Inaugural dissertation

for

obtaining the doctoral degree

of the

Combined Faculty of Mathematics, Engineering and Natural Sciences

of the

Ruprecht – Karls – University

Heidelberg

presented by
M.Sc. Jiao Zhao
born in: Jiangsu, China
Oral-examination: 28.07.2022

Roles of strigolactone signaling in the vascular development during secondary growth of *Arabidopsis thaliana*

Referees: Prof. Dr. Thomas Greb

Prof. Dr. Karin Schumacher

Acknowledgements

This project would not have been possible without the help and support of countless people. First of all, I would like to express my eternal gratitude to my supervisor Prof. Dr. Thomas Greb, who always generously takes time out of his schedule to provide me with professional guidance, invaluable opinion and feedback, as well as sincere mental support. His dedication to research and science is a source of inspiration; his responsibility to students is an origin of respect. I am so fortunate and grateful to be his student.

Also, I would like to express gratitude to my TAC committee members Prof. Dr. Karin Schumacher and Dr. Michael Raissig, who always provide me thoughtful, detailed feedback, crucial suggestions. Also, thanks for your encouraging words. All of these significantly contribute to the successful completion of my project. Thanks to Dr. Monika Langlotz from Flow Cytometry & FACS Core Facility for nuclei sorting service. Dr. David Ibberson from the Deep Sequencing Core facility who helped me with single nucleus RNA-sequencing service and I would like to express my gratitude to him. Great thanks especially to Dongbo, who constantly teaches me fundamental scientific skills and knowledge. I am so grateful for the great conversations in scientific topics. Thanks for providing me with precious opinions every single time I have doubts with my project. Many thanks to Theresa, who always gave me great mental supports when I was pregnant. Thanks to Xiaomin, who always gives me encouragement in the past months for writing. Thanks to Ilona, Aylin, Laura and Kiara, who always send their warming and sincere concern to me. At the beginning of my project, I had very little knowledge of vascular development and I always had questions. By then, I got many bits of help from Jiyan, Hyunwoo, Minhao, Vadir and Sophie. Thanks a lot for your time and suggestions. And to everybody I did not mention by name: Thanks for creating a pleasant working atmosphere and great working environment.

In addition, I also would like to express my great thanks to my friends and colleagues from Professor Dr. Jan Lohmann Group. A great thank to Xinai, who provides me with helpful infanticulture knowledge and is always a great mentor. Thanks also to Yanfei, Zhe, Jian, Pengfei for great conversations about scientific and personal topics.

Last, I would like to express my guilty and gratitude to my parents. I have not been back to China for 3 years and 3 months. I really miss them, and they miss me more. Thanks to my parents for always standing behind me, being there for me, and letting me live my dreams. Thanks to my parents for their consistent understanding and support of me. Thanks to my daughter, who makes my life alive and brings me lots of fun every day. Big thanks to my husband Changzheng, thanks a lot for everything he does for my daughter and me. I also would like to express my gratitude to the teachers from University Kita in INF685, who help me to take of my daughter since she was 3 months old and significantly enable me to complete this thesis.

Zusammenfassung

Das sekundäre Wachstum der Pflanzen trägt durch die Ablagerung von Zellwandmaterial im sekundären Xylem zur Produktion des größten Teils der Pflanzenbiomasse auf der Erde bei. Das sekundäre Xylem fungiert nicht nur als Transportkanal für Wasser und Mineralien durch den Pflanzenkörper, sondern liefert auch mechanische Unterstützung zur Aufrechterhaltung der Pflanzenarchitektur. Bei Gefäßpflanzen diffenziert sich das sekundäre Xylem vom vaskulären Kambium, welches parallel dazu und in entgegengesetzter Richtung Phloem erzeugt und damit das radiale Pflanzenwachstum antreibt. Für die Bildung des sekundären Xylems ist es entscheidend, die Identität von Xylemzellen ausgehend von vaskulären Stammzellen zu etablieren. Die Bildung des sekundären Xylems beginnt mit einer vaskulären Stammzelle, deren Tochterzellen sich in einer weitgehend unbekannten räumlich-zeitlichen Weise teilen und differenzieren. Eine gestörte oder verzögerte Bildung des sekundären Xylems hat starke Auswirkungen auf die radiäre Musterbildung in sekundären Geweben und auf das Pflanzenwachstum allgemein. Das Verständnis der räumlich-zeitlichen Regulationsnetzwerke hinter der sekundären Xylembildung ist insofern entscheidend für die Optimierung der Xylembildung und damit des pflanzlichen Wachstums und der Holzproduktion.

In dieser Studie deckte ich eine neue Rolle der Strigolacton (SL)-Signalübertragung in der Gefäßentwicklung von *Arabidopsis thaliana* auf: Der SL-Signalweg unterdrückt die Bildung sekundärer Gefäße in der Xylem-Phase I und hält die radiäre Hypokotyl-Musterbildung während der Xylem-Phase II stabil. Wie die Analyse der Promotoraktivität von dem Signalweg zugehörigen Genen zeigte, ist der SL-Signalweg in der Xylem-Phase I in hohem Maße mit den meisten differenzierten Geweben assoziiert. Im Vergleich dazu konnte ich in den sich entwickelnden Gefäßen eine relativ niedrige Aktivität des SL-Signalwegs feststellen. In der SL-Signalmutante *dwarf14* (*d14*) stellte ich sowohl durch Einzelkern-RNA-Sequenzierung (snRNA-seq) als auch durch histologische Analyse einen deutlicher Anstieg der sekundären Gefäßbildung fest, während ein Mangel an *SUPPRESSOR OF MAX2 1-LIKE6* (*SMXL6*), *SMXL7* und *SMXL8*-Genaktivität zu einer reduzierten sekundären Gefäßbildung führte. *SMXL7* reichte aus, um die Bildung von Sekundärgefäßen zu fördern, da eine vergleichbare verstärkte Gefäßbildung wie bei *d14*-

Mutanten auch in Linien mit stabilisiertem SMXL7 (SMXL7^{d53}) Protein zu beobachten war. Die Bildung von Größe und Anzahl der Gefäße wurde hingegen beeinträchtigt, wenn die Auxin-Signalübertragung in der *PHLOEM INTERCALATED WITH XYLEM* (*PXY*) Expressionsdomäne unterdrückt wurde. Interessanterweise wurd die Zunahme der Gefäßanzahl und -größe in *d14*-Mutanten durch die Unterdrückung der Auxin-Signalübertragung in der *PXY*-Expressionsdomäne gemildert. Dies zeigt, dass SL- und Auxin-Signale bei der Bildung von Sekundärgefäßen miteinander verbunden sind. In Phase II ist die radiale Hypokotylstrukturierung in *d14*-Mutanten gestört, begleitet von einer veränderten Auxinreaktion, die durch *DR5revV2:EYFP-ER* entlang der radialen Sequenz des Hypokotylgewebes dargestellt wird. Wichtig ist, dass die gestörte radiale Hypokotyl-Musterung in *d14*-Mutanten entweder durch Unterdrückung der Auxin-Signalübertragung in der *SMXL5*-Expressionsdomäne oder unter *Monopteros* (*MP*) -Mangelbedingungen vollständig in die Wildtyp-Musterung zurückgeführt werden kann. Dies zeigt, dass die SL-Signalübertragung für die Aufrechterhaltung der radialen Hypokotylstruktur entscheidend ist, indem sie das radiale Auxin-Reaktionsmuster moduliert, das hauptsächlich durch MP vermittelt wird.

Abstract

Secondary growth contributes to the production of most of the plant biomass by deposition of cell-wall material within the secondary xylem. Secondary xylem not only functions as a conduit transporting water and minerals throughout plant body, but also provides mechanical support for maintaining plant architecture. In vascular plants, secondary xylem differentiates from the vascular cambium, which in parallel generates phloem in the opposite direction and, thereby, driving radial plant growth. The determination of xylem cell identity from vascular stem cells is therefore crucial for the formation of secondary xylem. Formation of the secondary xylem initiates with a vascular stem cell whose cell lineages divide and differentiate in a largely unknown spatio-temporal manner. Impaired or delayed secondary xylem formation has destructive effects on radial vascular patterning and plant growth. Understanding the spatio-temporal pattern of the regulatory networks behind secondary xylem formation is therefore crucial to improve xylem formation, plant growth and wood production.

In this study, I report two novel roles of strigolactone (SL) signaling in vascular development in *Arabidopsis thaliana*: SL signaling suppresses secondary vessel formation at xylem phase I and maintains the radial hypocotyl patterning at xylem phase II. During xylem phase I, SL signaling is highly associated with most of the differentiated tissues as revealed by promoter activity analysis. In comparison, I detected a relatively low SL signaling level in developing vessel elements. A prominent increase in secondary vessel formation was detected in the SL signaling mutant *dwarf14* (*d14*) based on both single nucleus RNA-sequencing (snRNA-seq) and histological analysis, while deficiency in *SUPPRESSOR OF MAX2 1-LIKE6* (*SMXL6*), *SMXL7* and *SMXL8* gene activities resulted in reduced secondary vessel formation. SMXL7 was sufficient to promote secondary vessel formation, which I concluded based on a comparable enhancement of secondary vessel formation in *d14* mutants and in lines expressing a stabilized SMXL7 ($SMXL7^{d53}$) protein. Vessel size and number were reduced when auxin signaling was repressed in the *PHLOEM INTERCALATED WITH XYLEM* (*PXY*) expression domain in *d14* mutants. This suggested that SL and auxin signaling play interconnected roles in secondary vessel formation. During phase II, I observed a disrupted radial hypocotyl patterning in *d14* mutants accompanied by an altered auxin response along the radial

sequence of hypocotyl tissues as revealed by a *DR5revV2:EYFP-ER* reporter. Importantly, the disrupted radial hypocotyl pattern in *d14* mutants was completely recovered to a wild type-like pattern either by repressing auxin signaling in the *SMXL5* expression domain or under *MONOPTEROS* (*MP*) deficiency conditions. This demonstrated that SL signaling is crucial for maintaining the radial hypocotyl patterning via modulating the radial auxin response pattern which is mainly mediated by MP.

Abbreviations

ACL5	ACAULIS5
Agrobacteria	*Agrobacterium tumefaciens*
AHK4	ARABIDOPSIS HISTIDINE KINASE 4
AHP6	ARABIDOPSIS HISTIDINE PHOSPHOTRANSFER PROTEIN 6
AM	*Arbuscular mycorrhizal*
Arabidopsis	*Arabidopsis thaliana*
ARF	AUXIN RESPONSE FACTOR
AFB	AUXIN-RELATED F-BOX PROTEINS
ATHB8	ARABIDOPSIS THALIANA HOMEOBOX GENE 8
AXR3	AUXIN RESISTENT 3
BAK1	Brassinosteroid insensitive 1 associated Kinase 1
BES1	BRI1-EMS SUPPRESSOR 1
BRC1	BRANCHED1
BRI	BRASSINOSTEROID INSENSITIVE
bud2	*bushy and dwarf*
BZR1	BRASSINAZOLE-RESISTANT 1
CCD	Carotenoid cleavage dioxygenase
ChIP	Chromatin immunoprecipitation
CL	Carlactone
CLA	Carlactonoic acid
CLE	CLAVATA3/ESP-RELATED
CNA	CORONA/ATHB15
Col-0	Columbia-0
CFP	Cyan fluorescent protein
D14	DWARF14
D27	DWARF 27
D3	DWARF3 (MAX2)
D53	DWARF 53
DNA	Deoxyribonucleic acid
DO	Deoxyorobanchol
DS	Deoxy strigol

EAR	ETHYLENE RESPONSE FACTOR ASSOCIATED AMPHIPFATIC REPRESSION
EDTA	Ethylenediaminetetraacetic acid
EdU	5-ethynyl-2′-deoxyuridine
ER	Endoplasmic reticulum
E. coli	*Escherichia coli*
GSK3s	Glycogen Synthase Kinase 3 proteins
HD-ZIP III	Class III HOMEODOMAIN LEUCINE ZIPPER
IAA	Auxin indole-3-acetic-acid
KAI2	KARRIKIN INSENSITIVE 2
KAR	Karrikin
M	Molar
MAX4	MORE AXILLARY GROWTH 1-4
MeCLA	Methyl carlactonoate
MP	MONOPTEROS (ARF5)
MS	Murashige and Skoog
nCount-RNA	Number of molecules detected within a cell
NIB	Nuclei isolation buffer
NLS	Nuclear localization signal
NST	NAC SECONDARY WALL THICKENING PROMOTING FACTOR
PBS	Paraformaldehyde
PEAR	PHLOEM EARLY DOF
PFA	Paraformaldehyde
PHB	PHABULOSA
PHV	PHAVOLUTA
PIN	PIN-FORMED
PXY	PHLOEM INTERCALATED WITH XYLEM
REV	REVOLUTA
RNA	Ribonucleic acid
SAC51	SUPPRESSOR OF ACAULIS 51
X	

SCF	SUPPRESSOR OF KINETOCHORE PROTEIN1, Cullin , F-box
SERKs	SOMATIC EMBRYOGENESIS RECEPTOR KINASEs
SL	Strigolactone
SMAX1	SUPPRESSOR OF MAX2 1
SMXL	SUPPRESSOR OF MAX2 1-LIKE
snRNA-seq	Single nucleus RNA-sequencing
tbl29	*trichome birefringence-like 29*
TDIF	Tracheary Element Differentiation Inhibitory Factor
TIR	TRANSPORT INHIBITOR RESPONSE
TMSP	Thermospermine
TPL	TOPLESS
TPR	TPL-RELATED
UMAP	Uniform Manifold Approximation and Projection
UTR	Untranslated region
VND	VASCULAR-RELATED NAC-DOMAIN
WOX	WUSCHEL RELATED HOMEOBOX
wol	*wooden leg*
YFP	Yellow fluorescent protein

Table of contents

1 Introduction

Plants have evolved developmental plasticity as a result of being sessile to cope with changing environment conditions. As plant cells do not migrate (Dupuy et al. 2010), the developmental plasticity is significantly contributed by cell-to-cell communication. In multicellular organisms, cell-to-cell communication is a precondition for differentiation and development. Plant cell communicates to coordinate various complex signaling and regulatory networks in a precisely organized manner at the multicellular level, thereby determining cell fate and tissue-specific initials. Strict and tight control is subsequently imposed on timing and positioning of cell division, orientation of division plane, as well as differentiation to enable tissue establishment (Wendrich and Weijers 2013; De Rybel et al. 2014). Vascular tissues are established as a continuous system throughout the plant to conduct water, minerals, sucrose, and amino acids, which largely contribute to the success of plants in adapting to diverse terrestrial environments. As such, it is very important to investigate vascular development thus obtaining more knowledge in specification and differentiation of the vascular tissues.

1.1 The specification of xylem precursors in primary growth

In *Arabidopsis thaliana* roots, the primary vascular tissues are arranged into a bilateral symmetric pattern, with a central xylem axis flanked by two phloem poles and their intervening two domains of procambial cells (Růžička et al. 2015; De Rybel et al. 2016). The central xylem axis consists of protoxylem and metaxylem that occupy the marginal and central positions, respectively. The specification of the central xylem axis is tightly controlled by a high-auxin signaling domain in the protoxylem and a high-cytokinin signaling domain in the procambium (Bishopp et al. 2011; Růžička et al. 2015; De Rybel et al. 2016). By analysing an auxin responsive

reporter, an auxin response maximum is detected in the xylem axis, whereas cytokinin response peaks in the procambium visualized by cytokinin signaling reporters (Bishopp et al. 2011). Auxin signaling is compromised in *auxin resistant 3 - 1* (*axr3-1*) mutants, which causes disrupted protoxylem formation. It provides support for a positive role of auxin signaling in specifying protoxylem (Bishopp et al. 2011). By contrast, all vascular cells differentiated into protoxylem in *wooden leg* (*wol*) mutants which carry a mutation in a gene encoding a cytokinin receptor ARABIDOPSIS HISTIDINE KINASE 4 (AHK4), indicating that cytokinin function as a negative regulator of protoxylem cell fate (Mähönen et al. 2000). Protoxylem differentiation is also facilitated by ARABIDOPSIS HISTIDINE PHOSPHOTRANSFER PROTEIN 6 (AHP6), a cytokinin signaling inhibitor whose expression is strictly restricted to the protoxylem and induced by auxin (Mähönen et al. 2006; Bishopp et al. 2011). Thus, the protoxylem zone is a high-auxin domain characterised by high auxin and low cytokinin responses (Mähönen et al. 2006; Bishopp et al. 2011). In high-cytokinin signaling domains (the adjacent procambium zones), cytokinin in turn induces the expression of auxin-efflux carriers and thus transporting auxin towards the xylem axis, leading to the accumulation of auxin in the xylem related cells. Therefore, the mutually repressive feedback loop between auxin and cytokinin results in the establishment of protoxylem in a bilateral symmetric pattern (Bishopp et al. 2011).

1.2 Secondary xylem formation in the Arabidopsis hypocotyl

Vascular cambium originating from procambium whose activity contributes to secondary growth. Secondary xylem (wood) generated by the vascular cambium constitutes most of the plant biomass as a result of the deposition of cell-wall material. Wood as a kind of renewable fuel mainly derived from trees, and its generation encompasses a series of striking developmental processes. However, the long generation time of trees renders the study of genetic processes behind xylem

formation laborious. To accelerate the pace in studying wood formation, a model plant undergoing secondary growth would be extremely useful. Arabidopsis, despite of its herbaceous nature, has been proposed to be an excellent model to study the formation of secondary xylem (Chaffey et al. 2002; Zhang et al. 2011; Ragni and Hardtke 2014). Secondary growth in Arabidopsis occurs in stem, hypocotyl and root. Moreover, the composition of later stage xylem produced in the Arabidopsis hypocotyl tightly resembles the xylem in woody plants (Chaffey et al. 2002). In addition, recent progress in xylem development also revealed that conserved mechanisms existed between Arabidopsis and woody plants (Zhang et al. 2014a; Růžička et al. 2015; Ragni and Greb 2018). Therefore, *Arabidopsis* is now widely used as a model plant to study secondary xylem formation.

1.2.1 The onset and composition of secondary xylem in the *Arabidopsis* hypocotyl

In *Arabidopsis*, the initiation of periclinal cell divisions in procambium cells represents the activation of secondary growth, and the vascular cambium is derived from procambium cells that are in physical contact with primary xylem vessels (Smetana et al. 2019).

The vascular cambium, also known as vascular meristem, is usually organized in a cylindrical domain, which proliferates to generate secondary xylem towards the inside and phloem towards the outside, forming concentric vascular rings (xylem, cambium and phloem) (Figure 1.1 A) (Ragni and Greb 2018). The principal cell types of secondary xylem are xylem parenchyma, vessel elements and fibres, of which vessels are the main water-conducting cells and fibres function to provide mechanical support. In the Arabidopsis Columbia ecotype, secondary xylem development in hypocotyls is divided into two phases (phase I and phase II) according to its cell type composition (Chaffey et al. 2002; Ragni and Hardtke 2014). During phase I, secondary xylem comprises lignified vessel cells and non-lignified

xylem parenchyma cells (Figure 1.1 B). After the transition to phase II, which coincides with the bolting of the inflorescence stem, lignified fibre cells are produced instead of parenchyma cells (Figure 1.1 C). At last, the secondary xylem generated in phase II is massively occupied by lignified fibre cells combined with a minority of vessel elements, and forms a lignified tissue layer encompassing the xylem area produced in phase I (Chaffey et al. 2002).

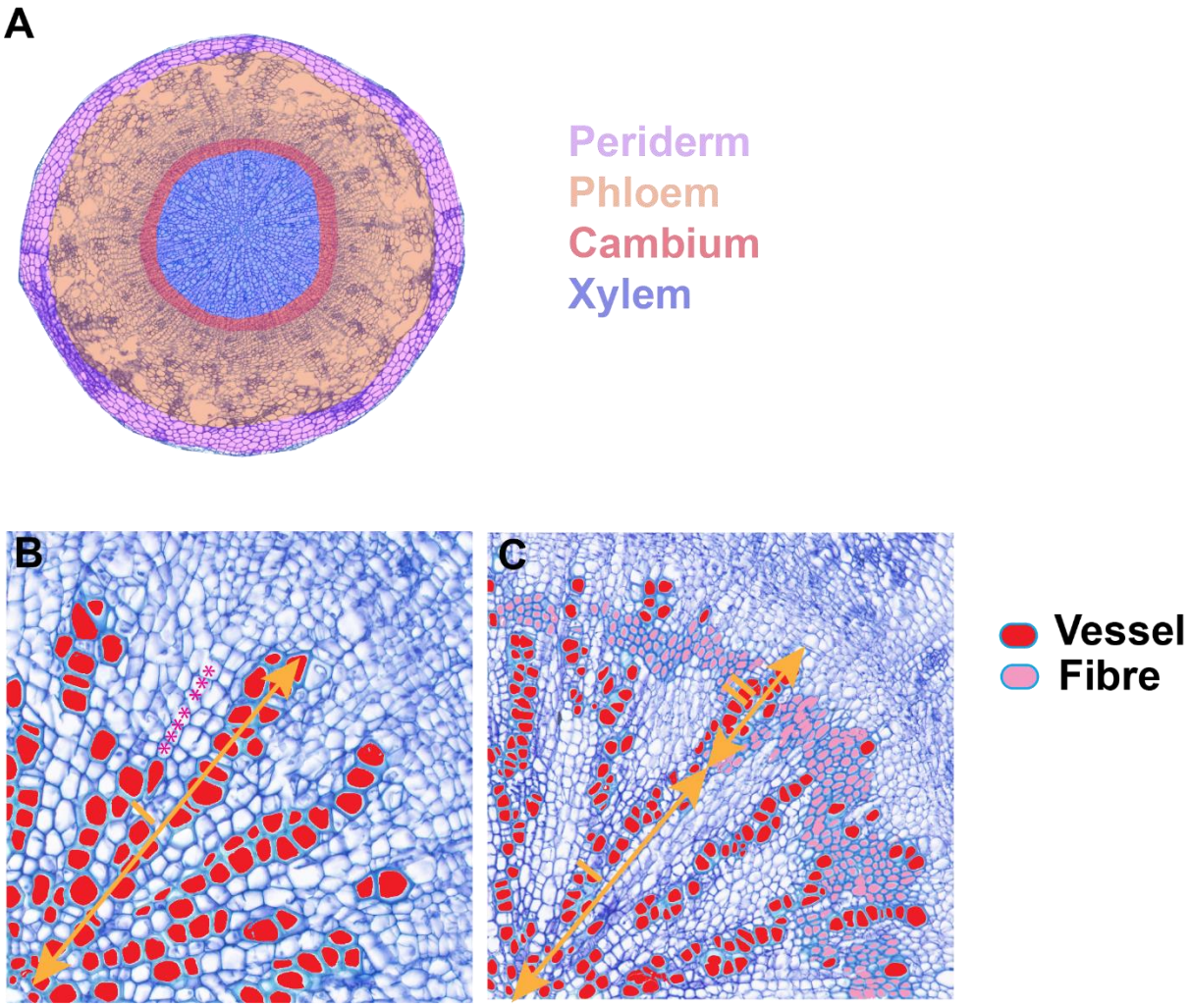

Figure 1.1: Vascular tissues in hypocotyl in Arabidopsis

A A schematic cross section at the hypocotyl illustrates main tissues organized in concentric cylindrical rings that are coloured according to the legend. B The phase I of secondary xylem development is characterized by the formation of vessels coloured in red and xylem parenchyma (indicated with purple asterisks). C The phase II of secondary xylem development consists of vessels in red and fibres in pink. The figure

is generated on information described in Chaffey et al. 2002, and Ragni and Hardtke 2014.

1.2.2 The regulation of xylem formation during secondary growth

Once all cell types are present in primary vascular tissues, (pro)cambium cells establishing xylem fate start differentiating into secondary xylem. The formation of secondary xylem is regulated by auxin, thermospermine, the CLAVATA3/ESR-RELATED 41/Tracheary Element Differentiation Inhibitory Factor (CLE41/TDIF) and PHLOEM INTERCALATED WITH XYLEM (PXY) module, and gibberellin. Also, several transcriptional master regulators have been identified to be involved in this process.

1.2.2.1 Auxin promotes xylem formation

$SCF^{TIR1/AFB}$ -mediated auxin signal transduction requires TRANSPORT INHIBITOR RESPONSE 1/AUXIN-RELATED F-BOX PROTEINS (TIR1/AFB) proteins, AUXIN/INDOLE-3-ACETIC ACID (AUX/IAA) repressors, and AUXIN RESPONSE FACTORs (ARFs) (Salehin et al. 2015). Auxin binding to the TIR1/AFB receptors prompts the degradation of AUX/IAA transcriptional repressors, thus releasing Aux/IAA repression on ARFs, and consequently derepresses the ARFs based transcription (Salehin et al. 2015). ARF5 also known as MONOPERTOS (MP) whose mutation results in defective tissue continuity within vascular strands, has previously been reported to be crucial for normal vascular tissue formation (Przemeck et al. 1996; Hardtke and Berleth 1998). A recent study demonstrated that *ARF5*, *ARF7* and *ARF19* display overlapping expression patterns in vascular tissues, and a substantial reduction in secondary xylem production is observed when *MP* is knocked down in an *arf7arf19* mutant background, suggesting that *MP* promotes

secondary xylem formation redundantly to *ARF7* and *ARF19* in roots (Smetana et al. 2019).

ARABIDOPSIS THALIANA HOMEOBOX 8 (*ATHB8*) functions downstream of auxin and its expression is directly and positively regulated by *MP* (Donner et al. 2009). In Arabidopsis, *ATHB8*, together with its homologous genes *PHABULOSA (PHB)*, *CORONA (CNA)/ATHB15*, *REVOLUTA (REV)*, and *PHAVOLUTA (PHV)* are characterised as homeodomain–leucine zipper (*HD–ZIP*) III genes, encoding for a family of transcription factors that is specific to plants (Prigge et al. 2005; Green et al. 2005; McConnell et al. 2001; Talbert et al. 1995; Baima et al. 2014; Baima et al. 2001). Interestingly, the activities of all five *HD-ZIP III* genes are active in vascular tissues (Prigge et al. 2005; Miyashima et al. 2013). In particular, *ATHB8* and *ATHB15* are highly active in procambium cells (Baima et al. 2001; Ohashi-Ito and Fukuda 2003; Ilegems et al. 2010). Besides, the expression of *ATHB8* is also detected in developing vessel elements, but neither in the phloem nor in fully differentiated vessels in the hypocotyl (Ilegems et al. 2010). In agreement with its expression in developing vessels, *ATHB8* has been proposed to promote xylem differentiation as the overproduction of *ATHB8* results in an excess of secondary xylem formation (Baima et al. 2001).

1.2.2.2 Thermospermine negatively regulates the proliferation of developing vessel elements

There are not many reports of mutants displaying over-proliferation of vessel-related cells, but mutants of the *ACAULIS5* (*ACL5*) gene display enhanced vessel formation in stems, roots and hypocotyls (Hanzawa et al. 1997; Imai et al. 2006; Muñiz et al. 2008; Vera-Sirera et al. 2015). However, the vessel increment is only observed in early-stage hypocotyls and no further secondary growth is detected in 5-week-old *acl5* mutants (Muñiz et al. 2008). Of note, *ACL5* encodes a thermospermine synthase, a structural isomer of spermine (Knott et al. 2007).

Another mutant, *bushy and dwarf* (*bud2*), displays a similar phenotype as *acl5* with regard to the over-proliferation of developing vessel elements. *BUD2* is one of the four genes encoding S-adenosylmethionine decarboxylases, enzymes required for the biosynthesis of polyamines in *Arabidopsis* (Ge et al. 2006). *ACL5* activity is specifically restricted to the developing vessel elements in stems and hypocotyls (Muñiz et al. 2008). The expression of *ACL5* is upregulated by auxin in poplar and downregulated when MP activity is abolished in *Arabidopsis* (Milhinhos et al. 2013; Tong et al. 2014; Vera-Sirera et al. 2015). Similarly, the expression of *BUD2* can also be induced by auxin (Cui et al. 2010). By contrast, exogenously application of thermospermine suppresses auxin-dependent xylem differentiation (Yoshimoto et al. 2012). A negative feedback loop is proposed to explain the homeostasis of thermospermine and the fine-tuning of xylem formation (Figure 1.2) (Baima et al. 2014; Milhinhos et al. 2013). As mentioned above, *MP* directly promotes the expression of *ATHB8*. Meanwhile, ATHB8 is demonstrate to directly promote the expression of *ACL5* and *BUD2*. As such, auxin positively regulates the expression of *ACL5*. Thermospermine, the enzymatic product of *ACL5*, subsequently enhances the activity of transcription factor *SUPPRESSOR OF ACAULIS 51* (*SAC51*), whose disruption represses the *acl5-1* phenotype (Imai et al. 2006; Kakehi et al. 2008). *SAC51* in turn negatively regulates auxin-related processes by an unrevealed mechanism, thereby balancing thermospermine synthesis and xylem differentiation (Baima et al. 2014).

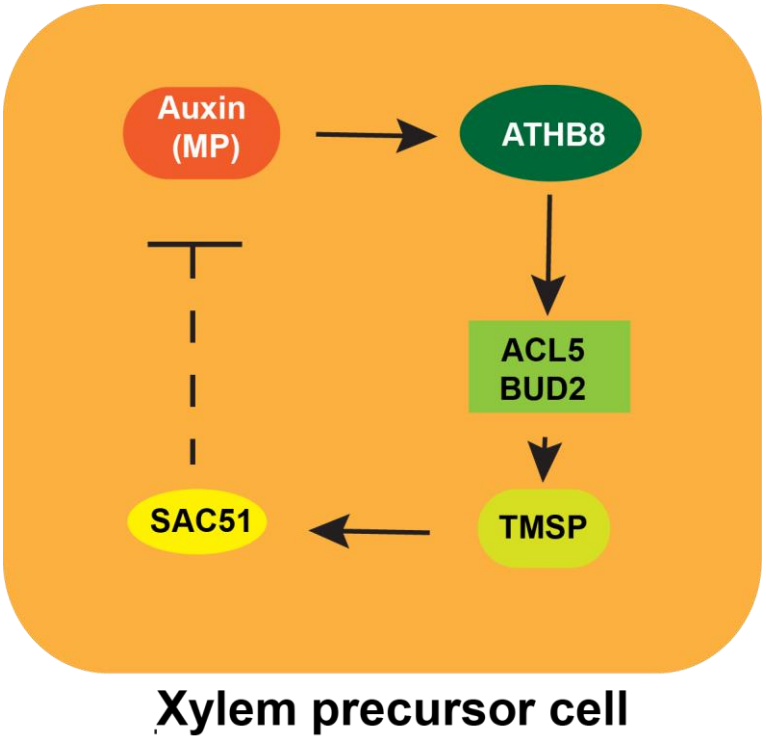

Figure 1.2: A negative feedback loop mediated by ATHB8/ACL5–BUD2 module
Auxin (MP) promotes the regulation of ATHB8. ATHB8 positively regulate the expression of ACL5 and BUD2, and consequently the synthesis of Thermospermine (TMSP). TMSP positively regulate the translation of the SAC51 which, in turn, potentially represses auxin signaling by an unrevealed mechanism (Milhinhos et al. 2013; Baima et al. 2014).

1.2.2.3 Roles of the CLE41/TDIF-PXY module in secondary growth

In *Arabidopsis*, TDIF is encoded by two genes: *CLV3/ESR1-LIKE 41* and *44* (*CLE41* and *CLE44*). CLE peptide CLE41/TDIF was initially isolated from a xylogenic culture system of Zinnia (*Zinnia elegans*) cells (Fukuda and Komamine 1980) and it was shown to suppress the differentiation of cultured cells into vessels (Ito et al. 2006). Similar effect in vessel formation was observed when plants are grown in a liquid medium containing CLE peptides (Hirakawa et al. 2008). High CLE peptide conditions inhibit xylem formation, but do not affect phloem differentiation. Besides, an evident promotion of stem cell divisions was observed by treating hypocotyls with CLE peptides (Hirakawa et al. 2008; Whitford et al. 2008). Nevertheless, xylem

inhibition and cambium proliferation effects disappear when TDIF RECEPTOR (TDR), also named PXY, activity is abolished. In addition, the crystal structure of TDIF binding to its receptor PXY has been illustrated (Zhang et al. 2016a). Therefore, PXY is demonstrated to be the receptor of TDIF. In hypocotyls and roots, both *CLE41/44* genes are active in the phloem region and the adjacent pericycle, while their receptor PXY shows specific expression in procambial cells (Hirakawa et al. 2008). As the peptides are detected in the procambial zone, it is proposed that TDIF is expressed in the phloem region and secreted to the adjacent cambium zone, where it is perceived by PXY to stimulate cambium cell division and suppress xylem differentiation (Hirakawa et al. 2008). Further studies demonstrated that these two TDIF-PXY module outputs are separately mediated by WUSCHEL HOMEOBOX RELATED 4 (WOX4)/WOX14 transcription factors, and Glycogen Synthase Kinase 3 proteins (GSK3s) (Hirakawa et al. 2010; Kondo et al. 2014; Etchells et al. 2013). A rapid increase in *WOX4* expression is detected when wild-type plants are subjected to TDIF treatment, whereas the induction is undetectable in *pxy* mutants, suggesting that *WOX4* acts as a transcriptional target of the TDIF-PXY module (Hirakawa et al. 2010). Moreover, under long-term TDIF treatment, wild-type plants show an increment in cambium cells, while this effect is absent in *wox4*. However, *wox4* mutants only show defects in cambium proliferation but not in xylem formation. These results suggest that WOX4 mediates the proliferation of cambium cells as an output of the TDIF-PXY module, whereas the xylem inhibition output is mediated by other factors (Hirakawa et al. 2010). GSK3s have been illustrated to interact with PXY within the plasma membrane via transient tobacco-based assays, and the perception of TDIF by PXY enhances GSK3s activity (Kondo et al. 2014). Importantly, xylem repression upon TDIF application is not detectable when GSK3 activity is abolished. BRI1-EMS SUPPRESSOR 1 (BES1) is a transcription factor that acts downstream of GSK3s in promoting xylem differentiation from cambium cells (Kondo et al. 2014). As such, GSK3s are demonstrated to be the downstream targets of the TDIF-PXY signaling pathway in suppressing xylem differentiation from cambium cells through the repression of BES1 (Kondo et al. 2014).

A cross-talk exists between the TDIF-PXY and brassinosteroid signaling pathways in regulating xylem formation (Kondo et al. 2014; Yin et al. 2002; Yin et al. 2005). However, the brassinosteroid signaling pathway has been indicated to promote xylem cell identity (Yamamoto et al. 2001; Yamamoto et al. 2007; Caño-Delgado et al. 2004). The gene activities of the brassinosteroid receptors, BRASSINOSTEROID INSENSITIVE (BRI), BRI-LIKE1 (BRL1), and BRL2 are detected broadly in vascular tissues (Caño-Delgado et al. 2004). In contrast to TDIF-PXY signaling, BRI, BRL1 and BRL2 mediated brassinosteroid signaling negatively regulates GSK3, the repression of BRASSINAZOLE-RESISTANT 1 (BZR1) therefore is released. BZR1 represents a class of plant-specific transcription factors and BES1 is the closest homolog of BZR1, both of which are verified to be master transcription factors in the BR signaling pathway by regulating expression of many target genes (Sun et al. 2010; Yu et al. 2008; Zhao et al. 2002). The activated BZR1 is subsequently transported into nucleus and promote the xylem differentiation (Caño-Delgado et al. 2004; Yamamoto et al. 2007; Etchells et al. 2013; Etchells et al. 2016).

1.2.2.4 GA signaling promotes wood formation

Gibberellic acid (GA) signaling is reported to stimulate polar auxin transport, thus promoting wood formation and fibre elongation in aspen (*Populus tremula*) (Björklund et al. 2007; Mauriat and Moritz 2009). It is reported that GA synthesis-related genes are expressed in the expanding xylem, while as the first executed GA biosynthesis enzyme, ent-copalyl diphosphate synthaseshows high expression levels in the phloem region, indicating GA precursor(s) probably are transported from phloem to the xylem in aspen (Israelsson et al. 2005). In *Arabidopsis*, mobile GA has also been verified to trigger the xylem expansion phase upon flowering, as well as fibre formation by the degradation of DELLA proteins (Ragni et al. 2011). Later study further suggests that plants respond to GA in aspect of triggering fiber differentiation

depends on the homeoboxtranscription factor BREVIPEDICELLUS/KNAT1 (BP) (Ikematsu et al. 2017; Ben-Targem et al. 2021).

1.2.2.5 Xylem formation regulators

The plant-specific NAC-domain transcription factors VASCULAR-RELATED NAC-DOMAIN 6 (VND6) and VND7 are master regulators of xylem formation (Kondo et al. 2015; Kubo et al. 2005; Yamaguchi et al. 2010). In roots, the expression activity of *VND6* is exclusively detected in metaxylem cells with reticulate or pitted secondary cell wall deposition, whereas *VND7* is detected in the protoxylem with annular or spiral secondary cell wall thickening (Kubo et al. 2005). Gene redundancy is reflected by normal development and growth of loss-of-function mutants of *VND6* or *VND7*. Intriguingly, trans-differentiation of various types of cells into xylem vessels is observed when VND6 and VND7 are expressed under the control of the ubiquitously active cauliflower mosaic virus 35S promoter (Kubo et al. 2005). In the hypocotyl, for instance, trans-differentiation occurs mainly in epidermis cells. During the deposition of secondary cell walls, however, the cell shape of the epidermis maintains unchanged (Kubo et al. 2005). Further studies identified several direct and indirect targets of VND7 in controlling secondary cell wall biosynthesis, including the transcription factors MYB46 and MYB83 (Yamaguchi et al. 2011; McCarthy et al. 2009; Turco et al. 2019). Two more NAC-domain transcription factors named SECONDARY WALL THICKENING PROMOTING FACTOR1 (NST1) and NST3 are key regulators of SCW formation in fibre cells. Their mutation results in the absence of secondary cell wall thickening in fibre cells in hypocotyls (Mitsuda et al. 2007). The activities of *NST1* and *NST3* are detected in developing vessel elements, and are strongly enhanced in cells destined to become fibres, suggesting the expression of *NST1* and *NST3* is closely correlated with a woody cell fate. In *nst1nst3* double mutants, long and narrow fibrous cells are observed in the position where fibre cells are located in WT, and these cells display strong *NST1* and *NST3* activities revealed

by promoter activity analysis, demonstrating that the fibre cell fate is maintained and independent of NST1 and NST3 (Mitsuda et al. 2007).

1.3 The asymmetry of cambium division

Cambium cell divisions are characterized by a very prominent asymmetry, by which xylem and phloem cells are spatially separated, with xylem towards its inside and phloem towards its outside. The spatial separation of xylem and phloem, however, is disturbed when the TDIF-PXY module is altered (Fisher and Turner 2007; Etchells and Turner 2010; Yang et al. 2020). *pxy* mutants displays a pattern defect meaning that phloem is intercalated with xylem in the stem, suggesting PXY maintains spatial separation in vascular development (Fisher and Turner 2007). A similar pattern defect was also observed in stems when *CLE41* was ubiquitously expressed or ectopically expressed in the xylem domain with phloem generated in a region where usually only xylem is formed (Etchells and Turner 2010). Moreover, plants with altered *CLE41* expression display a more severe phenotype in the hypocotyl, in which phloem and xylem tissues are completely interspersed. Therefore, it is proposed that localised expression of *CLE41* in phloem domain is essential for maintaining properly orientated cell divisions, thereby generating a well-ordered vascular pattern (Etchells and Turner 2010). Later, SOMATIC EMBRYOGENESIS RECEPTOR KINASEs (SERKs) were identified to serve as co-receptors in the PXY-CLE41module to promote the proliferation of procambial cells (Zhang et al. 2016b). One of the co-receptors, SERK3, also known as Brassinosteroid insensitive 1 associated Kinase 1 (BAK1), interacts with the NAC-domain protein XVP/ NAC003 (Yang et al. 2020). XVP suppresses TDIF-PXY signaling. The *xvp-d* mutant displays similar disruptive vascular organization as the *pxy* null mutant: the phloem tissue extends almost to the centre of hypocotyls and is interspersed with xylem probably caused by disruptive periclinal orientations during cambium cell division (Yang et al. 2020). These results suggest that the cell division

orientation in cambium shows a dependency on the TDIF-PXY module, which is important for the proper distribution of the two specialized and differentiated phloem and xylem tissues. In addition, the strict spatial separation of phloem and xylem can be disturbed by expressing constitutively active *MP* (*MPΔ*) in the phloem region (Smetana et al. 2019). The conditional expression of *MPΔ* directly induces the expressions of *PXY*, *WOX4* and *ATHB8*, followed by the formation of ectopic vessels. Subsequently, the activities of *PXY*, *WOX4* and *ATHB8* are induced in the adjacent cells of the *MPΔ* clones, and an early phloem marker *PHLOEM-EARLY-DOF 1* (*PEAR1*) appears in the surrounding cells, suggesting the *MPΔ* is sufficient for the generation of a vascular cambium in the phloem region (Smetana et al. 2019).

1.4 Strigolactones

Strigolactones (SLs) were initially isolated to act as rhizospheric signals that stimulate the germination of parasite plants (Cook et al. 1966). As rhizospheric signals, SLs were later revealed to promote a symbiotic relationship between arbuscular mycorrhizal (AM) fungi and their host plants by facilitating hyphal branching of AM (Akiyama et al. 2005). Importantly, SLs also act as endogenous hormonal signals to inhibit processes like plant shoot branching (Gomez-Roldan et al. 2008; Umehara et al. 2008). Since the revelation of SLs as phytohormones, extensive insights into SLs synthesis, perception and communication have been established.

1.4.1 The chemical structure of SLs compounds

SLs are a class of carotenoid-derived molecules, and can be classified into two groups according to their chemical structures: canonical and non-canonical SLs. Canonical SLs compromise tricyclic lactone moiety (ABC ring) connected to a butanolide moiety (D-ring) via an enol-ether bond (Al-Babili and Bouwmeester 2015).

With the help of bioassay-guided purifications, at least 23 canonical SLs have been identified from root exudates (Xie 2016). According to the stereochemical differences at the connection of the B and C rings, canonical SLs are divided into two subclasses, the 5-deoxy strigol (5DS) and 4-deoxyorobanchol (4DO) types (Yoneyama et al. 2018). Plants generally produce either strigol- or orobanchol-type SLs as their principal SLs, but still some species produce both types such as tobacco (*Nicotiana tabacum*) (Xie et al. 2013). However, compounds with SL-like activities that do not have tri-cyclic ABC structure (non- canonical SLs) are described (Yoneyama et al. 2010; Yoneyama et al. 2018; Yoneyama et al. 2009; Zwanenburg et al. 2009; Boyer et al. 2012). In contrast to non-canonical SLs, canonical SLs are routinely used in research, including the natural forms such as 5DS and 4DO, and their synthetic analogue (Flematti et al. 2016). The strigol-configured GR24 (*rac*-GR24), comprising GR24^{5DS} and its enantiomer GR24$^{ent\text{-}5DS}$, is widely used as an SL synthetic analog. Nevertheless, GR24^{5DS} behave as SL and Karrikin (KAR) that is a small butenolide compound (detailed description blow), and GR24$^{ent\text{-}5DS}$ is shown to act as a KAR (Scaffidi et al. 2014; Villaécija-Aguilar et al. 2019), raising the risk to use GR24 as SLs to evaluate the impact of plants responding to exogenous SLs. Another pair of enantiomers of GR24 is GR24^{4DO} and GR24$^{ent\text{-}4DO}$, and they were shown to behave as SL and KAR, respectively (Scaffidi et al. 2014). And indeed, the SL specificity of GR24^{4DO} was further confirmed in later studies (Wang et al. 2020a; Song et al. 2022).

1.4.2 SL biosynthesis

SL biosynthesis starts with the carotenoid isomerase DWARF27 (D27), which transforms all-trans-β-carotene to 9-cis-β-carotene (Alder et al. 2012). Sequential reactions involve carotenoid cleavage dioxygenase 7 (CCD7) and CCD8 in catalysing 9-cis-β-carotene to carlactone (CL) (Alder et al. 2012). In *Arabidopsis*, the carotenoid isomerase is encoded by *AtD27*, whereas carotenoid cleavage dioxygenases CCD7 and CCD8 are encoded by the *MORE AXILLARY GROWTH 3*

(*MAX3*) and *MAX4* genes, respectively (Xie et al. 2010). The intermediate CL molecule is subsequently oxidized by MORE AXILLARY GROWTH 1 (MAX1) to yield carlactonoic acid (CLA). Afterwards, CLA is modified by an unknown methyltransferase into methyl carlactonoate (MeCLA) (Abe et al. 2014). Of note, MeCLA but not CL and CLA is able to interact with the SL receptor, indicating MeCLA supresses branching in *Arabidopsis* (Abe et al. 2014). Further action by a novel SL biosynthetic gene, *LATERAL BRANCHING OXIDOREDUCTASE* (*LBO*), converts MeCLA into an unknown molecule that is probably more potent than MeCLA (Brewer et al. 2016). As only MeCLA and its derivatives so far are identified, it is still disputable whether canonical SLs are produced in *Arabidopsis* (Abe et al. 2014; Kohlen et al. 2011; Xie 2016). In rice, five homologs of MAX1 exist, one of which acts as a CL oxidase that directly oxidize CL to 4-deoxyorobanchol, being the precursor for natural canonical orobanchol-type SLs (Zhang et al. 2014b).

1.4.3 The strigolactone signaling perception mechanism in planta

Similar to the way auxin, jasmonate, and gibberellin are perceived, SL signal transduction requires hormone-activated proteolysis of targeted substrates (Waters et al. 2017). The proteolysis is mediated by an F-box E3 ubiquitin ligase which is part of a Skp1–Cullin–F-box (SCF) complex, and the 26S proteasome, respectively (Waters et al. 2017). Numerous studies have focused on finding the F-box targets, as well as the activation mechanism of SCF complex mediated polyubiquitination.

1.4.3.1 Strigolactone perception

Genetic studies in *Arabidopsis*, rice, *Petunia hybrida*, and *Pisum sativum* revealed the nature of the SL receptors (de Saint Germain et al. 2016; Arite et al. 2009; Hamiaux et al. 2012; Waters et al. 2012). In both *Arabidopsis* and rice, the SL

receptor is known as DWARF14 (D14), belonging to the α/β-fold hydrolase enzyme family (Figure 1.3). The transduction of the SL signal is also coordinated by the F-box protein MORE AXILLARY GROWTH2 (MAX2) in *Arabidopsis* or D3 in rice (Figure 1.3). D14 shows hydrolase activity for some SLs, by which SLs are cleaved into ABC-ring and D-ring moieties (Abe et al. 2014; Hamiaux et al. 2012; de Saint Germain et al. 2016; Yao et al. 2016; Zhao et al. 2013). A covalent modification between the cleaved D-ring derivative and the active site in Ser and His residues of D14 induces conformational changes in the AtD14 protein (de Saint Germain et al. 2016; Yao et al. 2016). The modification has been proposed to prompt the binding of D14 with MAX2/D3, together with the SMXL proteins in *Arabidopsis* and D53 in rice, triggering ubiquitination and degradation of the SMXL/D53 proteins (de Saint Germain et al. 2016; Yao et al. 2016; Yao et al. 2017). Another model proposes that the binding of D14 to the intact SL directly triggers the association with MAX2 and SMXL proteins, which subsequently are ubiquitinated and degraded. Afterwards, SL is destroyed due to the hydrolysis by D14 (Seto et al. 2019). The conformational switch of D3 is also crucial for the hydrolase activity of D14, recruitment of D53 to $SCF^{D3\text{-}D14}$, and thus transduction of SL signaling (Shabek et al. 2018).

1.4.3.2 Proteolytic Targets (mediators) of Strigolactone Signaling

A screen for genetic mediators of *max2* phenotypes in Arabidopsis initially identified SUPPRESSOR OF MAX2 1 (SMAX1), while the *smax1* mutant was later shown to repress KAR-related phenotypes of *max2* (Soundappan et al. 2015; Stanga et al. 2013). In rice, a dominant SL-insensitive *d53* mutant displays higher tillering phenotype as also observed in *d3* and *d14*, and D53 is identified as a mediator of SL signaling (Jiang et al. 2013; Zhou et al. 2013). Later, SMAX1-LIKE6 (SMXL6), SMXL7, and SMXL8 were demonstrated to be mediators of SL-associated alterations of the *max2* phenotype (Soundappan et al. 2015). The mediators D53 in rice and SMXL7 in *Arabidopsis* both were shown to physically interact with D14 in an SL-

dependent manner. Moreover, D53 and SMXL7 degradation upon GR24 treatment depends on D14 and MAX2/D3 (Soundappan et al. 2015; Jiang et al. 2013; Zhou et al. 2013; Umehara et al. 2015; Liang et al. 2016; Wang et al. 2015), demonstrating that SMXL7 in *Arabidopsis* and D53 in rice are the proteolytic targets of SL signaling (Figure 1.3). The dominant *d53* isoform carries a small deletion in a conserved C-terminal Arg-Gly-Lys-Thr motif, and an equivalent mutation to that observed in *d53* occurs in SMXL6 and SMXL7, which renders D53, SMXL6 and SMXL7 undegraded, resulting in a similar branchy phenotype as found in *d14* mutants (Liang et al. 2016; Wang et al. 2015; Jiang et al. 2013; Zhou et al. 2013).

1.4.4 SMXL proteins act as transcription factors

SMXL/D53 proteins are reported to contain a well-conserved ETHYLENE RESPONSE FACTOR–associated amphiphilic repression (EAR) motif (Ohta et al. 2001; Bennett and Leyser 2014). The EAR motifs are crucial for the interactions with the transcriptional corepressors - TOPLESS (TPL)/TOPLESS-RELATED (TPR) (Szemenyei et al. 2008). This is reminiscent to the proteolytic targets of auxin and jasmonate signaling which likewise contain EAR motifs and act as transcriptional repressors via interaction with TPR proteins (Pauwels et al. 2010; Szemenyei et al. 2008). As such, SMXL proteins are assumed to act in a similar manner. The EAR motifs in SMXL proteins are essential for the interaction between SMXL proteins and TPL/TPR proteins and thus for transcriptional repression (Soundappan et al. 2015; Wang et al. 2015). However, some observations challenge the hypothesis of EAR-mediated transcriptional repression (Mashiguchi et al. 2009; Liang et al. 2016; Shinohara et al. 2013). For example, shoot related defects of *smxl6*;*smxl7*;*smxl8*;*max2* quadruple mutants are restored by a SMXL7 variant lacking the EAR motif (Liang et al. 2016). More recent work revealed that SMXL6 can function as a transcription factor in an EAR dependent manner by directly binding DNA (Wang et al. 2020a). Moreover, this work identified *BRANCHED 1* (BRC1), *TCP*

DOMAIN PROTEIN 1 and *PRODUCTION OF ANTHOCYANIN PIGMENT 1* to function downstream of SL signaling in regulating shoot branching, leaf shape and anthocyanin accumulation, suggesting that different SL responses are mediated by distinct downstream targets (Wang et al. 2020a). Furthermore, SMXL6 and SMXL7 directly binds to the promoters of SMXL6, SMXL7 and SMXL8 to maintain the homeostasis of SL signaling (Figure 1.3) (Wang et al. 2020a).

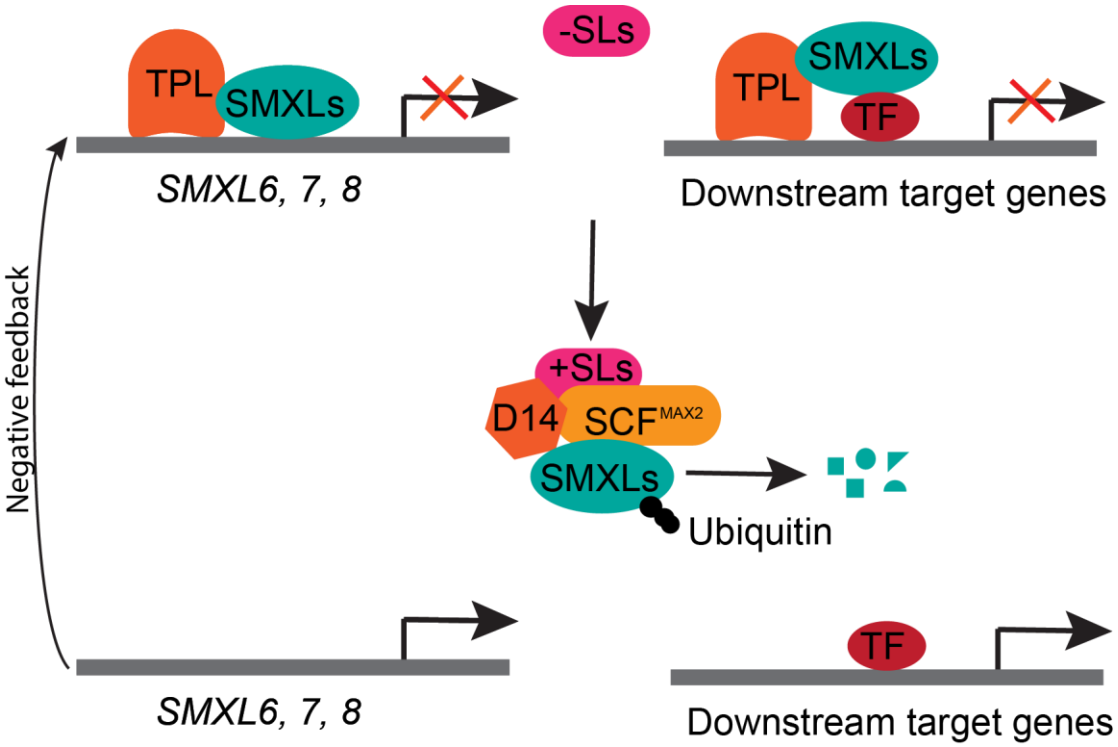

Figure 1.2: The core SL signaling pathway and proposed model of transcriptional regulation by SMXLs

When SLs is absent, SMXLs and TPL act as repressive transcription factors by directly binding to the promoters of *SMXL6*, *7*, *8*. Meanwhile, SMXLs represses the transcription of target genes by forming a complex with unknown transcription factors that recognize and bind to the promoter of the target genes. In the presence of SLs, D14 perceives SLs, which consequently promotes the formation of the D14/SCF^{MAX2}/SMXLs complex, thereby triggering the ubiquitin-mediated degradation of SMXLs. This can derepress transcription of *SMXL6*, *7*, *8*. Freshly synthesized SMXLs proteins in turn inhibit expression to form a negative loop. Likewise, the degradation of SMXLs also releases the transcriptional repression of other downstream targets to activate SL signaling cascades mediated in multiple

developmental aspects (Wang et al. 2020; Soundappan et al. 2015; Jiang et al. 2013; Zhou et al. 2013; Umehara et al. 2015; Liang et al. 2016; Wang et al. 2015).

1.4.5 Strigo-D2 sensor

Strigo-D2, as a genetically encoded ratiometric SL signaling sensor, responds rapidly to altered SL levels, thus rendering it capable of examining the distribution of SL signaling at cellular resolution in *Arabidopsis* (Song et al. 2022). Strigo-D2 comprise two expression cassettes. The two expression cassettes are cloned in the same construct and both are driven by the 35S promoter (*35S:SMXL6-D2-mVenus_35S:mCherry-NLS*). As the D2 domain of D53 in rice has been reported to be sufficient to trigger the hormone-induced $SCF^{MAX2–D14}$-catalysed protein turnover (Shabek et al. 2018), the correspondent D2 domain of SMXL6 (D3 homologous gene in *Arabidopsis*) is cloned into the construct, instead of intact SMXL6. The fusion protein between D2 and mVenus which should lead to the degradation and loss of mVenus fluorescence in case of active strigolactone signaling; this part is combined with an internal reference consisting of mCherry linked to a nuclear localization signal (NLS) which should be stable under every condition. As such, the SL signaling activity can be revealed by the intensity ratio of mVenus to mCherry. And indeed, the degradation of mVenus was captured when plants carrying Strigo-D2 are treated with SLs, meanwhile mCherrry remains stable. Moreover, Strigo-D2 displays insensitivity to pharmacological induction of SL-signaling in *d14* mutant background, indicating Strigo-D2 specifically responds to D14 mediated SL signal transduction in planta (Song et al. 2022).

1.4.6 Roles of SL signaling in plant development

SL signaling has been proposed to be involved in multiple aspects of plant development, such as shoot branching, anthocyanin accumulation, shoot

gravitropism, leaf shape, internode elongation and senescence, root architecture, cambium activity, and adaptation to drought and nutrient availability (Sorefan et al. 2003; Stirnberg et al. 2002; Snowden et al. 2005; Arite et al. 2007; Gomez-Roldan et al. 2008; Umehara et al. 2008; Drummond et al. 2009; Agusti et al. 2011; Lin et al. 2009; Sang et al. 2014; Wang et al. 2015; Bu et al. 2014; Akiyama et al. 2005; Czarnecki et al. 2013; Van Ha et al. 2014)

1.4.6.1 Inhibition of shoot branches

Among of these roles, the best-characterized SL role is in the control of shoot branching by the core D14-MAX2-D53/SMXLs signaling mechanism (Soundappan et al. 2015; Wang et al. 2015; Zhou et al. 2013; Jiang et al. 2013). However, downstream effects of SMXL protein degradation remain disputable and two main models have been proposed for shoot branching regulation: the direct-action model and the canalization model (Domagalska and Leyser 2011). The direct-action model proposes that SLs act as a second messenger of auxin to directly regulate the expression of *BRC1* in buds (Domagalska and Leyser 2011; Dun et al. 2012). BRC1 is a key repressor of bud outgrowth, whose mutation results in increased shoot branching (Aguilar-Martínez et al. 2007). Wang et al recently confirmed that BRC1 acts downstream of SMXL6 to modulate shoot branching in an EAR motif-dependent manner (Wang et al. 2020a; Aguilar-Martínez et al. 2007; Braun et al. 2012; Brewer et al. 2009; Dun et al. 2012), which supports the direct-action model for shoot branching regulation (Domagalska and Leyser 2011; Dun et al. 2012). However, some more recent evidences challenge the direct-action model. The binding of SMXL6 to the promoter of *BRC1* is detected via chromatin immunoprecipitation sequencing (ChIP–seq) assays but not in electrophoretic mobility shift assays (EMSAs), indicating the repression in BRC1 expression may be completed by the cooperation of SMXL6 and other unknown transcription factors(Wang et al. 2020a). In addition, the branch difference in amount is similar between *brc1* and SL mutants,

and *d14;brc1* double mutants display significantly more branches than the single mutants, indicating that BRC1 and other SL-related genes hold partially non-overlapping roles in shoot branching (Chevalier et al. 2014). The canalization model proposes that buds, being auxin sources, can grow into branches only if a canalized auxin transport route to the main stem was formed (Prusinkiewicz et al. 2009). This model is based on the observation that SLs promote removal of PIN1 from the plasma membrane: *rac*-GR24 application leads to a fast reduction of PIN1 levels at the basal plasma membrane of xylem parenchyma cells. Meanwhile, several SL-related mutants show enhanced PIN1 accumulation within the plasma membrane (Bennett et al. 2016; Bennett et al. 2006; Crawford et al. 2010; Shinohara et al. 2013). In addition, the loss of SMXL6, SMXL7 and SMXL8 functions completely represses increased PIN1 accumulation occurring in *max2* mutants. Along these lines, PIN1 levels raise when SMXL7 is stabilized in stems (Liang et al. 2016; Soundappan et al. 2015). As such, SL signaling weakens sink strength by counteracting PIN1 protein accumulation, thus reducing the number of branches and auxin exporting (Prusinkiewicz et al. 2009). Likewise, some of observations contradict this model by showing SLs suppress branching in a manner independent of polar auxin transport (Brewer et al. 2015). Conclusively, it is important to recognize that the direct-action and canalization models are not mutually exclusive. Further research may focus more on mechanistic understanding of the canalization model.

1.4.6.2 Promotion of cambium activity

SL signaling has been reported to promote the thickening of stem by stimulating cambium activity (Agusti et al. 2011). Genetically, reduced cambium cell layers are found in both SL biosynthetic and signaling mutants, and the reduced secondary growth in *max2* mutants is fully rescued by the expression of *MAX2* driven by the cambium-specific *WOX4* promoter (Agusti et al. 2011). In addition, cambium-like cell divisions are stimulated in the *Arabidopsis* stem by local GR24 treatments

(Agusti et al. 2011). Interestingly, BES1 also plays a negative role in cambium activity via direct repression of *WOX4* activity (Hu et al. 2022). The complex roles of SL signaling in secondary growth regulation are further revealed by the observations that both *smxl6;smxl7;smxl8* and *max2;smxl6;smxl7;smxl8* mutants show reduced stem diameter, while expression of a stabilized SMXL7 protein is able to increase stem diameter (Liang et al. 2016). Besides, the expression of the SL signaling related genes *MAX2*, *D14*, *SMXL6*, *SMXL7* and *SMXL8* is strong in vascular tissues in roots, indicating important roles of SL signaling in vascular development (Chevalier et al. 2014; Soundappan et al. 2015; Zhao et al. 2018). Still, the actual roles of the mediators of SL signaling SMXL6, SMXL7 and SMXL8 remain largely obscure in this regard. In this study, I used histological, genetic and single nucleus RNA-sequencing (snRNA-seq) assays to investigate the biological roles SL signaling in secondary growth regulation.

1.4.7 Crosstalk between SL and KAR signaling

Like SLs, KARs are small butenolide compounds, which in this case are present in the smoke of burning plants to trigger germination of fire-following plants, including *Arabidopsis* (Flematti et al. 2004; Nelson et al. 2010). Genetic studies lead to the identification of KAR perception components, which are MAX2 and the α/β-fold hydrolase receptor KARRIKIN INSENSITIVE 2 (KAI2) (Nelson et al. 2011; Waters et al. 2012). Therefore, SLs and KARs are perceived by the paralogous α/β-fold hydrolases D14 and KAI2, respectively. Importabtly, both signal transductions require the F-box protein MAX2. The mediators of KAR signaling are identified via forward genetic screens, belonging to the same SMXL family with the mediators of SL signaling (Stanga et al. 2013; Stanga et al. 2016). In particular, SMAX1 /and SMXL2 function in KAR signaling in controlling seed germination and hypocotyl growth (Soundappan et al. 2015; Stanga et al. 2016; Stanga et al. 2013). SMXL3, SMXL4, and SMXL5 are regulators of phloem formation in a SL or KAR independent manner

(Wallner et al. 2017). As above mentioned, SMXL6, SMXL7, and SMXL8 act as mediators of SL signaling in multiple aspects of plant development processes (Wang et al. 2015; Soundappan et al. 2015). It is therefore normally proposed that SL and KAR signaling are moderated by distinct clades of the SMXL protein family. However, a very recent study demonstrates that SMXL2 functions as a mediator of both SL and KAR signaling in hypocotyl elongation, forming a convergent pathway and being in line with the close crosstalk between SL and KAR transduction pathways (Wang et al. 2020b).

2 Material

2.1 Organism

2.1.1 *Arabidopsis thaliana*

The ecotype Columbia-0 (Col-0) of *Arabidopsis thaliana* (L.) Heynh. was utilized in this work. The used plant lines are listed in table 2.1.

Genotype	Gene locus	Construct	Origin	Reference
smxl6-4 ***smxl7-3*** ***smxl8-1***	AT1G07200 AT2G29970 AT2G40130	*SALK_049115* *WiDsLox339_C04* *SALK_025338C*	David Nelson	Soundappan et al. 2015
smxl6-4 ***smxl7-3*** ***smxl8-1*** ***max2-1***	AT1G07200 AT2G29970 AT2G40130 AT2G42620	*SALK_049115* *WiDsLox339_C04* *SALK_025338C* *Tilling (point mutation)*	David Nelson	Stanga et al. 2013
smxl6-4 ***smxl7-3*** ***smxl8-1*** ***d14-1***	AT1G07200 AT2G29970 AT2G40130 AT3G03990	*SALK_049115* *WiDsLox339_C04* *SALK_025338C* *WiscDsLoxHs137_07E*	Tom Bennett	unpublished
d14-1	AT3G03990	*WiscDsLoxHs137_07E*	David Nelson	Waters et al. 2012
max2-1	AT2G42620	*Tilling (point mutation)*	Ottoline Leyser	Stirnberg et al. 2007
brc1-2	AT3G18550	*SALK_091920*	NASC	Niwa et al. 2013
mp-S319	AT1G19850	*SALK_021319*	NASC	Brackmann et al. 2018
d14-1 ***mp-S319***	AT3G03990 AT1G19850	*WiscDsLoxHs137_07E* *SALK_021319*	This study	unpublished
WT	-	*SMXL6:mTurquoise2-ER* (pJZ18)	This study	unpublished
WT	-	*SMXL7:mTurquoise2-ER* (pJZ24)	This study	unpublished
WT	-	*SMXL8:mTurquoise2-ER* (pKR15)	This study	unpublished
WT	-	*MAX2:mTurquoise2-ER_WOX4:Venus-ER* (pVJ47)	This study	Song et al. 2022

WT	-	*D14:mTurquoise2-ER_WOX4:Venus-ER* (pVJ33)	This study	Song et al. 2022
WT	-	*35S:SMXL6-D2-mVenus_35S:mCherry-NLS* (PJZ27)	This study	Song et al. 2022
WT	-	*PXY:mTurquoise2-ER_SMXL5:Venus-ER* (pVL78)	Greb Group	Shi et al. 2019
d14-1	AT3G03990	*WiscDsLoxHs137_07E PXY:mTurquoise2-ER_SMXL5:Venus-ER* (pVL78)	This study	unpublished
WT	-	*APL:ECFP-ER* (pPS10)	Greb Group	unpublished
d14-1	AT3G03990	*WiscDsLoxHs137_07E APL:ECFP-ER* (pPS10)	Greb Group	unpublished
mp-S319	AT1G19850	*SALK_021319 DR5revV2:YFP (pKB46)*	Greb Group	Brackmann et al. 2018
d14-1 mp-S319	AT3G03990 AT1G19850	*SALK_021319 DR5revV2:YFP (pKB46)*	this study	unpublished
WT	-	*SMXL7:SMXL7^{d53}-Venus*	Tom Bennette	Liang et al. 2016
WT	-	*PXY:GR-LHG4_OP4:mTurqouise2* (pVL45) *OP4:SMXL7^{d53}*-mVenus (pJZ62)	This study	unpublished
smxl6-4 smxl7-3 smxl8-1 d14-1	AT1G07200 AT2G29970 AT2G40130 AT3G03990	*SALK_049115 WiDsLox339_C04 SALK_025338C WiscDsLoxHs137_07E SMXL7:SMXL7:3xHA*	This study	unpublished
WT	-	*PXY:Myc-GR-bdl* (pKB45)	Greb Group	Brackmann et al. 2018
d14-1	AT3G03990	*WiscDsLoxHs137_07E PXY:Myc-GR-bdl* (pKB45)	This study	unpublished
WT	-	*SMXL5:Myc-GR-bdl* (pJQ1)	Greb Group	Brackmann et al. 2018
d14-1	AT3G03990	*WiscDsLoxHs137_07E SMXL5:Myc-GR-bdl* (pJQ1)	This study	unpublished

WT	-	*PXY:GR-MPΔIII/IV* (pKB25)	Greb Group	Brackmann et al. 2018
d14-1	AT3G03990	*WiscDsLoxHs137_07E PXY:GR-MPΔIII/IV* (pKB25)	This study	unpublished
WT	-	*NST3:ER-ECFP-HDEL* (pPS31)	This study	unpublished
d14-1	AT3G03990	*NST3:ER-ECFP-HDEL* (pPS31)	This study	unpublished
WT	-	*CLE41:ER-YFP-HDEL* (pNG4)	This study	unpublished
d14-1	AT3G03990	*CLE41:ER-YFP-HDEL* (pNG4)	This study	unpublished
WT	-	*VND7-ER-mTurqouise2-HDEL* (pJZ35)	This study	unpublished
d14-1	AT3G03990	*VND7-ER-mTurqouise2-HDEL* (pJZ35)	This study	unpublished

Table 2.1: Arabidopsis lines used in this study.

2.1.2 Bacterial strains for this study

2.1.2.1 *Escherichia coli* (*E. coli*)

All the molecular cloning for this study was performed in the DH5α.

2.1.2.2 *Agrobacterium tumefaciens* (Agrobacteria)

The *Agrobacterium tumefaciens* (Agrobacteria) strain C58C1: RifR with pSoup plasmid (TetR) + plasmid (TetR) was used to mediate plant transformation.

2.2 The plasmids for this study

2.2.1 Basic vectors

Name	Description	Resistance for bacteria	Origin	Reference
pGGZ003	GreenGate destination vector	Spectinomycin	Jan Lohmann	Lampropoulos, et al. 2013
pGGM000	Intermediate Module	Kanamycin	Jan Lohmann	Lampropoulos, et al. 2013
pGGN000	Intermediate Module	Kanamycin	Jan Lohmann	Lampropoulos, et al. 2013
pGGG001	F-H short adaptor	-	Jan Lohmann	Lampropoulos, et al. 2013
pGGG002	H-A short adaptor	-	Jan Lohmann	Lampropoulos, et al. 2013
pGGA000	GreenGate entry Module A	Ampicillin	Jan Lohmann	Lampropoulos, et al. 2013
pGGB000	GreenGate entry Module B	Ampicillin	Jan Lohmann	Lampropoulos, et al. 2013
pGGC000	GreenGate entry Module C	Ampicillin	Jan Lohmann	Lampropoulos, et al. 2013
pGGD000	GreenGate entry Module D	Ampicillin	Jan Lohmann	Lampropoulos, et al. 2013
pGGE000	GreenGate entry Module E	Ampicillin	Jan Lohmann	Lampropoulos, et al. 2013
pGGF000	GreenGate entry Module F	Ampicillin	Jan Lohmann	Lampropoulos, et al. 2013

Table 2.2: Vectors used in this study.

2.2.2 Constructs specially generated for this study

The constructs generated in this work were cloned by GreenGate cloning using the GreenGate modules *pGGA000-pGGF000* and the destination vector *pGGZ000* (Lampropoulos et al. 2013). Some constructs named with '*pKR*' were generated by Konrad Reichel (rotation student at the Greb lab) and are listed in the Greb lab database. Most of the constructs were based on plasmids from Vadir López-Salmerón (*pVL*).

Name	Vector	Aim for	Description	Reference
pJZ12	*pGGE000*	*SMXL6 terminator*	Cloning of *pJZ18*	unpublished
pJZ13	*PGGA000*	*SMXL6 promoter*	Cloning of *pJZ18*	unpublished
pJZ18	*PGGZ003*	*SMXL6:mTurquoise2-ER* (GreenGate reaction with pVL11, pVL56, pJZ12, pVL71, pVL67, pVL63, pJZ13)	Transformation into WT	unpublished
pJZ22	*PGGA000*	*SMXL7 promoter*	Cloning of *pJZ24*	unpublished
pJZ23	*pGGE000*	*SMXL7 terminator*	Cloning of *pJZ24*	unpublished
pJZ24	*pGGZ000*	*SMXL7:mTurquoise2-ER* (GreenGate reaction with pVL11, pVL56, pJZ22, pVL71, pVL67, pVL63, pJZ23)	Transformation into WT	unpublished
pKR13	*PGGA000*	*SMXL8 promoter*	Cloning of *pKR15*	unpublished
pKR14	*pGGE000*	*SMXL8 terminator*	Clonging of *pKR15*	unpublished
pKR15	*pGGZ000*	*SMXL8:mTurquoise2-ER* (GreenGate reaction with pVL11, pVL56, pKR13, pVL71, pVL67, pVL63, pKR14)	Transformation into WT	unpublished
pKR07	*pGGC000*	*SMXL7 CDS* (Amplified from pEW71 with primers SMXL7_ModuleC_fwd and SMXL7_ModuleC_rev)	Cloning of SMXL7 CDS	unpublished
pJZ60	*pGGC000*	*Mutagenesis of SMXL7* (pKR07 as template)	Clonging of SMXL7^{d53}	unpublished
pJZ61	*pGGZ000*	*SMXL7:SMXL7^{d53}-GR* (GreenGate reaction with pVL11, pVL56, pJZ22, pJZ23, pVL82, pJZ60, pVL50)	Transformation into WT	unpublished
pJZ62	*pGGZ000*	*OP6:SMXL7^{d53}* (GreenGate reaction with pVL11, pVL56, pVL95, pVL54, pVL51, pJZ60, pVL50)	Transformation into Dex driver line *PXY:GR-LhG4*	unpubllished

pJZ63	*pGGZ003*	*SMXL7:SMXL7^{d53}-3xHA* (GreenGate reaction with pVL11, pVL56, pJZ22, pJZ23, pGGD014, pJZ60, pVL50)	Transformation into WT	unpublished
pJZ25	*pGGC000*	*SMXL6-D2* in pGGC	Cloning of truncated SMXL6	Song et al. 2022
pJZ26	*pGGM000*	*35S:SMXL6-D2-mVenus in pGGM000* (GreenGate reaction with pDS34, pVL50, pJZ25, pGGD-mVenus, pVL66, pVL01, pVL34)	Cloning the first cassette of the SL sensor	Song et al. 2022
pJZ27	*pGGZ000*	*35S:SMXL6-D2-mVenus_35S-mCherry-NLS* (GreenGate reaction with pVL11, PJZ26, pCS7)	Transformation into WT	Song et al. 2022
pJZ35	*pGGZ000*	*VND7-ER-mTurqouise2-HDEL* (GreenGate reaction with pVL11, pVL56, pVL21, pVL71, pVL67, pVL63, pVL23)	Transformation into *d14*	unpubllished

Table 2.3: Constructs specially generated for this study.

2.3 Primers used in this study

In this study, the primers used for cloning were designed by adding *Eco31I* recognition sites and module specific overhang in the 5' ends of forward and reverse primers.

	Aim for	Primer name	Sequence (5' → 3')
genotyping	*brc1-2*	*SALK_091920-LP*	TGTAGAACAACCCACTGAGCC
		SALK_091920-RP	ATCGATGGTGGTGCATTAGTG
	smxl6-4	*SALK_050363-LP*	AGCCAGAGAAAGACTCGAACC
		SALK_050363-RP	TCCGAAATTAAGCTCGATGTG
	smxl7-3	*WiscDsLox339C04_LP*	GATCAAGAAACGAACGCTGAG
		WIscDsLox339C04_RP	CGTATTAGCCTCTCGGATTCC
	smxl8-1	*SALK_025338_LP*	GAATCACAAATTCTGCATGGC

		SALK_025338_RP	CTGACGAAGCTCCACTTTCAC
	d14-1	*WiscDsLoxHs137_07E_LP*	AAGAATATGGCAAGTGCAAC
		WiscDsLoxHs137_07E_RP	GATGATTCCGATCATAGCG
	mpS319	*SALK_021319_LP*	TCTTCCTTCCAGTCTCTTGCC
		SALK_021319_RP	TTAAGATCGTTAATGCCTGCG
	max2-1	*max2-1_dCAPSfor*	TGTCCGAATTTGGAAGAGATTAG G
		max2-1_dCAPSrev	CAAGAAGAATCTTTCCCATAAAC TCGAAT
Cloning	*SMXL6-D2*	*SMXL6-D2_F*	AACAGGTCTCAGGCTCA ATGCAGAAAGATTTCAAGTCTC
		SMXL6-D2_R	AACAGGTCTCACTGA CCATATCACATCCACCTTCGCC
	pJZ12	*SMXL6terminator_F*	AACAGGTCTCACTGCC ATGCATATATATAAATGAGGTAAT AAT
		SMXL6terminator-R	AACAGGTCTCATAGTCATTCAAA ACAAGAT ATGAACATC
	pJZ13	*SMXL6promoter_F*	AACAGGTCTCAACCT CTTCTGAAACTTAGGGTTTTTCG
		SMXL6promoter_R	AACAGGTCTCATGTTCGCCGGC AAAAAAAAAGTC
	PJZ22	*SMXL7promoter_F*	*AACAGGTCTCAACCT TGTGACAGTTTGGATTTGTTGAG*
		SMXL7promoter_R	AACAGGTCTCATGTT CGTCGCCGGTTTAGTTA
	pJZ23	*SMXL7terminator-F*	AACAGGTCTCACTGCTTATTGTT GTTGTAATTTTATG
		SMXL7terminator-R	AACAGGTCTCATAGTATGGAGGT AATGCAAATCCTC
	pKR13	*SMXL8promoter_F*	AACAGGTCTCAACCTTTCAAGG AACTCCGACGAC
		SMXL8promoter_R	AACAGGTCTCATGTTCGCCGAC GACCATATATAAC
	pKR14	*SMXL8terminator_F*	AACAGGTCTCACTGCGTTAAAG AGAACTTTATATGGA
		SMXL8terminator_R	AACAGGTCTCATAGTCTAACACA TCCTCTAACTATC
	pKR07	*SMXL7_ModuleC_fwd*	AACAGGTCTCAGGCTCAATGCC GACACCAGTAACCAC
		SMXL7_ModuleC_rev	AACAGGTCTCACTGAGA TCACTTCGACTCTCGCCGGA

Mutagenesis	*pJZ60*	*SMXL7^{d53}-F*	CTTGACGATAGATTCACAGATTACATTGCTGGC
		SMXL7^{d53}-R	GCCAGCAATGTAATCTGTGAATCTATCGTCAAG

Table 2.4: Primers used in this study

2.4 Dyes

Direct Red 23 #212490 (Sigma-Aldrich, St. Louis, USA)

Toluidine blue #52040 (AppliChem, Darmstadt, Germany)

Calcofluor white #18909 (Sigma-Aldrich, St. Louis, USA)

Ethidium bromide solution 0,025 % (Roth, Karlsruhe, Germany)

2.5 GR24^{4DO}

The strigolactone-analogue GR24^{4DO} was ordered from StrigoLab (Torino, Italy), and 10 mM GR24^{4DO} stock solution dissolved in acetone was stored at -20°C.

2.6 Media, buffers and solutions

Murashige and Skoog (MS)-medium (1000 ml)

4.3 g Murashinge-Skoog salt

10 g Sucrose

0.5 g MES hydrat

8 g Phyto Agar

pH 5.7, autoclaved

Half-strength

Murashige and Skoog (MS)-medium (1000 ml)

2.15 g Murashinge-Skoog salt

10 g Sucrose

0.5 g MES hydrat

8 g Phyto Agar

pH 5.7, autoclaved

Genomic DNA extraction buffer (Edward's extraction buffer) (10 ml)

200 mM Tris HCl (pH8.0)

250 mM NaCl

0.5% SDS

25 mM EDTA

Nucleus isolation buffer (10 ml)

2.5 ml Nuclei Isolation Buffer 4X (NIB)

(# CELLYTPN1, Sigma-Aldrich, St. Louis, USA)

7.5 ml Nuclease free water (#AM9937, Thermo-Scientific, Waltham, USA)

100 µl Hoechst 33342 (1mg/ml, #B2261-25MG, Sigma-Aldrich, St. Louis, USA)

NIB RI (1.5 ml)

1.5 ml Nuclei isolation buffer

20 µl RiboLock RNase Inhibitor (40 U/µL, #EO0382, Thermo-Scientific, Waltham, USA)

10x Sorting Buffer (for 50,000 nuclei)

10 µl PBS Corning (#21-040-CV, Corning)

5 µl UltraPure™ BSA (50 mg/ml) (#AM2616, Thermo-Scientific, Waltham, USA)

6 µl Ambion™ RNase Inhibitor, 40 U/µL (#AM2682, Thermo-Scientific, Waltham, USA)

12 µl SUPERase In™ RNase Inhibitor (20 U/µl) (#2694, Thermo-Scientific, Waltham, USA)

Infiltration medium (plant transformation)

5 % Sucrose

0.02 % Silwet L-77

Seed sterilization

70 % ethanol

0.2 % Tween 20

1x Phosphate buffered saline (PBS)

1 tablet dissolved in 200 ml ddH2O (#P4417, Sigma-Aldrich, St. Louis, USA)

4 % PFA (50 ml)

2 g of Paraformaldehyde dissolved in 1X PBS by heating in a 60°C water bath (JB series)

25 mM Dexamethasone stock (15 ml)

147 mg Dex (D4902-500MG, Sigma-Aldrich, St. Louis, USA) dissolved in 15 ml DMSO

2.7 Kits

Wizard® SV Gel and PCR Clean-Up System (Promega, Madison, USA)

Click-iT® Plus EdU Imaging Kits (Thermo-Scientific, Waltham, USA)

QuickChange Site-Directed Mutagenesis Kit (Agilent, Santa Clara, USA)

T4 DNA Ligase (Thermo-Scientific, Waltham, USA)

RevertAid First Strand cDNA Synthesis Kit (Thermo-Scientific, Waltham, USA)

JumpStartTMREDTaq® ReadyMixTM (Sigma-Aldrich, St. Louis, USA)

Phusion High-Fidelity DNA Polymerase (2 U/µL) (Thermo-Scientific, Waltham, USA)

QIAprep Spin Miniprep Kit (QIAGEN, Venlo, Netherlands)

2.8 ImageJ macros

The image processing in this study was based on the ImageJ 1.53c version.

2.8.1 Toluidine blue staining vessel selection

Macros for selecting vessel cells based on colour deconvolution and shape circularity.

```
run("Stack to RGB");
rename("countvessels");
waitForUser("Pause", "please select ROI");
run("Crop");
run("Colour Deconvolution", "vectors=[Alcian blue & H]");
selectWindow("Colour Deconvolution");
close();
selectWindow("countvessels-(Colour_3)");
close();
run("Calculator Plus", "i1=[countvessels-(Colour_1)] i2=[countvessels-(Colour_2)] operation=[Divide: i2 = (i1/i2) x k1 + k2] k1=20 k2=0");
selectWindow("countvessels-(Colour_1)");
close();
selectWindow("countvessels-(Colour_2)");
setAutoThreshold("Default dark");
setOption("BlackBackground", true);
run("Convert to Mask");
run("Gray Morphology", "radius=1.5 type=circle show operator=close");
selectWindow("countvessels-(Colour_2)");
setOption("BlackBackground", false);
run("Make Binary");
run("Invert");
run("Set Measurements...", "area mean min limit display redirect=[countvessels-(Colour_2)] decimal=3");
run("Analyze Particles...", "size=800-18000 show=Outlines display exclude circularity=0.3-1.00 add");
selectWindow("countvessels");
waitForUser("Pause", "Check and Save");
run("Close All");
```

2.8.2 Selection of vessel visualized under UV excitation

Macros for selecting vessel cells based on grey value and shape circularity.

```
run("Duplicate...", "title=copy duplicate");
selectWindow("copy")
run("Z Project...", "projection=[Max Intensity]");
run("Split Channels");
selectWindow("C2-MAX_copy");
close();
selectWindow("C1-MAX_copy");
run("Duplicate...", "title=copy1 duplicate");
```

```
selectWindow("C1-MAX_copy");
setAutoThreshold("Default");
setThreshold(0, 40);
setOption("BlackBackground", true);
run("Convert to Mask");
selectWindow("C1-MAX_copy");
setOption("BlackBackground", false);
run("Make Binary");
run("Invert");
run("Set Measurements...", "area mean min limit display redirect=C1-MAX_copy decimal=3");
waitForUser("Pause", "please select ROI");
run("Analyze Particles...", "size=2-100 show=Outlines display exclude circularity=0.3-1.00 add");
waitForUser("Pause", "Check and Save");
```

2.9 Technical equipment

Confocal microscope TCS SP8 (Leica, Mannheim, Germany)

Stereomicroscope (Nikon, Tokyo, Japan)

Microtome RM2235 (Leica Microsystems, Mannheim, Germany)

Leica ASP 200S (Leica Microsystems, Mannheim, Germany)

Pannoramic SCAN II (3DHistech, Budapest, Hungary)

Precision balance (Kern & Sohn, Balingen, Germany)

Nanodrop ND-1000 (Nanodrop, Wilmington, USA)

Basic pH meter PB-11 (Sartorius, Göttingen, Germany)

Ice machine (Ziegra Eismaschinen, Isernhagen, Germany)

2.10 Software

CLC Main Workbench 7.6.1 (CLC Bio Qiagen, Aarhus, Denmark)

ImageJ 1.53c (National Institute of Health, Bethesda, USA)

Adobe Illustrator CS6 (Adobe, San Jose, USA)

R (https://cran.r-project.org/)

R Studio (https://www.rstudio.com/)

CaseViewer 2.2 (3DHistech, Budapest, Hungary)

3 Methods

3.1 Plant material and growth conditions

Arabidopsis thaliana (L.) Heynh. accession Col-0 plants were used as a genetic background. The *max2-1* mutant (Stirnberg et al. 2002), *d14-1* mutant (Waters et al. 2012) (in this study was mentioned as *d14*), triple mutant *smxl6-4;smxl7-3;smxl8-1* (Soundappan et al. 2015), *brc1-2* (Niwa et al. 2013), *mp-S319* (Brackmann et al. 2018), and transgenic line *SMXL7:SMXL7^{d53}-Venus* (Liang et al. 2016), *PXY:Myc-GR-bdl*, *SMXL5:Myc-GR-bdl,* and *PXY:GR-MPΔIII/IV* (Brackmann et al. 2018) have been described previously. The quadruple mutant *d14;smxl6-4;smxl7-3;smxl8-1* was obtained from Tom Bennett (University of Leeds, UK). The double mutant *d14;mp-S319* was generated by crossing homozygous *d14-1* and heterozygous *mpS319*+/- plants. The F2 progenies were genotyped to find heterozygous *mpS319*+/- among *d14-1* homozygous plants. The seeds of *d14;mp-S319+/-* were harvested and sown to obtain *d14;mp-S319* double mutants. *Arabidopsis* seeds were surface sterilized with 70% ethanol containing 0.02% Tween-20, stratified at 4°C for 2-3 days in the dark, sown on half-strength MS medium solidified with 0.8% agar if not mentioned otherwise, and then transferred to growth chambers under short day conditions with10 h light and

14 h dark (65% humidity at 22°C). For morphological observations and reporter activities analyses, 5-day-old seedlings were transferred to pots filled with 4:1 mixture of soil and vermiculite. After 21 days, plants were transferred to long day conditions with16 h light and 8 h dark,at 22°C with 65% humidity, if not mentioned otherwise.

3.2 Tissue staining and microscopy

3.2.1 Direct Red 23 staining

Harvested hypocotyls were embedded in 5 % low melting agarose, and then sectioned by razor blades (Wilkinson basic). The hand sectioned hypocotyls were counterstained with 0.1% (w/v) solution of Direct Red 23 (#212490, Sigma-Aldrich, St. Louis, USA) dissolved in PBS for at least 5 min, washed twice with PBS, and put into a 2-well glass-bottom dish (#80287, ibidi, Gräfelfing Germany) for analysis by confocal microscopy.

3.2.2 Calcofluor White staining

Harvested hypocotyls were immediately put in 4 % PFA solution, and stored overnight at 4°C. The fixed hypocotyls were embedded in 5% low melting agarose, and then sectioned by razor blades (Wilkinson basic). Subsequently, the sections were stained with 0.1% Calcofluor White dissolved in PBS for 5 min. Afterwards, sections were washed twice with PBS, analyzed by confocal microscopy and put into a 2-well glass-bottom dish (#80287, ibidi, Gräfelfing Germany).

3.2.3 Basic Fuchsin staining

To observe the xylem strands in roots, 5 DAG seedlings were stained and fixed in 0.2 % (m/v) Basic Fuchsin dissolved in ClearSee (10 % xylitol, 15% sodium

deoxycholate, and 25 % UREA) solution overnight. Next the fuchsin solution was removed and samples were washed once with ClearSee for 30 min. Subsequently, seedlings were stored in ClearSee solution and analysed using a microscope.

3.2.4 Microscopy

Images were taken by a Leica TCS SP8 confocal microscope (Leica Microsystems, Mannheim, Germany) with a water immersion 20x objective lens. 458 nm, 514 nm and 561 nm lasers were used to excite, mTurquoise2 (CFP), YFP (mVenus), and mCherry/Direct Red/ Basic Fuchsin, and emissions were detected at 465-509 nm, and 524-540 nm and 571-630 nm, respectively. Hoechst 33342 and Calcofluor White, together with lignin in differentiated xylem vessels were visualized using a 405 nm laser, and the emission was collected at 410-450 nm.

3.3 Histological analysis

The harvested hypocotyls from 5-week-old (3 week SD+2 week LD) plants were infiltrated in 70 % ethanol for at least 3 days at 4°C before being processed by the Leica ASP200 S processor (Leica Microsystems, Mannheim, Germany). After embedding in paraffin, the microtome RM2235 (Leica Microsystems, Mannheim, Germany) was used to produce 10-µm thick sections. Dry sections were deparaffinized, stained with 0.05 % toluidine blue (#52040, AppliChem, Darmstadt, Germany) and fixed by Micromount Mounting Media (Leica) in microscope slides (Thermo Scientific; Wal-tham, USA). Slides were scanned using Pannoramic SCAN II scanner (3DHistech, Budapest, Hungary) and analysed by the CaseViewer 2.2 software (3DHistech, Budapest, Hungary). Detailed processing steps were described as follows:

3.3.1 Fixation and dehydration, embedding, cutting, and floating

The harvested hypocotyls from 5-week-old (3 week SD+2 week LD) or 15-20 cm-bolting plants were infiltrated by 70% ethanol for at least 3 days before being processed by the Leica ASP200S infiltrator (Leica Microsystems, Mannheim, Germany) with the following steps:

Hypocotyls were sunk in FAA solution for 15 min.

Hypocotyls were put in the Leica ASP200s processor, followed by a fixation program showed below:

4 hr	FAA fix	1 hr	Xylene
1 hr	70% Ethanol	1 hr	Xylene
1 hr	90% Ethanol	1 hr and 15 min	Xylene
1 hr	90% Ethanol	1 hr	Wax I
1 hr	99.8% Ethanol+Eosin	1 hr	Wax II
1 hr	99.8% Ethanol	3 hr	Wax III
1 hr	Absolute Ethanol		

Samples were embedded

Embedded samples were dissected with microtome in 10 μm section thickness.

3.3.2 Toluidine blue staining

10 min	Histoclear	1 min	H2O
10 min	Histoclear	5 min	Toluidine Blue (50 mg in 100 ml water)
1 min	Absolute Ethanol	30 S	H2O
1 min	Absolute Ethanol	30 S	H2O
1 min	95% Ethanol	30 S	85% Ethanol

1 min	85% Ethanol	30 S	95% Ethanol
1 min	50% Ethanol	30 S	Absolute Ethanol
1 min	30% Ethanol	30 S	Absolute Ethanol
1 min	H2O		

Micromount Mounting Media (Leica) were added to the slide and cover it with a 20*54 cm coverslip.

Slide were scanned with scanner Pannoramic SCAN II (3DHistech, Budapest, Hungary).

Images are analysed using the software CaseViewer 2.2 (3DHistech, Budapest, Hungary) and ImageJ 1.53c.

3.4 Pharmacological treatment and experimental conditions

3.4.1 Dexamethasone treatment:

a) *PXY:GR-MP*∆ and *PXY:Myc-GR-bdl* transgenic lines. Stock solution of 25 mM Dex was dissolved in DMSO, and the 15 µM work solution was freshly prepared by diluting stock solution with tap water. Control treatments contained an equivalent amount of solvent. Plants were initially grown in SD conditions for 3 weeks without treatment, and then transferred to LD conditions. For a) *PXY:GR-MP*∆ and *PXY:Myc-GR-bdl* transgenic lines, treatment immediately started when plants were grown in LD conditions by watering with either 15 µM Dex or mock solution for 50 ml per pot. The treatment lasted for 2 weeks and in total 3 treatments were conducted before plants were harvested. For b) *SMXL5:Myc-GR-bdl* transgenic lines, the treatment started 4-weeks after germination by watering with either 15 µM Dex or mock solution for 50 ml per pot. This treatment continued until the plants' bolt length was around 15 cm. All the pots were put on petri dishes (with lids removed) (92 mm x 16 mm, SARSTEDT).

3.4.2 GR24^{4DO} application

GR24^{4DO} (10 µM) was prepared by 1000x dilution of a stock solution (10 mM GR24^{4DO} dissolved in acetone). Seedlings were initially grown in MS medium plates for two weeks (SD conditions) without treatment, subsequently transferred to plastic containers (PP-BECHER) supplemented either with 10 µM GR24^{4DO} or mock solution (contained an equivalent amount of acetone), grown for another two weeks (1 week SD + 1 week LD) and harvested for histological analyses.

3.5 EdU incorporation assay

Stock solution of 10 mM EdU supplemented in DMSO was freshly prepared. After 100 times dilution with tap water, the EdU working solution was ready to use. To improve the EdU incorporation efficiency, I stopped watering the plants around one week before EdU treatment (plants were healthy without obvious drought stress). The plants were treated by directly watering with 50 ml EdU solution from the top of each pot. After 3 days incorporation, the hypocotyls were harvested and fixed in 4 % (m/v) PFA overnight at 4°C. The next day, fixed hypocotyls were washed once with PBS, subsequently embedded in 5 % low melting agarose (#A4018, Sigma-Aldrich, St. Louis, USA), and sectioned with razor blades (Wilkinson, basic). The sections were kept in a Corning Costar 24 cell culture plate (Corning, CLS3527) and were ready for staining. The staining procedure was according to the protocols provided by Click-iT Plus EdU Imaging Kits (Thermo Fisher, C10639) with minor modifications. The detailed staining steps were performed as follows:

Sections were washed in each well twice with 500 µl of 3 % BSA dissolved in PBS.

Sections were incubated for 20 min with 1 ml of 0.5 % Triton X-100 solution supplemented in PBS at room temperature.

The Click-iT Plus reaction cocktail (within 15 min before using) was prepared with the following components (for 5 ml system, and can be adjusted with the same ratios for each component):

a. 2.25 ml reaction buffer

b. 50 µl Copper protectant

c. 6 µl Alexa Fluor picolyl azaide

d. 250 ml reaction buffer addictive

Triton X-100 solution in step 2 was removed, and the sections were washed in each well with 0.5 ml of 3% BSA in PBS.

The sections were incubated with 0.5 ml of reaction cocktail for another 30 mins protected from light. Gentle agitation is recommended to distribute the reaction cocktail evenly.

The reaction cocktail was removed and the sections were washed with 3% BSA in PBS.

Sections were washed with PBS.

500 µl, 10 µg/ml of Hoechst 33342 was added to each well, and the sections were incubated for 30 min. Subsequently, the sections were washed with PBS twice and ready for microscopy.

3.6 Generation of plasmids and transgenic lines

The generation of *pKB45*, *pKB46*, *pKB25*, *pJQ1*, *pVL78*, *pVJ33* as well as *pVJ47* was described previously (Brackmann et al. 2018; Song et al. 2022). *SMXL6:ER-mTurquoise2* (*pJZ18*), *SMXL7:ER-mTurqoise* (*pJZ24*), *SMXL8:ER-mTurquoise2* (*pKR15*), *OP4:SMXL7-d53* (*pJZ62*), *VND7-ER-mTurqouise2-HDEL* (*pJZ35*), as well as *SMXL7:SMXL7-3xHA* (*pJZ54*) constructs were generated based on GreenGate cloning system (Lampropaulos et al. 2013). And primers used for amplifying the target fragments, the entry modules, as well as destination modules are listed in supplemental Table 2.3 and 2.4. All these constructs were introduced into the *Agrobacterium tumefaciens* strain C58C1 (Rif, together with TetR for pSoup plasmid) and transformed into *Arabidopsis thaliana*.

3.7 RNA extraction from hypocotyls

Hypocotyls of 4-week-old plants were harvested. The hypocotyls were frozen in liquid nitrogen and pulverized in a mortar by a pestle. The RNA extraction was conducted following the introductions of RNeasy Mini Kit (Mallory and Vaucheret 2010). The RNA concentration was measured by a NanoDrop ND-1000 (Thermo Scientific; Wal-tham, USA). DNase was used to treat extracted RNA to remove genomic DNA contamination by referring to the protocol of TURBO DNA-free™ Kit (Thermo Scientific; Wal-tham, USA). The cDNA synthesis was conducted according to the instructions of the Thermo Revert Aid Kit (Thermo Scientific; Waltham, USA).

3.8 Sample preparation for nucleus sorting

Plants were grown in a large culture vessel (#C1958, SteriCon™ 4, Bayswater, Australia) and incubated in a growth cabinet (poly klima, PK 520-LED, Freising, Germany) for 19 days under SD condition before harvesting. The whole hypocotyl was harvested and collected in a petri dish using a razor blade (Classic, Wilkinson). Around 200 hypocotyls were collected and the whole process was conducted on ice. Subsequently, the harvested hypocotyls were chopped into small pieces by a razor blade (Classic, Wilkinson) for several minutes after rinsing with 1.2 ml NIB-RI buffer. The 50 µm filters (#04-004-2327, CellTrics, Wolflabs, York, UK) were pre-wetted and cell-strainer cap incorporated with 35 µm nylon mesh (#352235, Corning, Arizona, USA) by using 500 µl NIB buffer, respectively. The chopped pieces were then filtered into a LoBind tube (#EP0030108132-100EA, Sigma-Aldrich, St. Louis, USA) with a pre-wetted 50 µm filter. Afterwards, filtered samples were transferred through the pre-wetted cell-strainer cap into a round bottom tube (#352235, Corning, Arizona, USA). Cell sorting was conducted at the Flow Cytometry & FACS Core Facility (FFCF), ZMBH, at the University of Heidelberg. For each sample, 50,000 nuclei were sorted and collected in a LoBind tube (#EP0030108132-100EA, Sigma-Aldrich, St. Louis, USA) containing 33 µl sorting buffer. The sorted nuclei were immediately brought to the Deep

Sequencing Core Facility at the University of Heidelberg for library construction and 10x Genomics snRNA-seq.

3.9 snRNA-seq analysis

3.9.1 Pre-processing of raw snRNA-seq data

Raw files of snRNA-seq data were processed by Dr. Changzheng Song using Cell Ranger 6.0.1 (10x Genomics). Aligner STAR (STAR-2.7.8a) was used to align the reads in the samples to the TAIR10 reference genome and more than 96% of reads in all the samples were aligned. The ratio of the number of fraction reads in cells to total number of reads for wild type and *d14* were 27.8% and 31.8%, respectively. The detailed Cell Ranger reports were shown in Table 3.1.

Sample ID	**WT**	***d14***
Depth (Number of Reads)	220 M	272 M
Cell Ranger V6.1.1 Raw Cells	3,770	4,085
Mean Reads per Cell	58,531	66,731
Median Genes per Cell	638	657
Valid Barcodes	87.10%	84.70%
Sequencing Saturation	85.80%	87.40%
Fraction Reads in Cells	27.80%	31.80%
Reads Mapped to Genome	97.00%	96.90%
Reads Mapped Confidently to Intergenic Regions	4.20%	4.50%
Reads Mapped Confidently to Intronic Regions	3.80%	4.00%
Cell Ranger Version	6.1.1	6.1.1

Table 3.1: Cell Ranger reports of WT and *d14* samples.

3.9.2 Data integration and clustering

The clustering analysis was performed using Seurat package. Quality control was performed on wild type and *d14* samples separately. The low-quality cells and genes were filtered as follows: a. the cells with a total number of molecules detected above 15,000 and below 1500 were filtered out; b. the cells with more than 20% percent mitochondrial genes were excluded. Afterward, data from wild type and *d14* samples were merged. Clusters were visualized by performing Uniform Manifold Approximation and Projection (UMAP) analysis. The visualization of expression profiles of interested genes was conducted using R by FeaturePlot and VlnPlot

3.10 Accession Numbers

The genes accession numbers used in this study are as follows: *D14* (AT3G03990), *MAX2* (AT2G42620), *SMXL6* (AT1G07200), *SMXL7* (AT2G29970), *SMXL8* (AT2G40130), *BRC1* (AT3G18550), *MP* (AT1G19850), *BDL* (AT1G04550), *KAI2* (AT4G37470).

3.11 Statistical analyses

Statistical analyses were performed using R version 3.5.1 (https://www.r-project.org/). The statistical differences of nuclei abundance for each cluster in a combined dataset with wild type and *d14*.were determined by Fisher's exact test. Other statistically different groups were either determined by a One-way ANOVA or Two-way ANOVA with a confidence interval (CI) of 95 %, followed by post-hoc Tukey HSD test and post-hoc Bonferroni, respectively. Plots were generated using ggplot2 package or Excel (Microsoft, Redmond, USA). Boxplots show median (centre line), mean (blank diomond) first quartile (lower hinge), third quartile (upper hinge). Whiskers show the maximum or minimum.

3.12 Figure creation

Adobe Illustrator CS6 was used to assemble all data shown in this study into figures (Adobe, San Jose, USA). Adobe Photoshop CS6 (Adobe®, San Jose, USA) was used to generate schemes illustrated in Figures 1.1.

4 Results

4.1 The role of SL signaling during xylem phase I

SL signaling in *Arabidopsis* fulfils different regulatory roles in late developmental processes, such as branching and cambium activity in stem (Soundappan et al. 2015; Agusti et al. 2011). Inhibition of shoot branching is among the best-understood biological roles of SL signaling in angiosperms, and branches were generated and connected to the main stem mainly via vascular tissues. This prompted us to explore whether SL signaling exerts more roles in vascular development by investigating secondary growth in the hypocotyl. However, once all cell types are present in the vascular tissues, secondary growth already starts. To elucidate the roles of SL signaling in the whole secondary growth process, I first determined the SL signaling distribution and mutant phenotypes at early developmental stage.

4.1.1 SL signaling is highly associated with differentiated vascular tissues

I first examined the expression pattern of SL signaling related genes using transgenic lines expressing ER-localized mTurquoise2 fluorescent proteins under the control of the respective native promoters. The promoters were chosen based on an earlier study with around 3000 base pair in length (Soundappan et al. 2015). As a result, *SMXL6:mTurquoise2-ER* activity was preferentially observed in the phloem, periderm, and at lower levels in xylem parenchyma (Figure 4.1 A), whereas promoter activities of *SMXL7* and *SMXL8* genes both were detected in xylem parenchyma cells and phloem poles (Figure 4.1 B and C). *D14:mTurquoise2-ER* activity was mostly found in xylem parenchyma (Figure 4.1 D), and with lower intensity in the phloem area. In comparison, the activity of the *MAX2* reporter was detected broadly and with high intensity in the stele (Figure 4.1 E). As can be seen in Figure 4.1 B', D' and E', the promoter activities of *SMXL7*, *D14* and *MAX2* were also be active in

developing vessel cells. Collectively, these observations argued for SL signaling being active in differentiated vascular tissues.

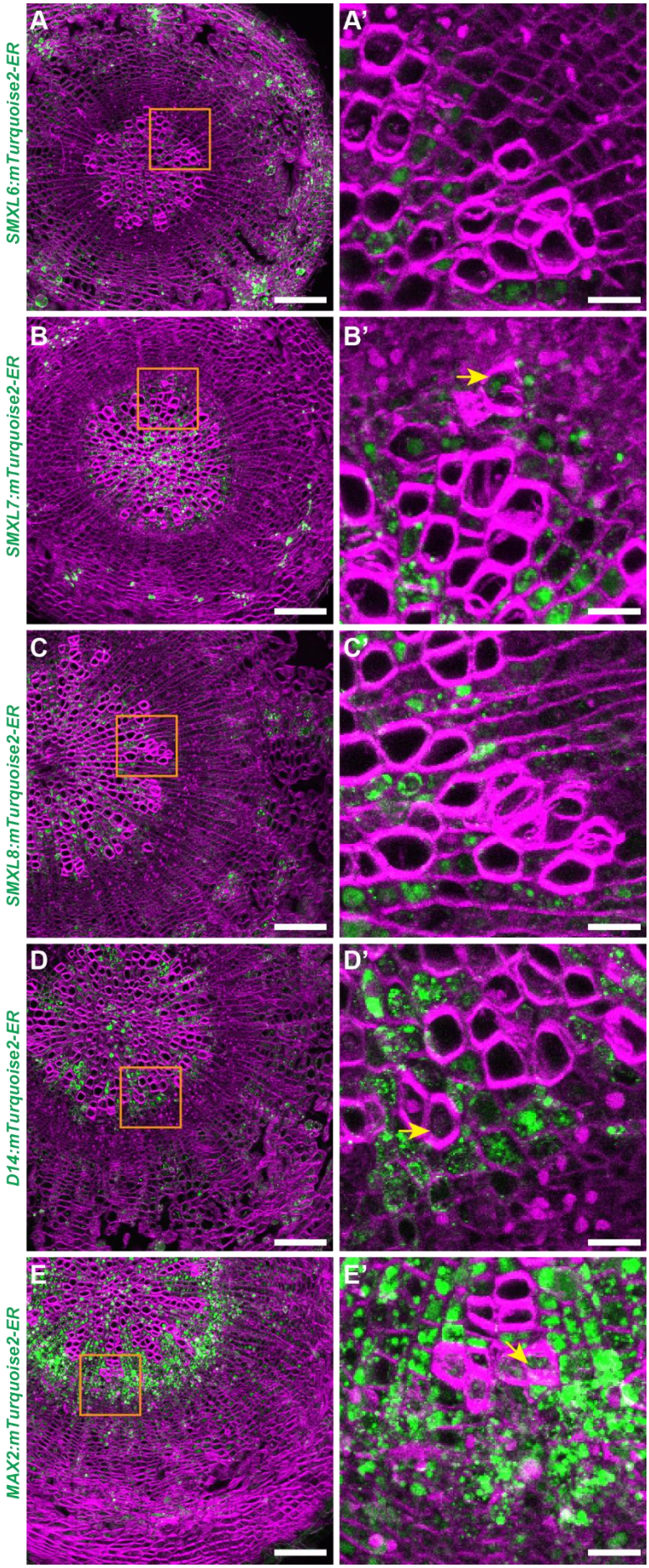
A
A'
SMXL6:mTurquoise2-ER
B
B'
SMXL7:mTurquoise2-ER
C
C'
SMXL8:mTurquoise2-ER
D
D'
D14:mTurquoise2-ER
E
E'
MAX2:mTurquoise2-ER

Figure 4.1: The expression of SL signaling related genes are more active in differentiated vascular tissues

A-E Hypocotyl cross-sections of 4-week-old transgenic plants carrying *SMXL6:mTurquoise2-ER*, *SMXL7:mTurquoise2-ER*, *SMXL8:mTurquoise2-ER*, *D14:mTurquoise2-ER*, and *MAX2:mTurquoise2-ER* constructs. mTurquoise2 signals were shown in green. Cell walls were stained with Direct Red 23 (in Magenta). Scale bars represent 100 µm in (A-E).

A'-E' Magnification of expression region marked by orange squared frame in (A-E). Yellow arrows indicate developing vessel elements. Scale bars represent 20 µm in (A'-E').

In parallel, I analyzed the activity of SL signaling in the hypocotyl via the ratiometric Strigo-D2 sensor (*35S:SMXL6-D2-mVenus_35S:mCherry-NLS*), which was characterized in several genetic backgrounds before and reveals the level of SL signaling in *Arabidopsis* (Song et al. 2022). Consistent with the analysis of the promoter activities of genes associated with SL signaling, high SL signaling levels were detected in xylem parenchyma and phloem regions, which was indicated by the low mVenus to mCherry ratio (Figure 4.2 A-E and F). In comparison, SL signaling activity was relatively low in the cambium zone supported by the high mVenus/mCherry value (Figure 4.2 A-E and F). Strikingly, a comparable high mVenus/mCherry ratio was observed in developing vessel elements (Figure 4.2 E-F and E'), demonstrating that SLs signaling in this cell type is low. Collectively, levels of SL signaling were relatively high in most differentiated vascular tissues, but low in cambium cells and in developing vessel elements.

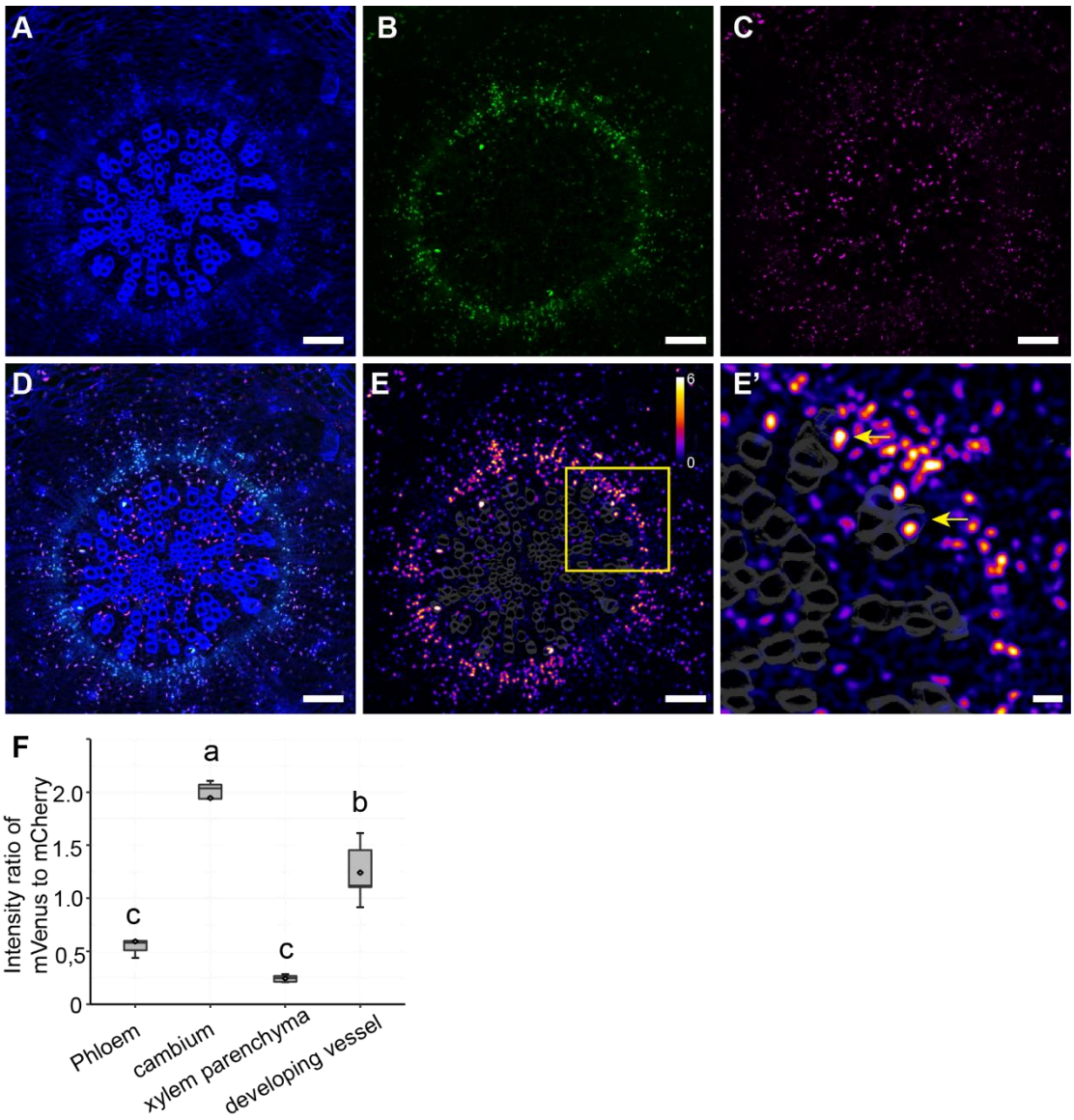

Figure 4.2: SL signaling level is high in differentiated cells but low in developing vessels

A-E Hand sectioned 5-week-old hypocotyl cross-sections of plants expressing *35S:SMXL6-D2-mVenus_35S:mCherry-NLS.* Hoechst33342 and Calcofluor white were used to stain nuclei and cell wall, respectively, which were shown in blue (A). mVenus signals were depicted in green (B) and mCherry signals were depicted in red (C). Merged channels of bule, green and magenta were shown in (D). False colour of merged channels was shown in (E). Scale bars represent 100 µm in (A-E).

E' Close-up of yellow squared frame in (E) marking the sensor expression pattern in the xylem region. Yellow arrows mark the developing xylem vessels. Scale bar represents 20 µm in E'.

F The fluorescence intensity ratio of mVenus to mCherry was compared between vascular tissues (n=5). Statistical groups were indicated by letters and assessed by a one-way ANOVA with post-hoc Tukey-HSD (95 % CI).

4.1.2 More vessel cells were detected in *d14* mutant by snRNA-seq analysis

To characterise the role of SL signaling in hypocotyl development in individual nucleus, I performed snRNA-seq (10x Genomics) comparing *d14* mutant with wild type. Plants were grown in plastic culture vessels, and around 150 hypocotyls were harvested to extract nuclei for each genotype at 19 DAG (referred to Dongbo et al. unpublished). I filtered out the data of nuclei with very few reads, or unspecific gene expressions that are likely to be noise by controlling the number of molecules detected within a nucleus (nCount-RNA) over 1500. In the end, I included 684 wild type and 822 *d14* nuclei in my analysis. The transcriptomes from wild type and *d14* were plotted into two dimensions by performing Uniform Manifold Approximation and Projection (UMAP) analysis, and 15 clusters were identified in a combined dataset with wild type and *d14* (Figure 4.3 A).

To assign cell identity to the clusters, I explored the specificity of transcripts of known marker genes in both genotypes (Figure 4.4). Cambium stem cells were found in cluster 4, indicated by all high enrichment of cambium stem-cell marker gene: *PXY* (proximal cambium where xylem initiation takes place), *SMXL5* (distal cambium in which phloem initiation occurs), *ATHB8*, *WOX4*, and *ANT* (Shi et al. 2019; Haas et al. ; Smetana et al. 2019), as well as early phloem marker *PEAR1* (Miyashima et al. 2019) (Figure 4.4). Enrichment of transcripts of *PXY*, *ATHB8*, *WOX4*, and *ANT* was also detected in cluster 8, but the transcripts of *SMXL5* and *PEAR1* is absent (Figure 4.4), which indicated that cluster 8 comprised xylem precursor cells. And this is

further confirmed by the high enrichment of *ACL5* in cluster 8 (Figure 4.4), whose mutation results in vessel development defect, and its promoter activity is specifically expressed in the vessel elements (Muñiz et al. 2008). Phloem precursor cells were found in cluster 1, suggested by the high enrichment of *ATHB8*, *ANT*, *PEAR1*, and *SMXL5* (Figure 4.4). Enrichment of transcripts of *ACL5*, *PXY*, *MP*, *ATHB8*, and master regulators of xylem vessel formation *VND6* and *VND7* (Kubo et al. 2005) (Figure 4.4), indicated that cluster 6 comprised developing vessel cells. *GLR3.6* is expressed in xylem parenchyma (Zandalinas et al. 2020). The specific enrichment of *GLR3.6* in cluster 10 (Figure 4.4), suggests that this cluster consisted of xylem parenchyma cells. Cluster 14 comprised phloem companion cells, as specific high enrichments of phloem companion markers, *SUC2,* and *APL* (Cayla et al. 2015; Absmanner et al. 2013) were found in this cluster (Figure 4.4). The transcripts of phloem sieve element marker *SEMA1* (Graeff and Hardtke 2021) were enriched in cluster 0 (Figure 4.4), suggesting cluster 0 included cells with sieve element identity. However, the other sieve element marker *SEOR1* (Cayla et al. 2015) showed very low expression in each cluster. *MYB84* as a marker for periderm (Wunderling et al. 2018), showed specific transcript enrichment in cluster 3, together with high expression of *WOX4* and *ANT* (Figure 4.4), suggesting that cluster 3 includes periderm cells.

The relative abundance of nuclei displayed certain differences within some clusters (Figure 4.3 B). Strikingly, cluster 6 showed a 3-fold nuclei abundance increment in *d14* relative to wild type. As cluster 6 showed the most dramatic difference between these two genotypes, the cell identity represented by that cluster was further confirmed by checking some known vascular markers by observing the promoter activities of *VND7:mTurqouise2-ER*, *PXY:ECFP-ER* (pPS19), *MP:EYFP-ER* (pKB24) in hypocotyl. As shown, the expression of the *VND7* reporter was specifically detected in developing vessels (Figure 4.3 C). The activities of *PXY* and *MP* reporters were broader, however, both were strongly detected in developing vessels (Figure 4.3 D and E). These results demonstrated that cluster 6 comprised

developing vessel cells, and probably more vessels were produced in *d14* mutant in contrast with wild type.

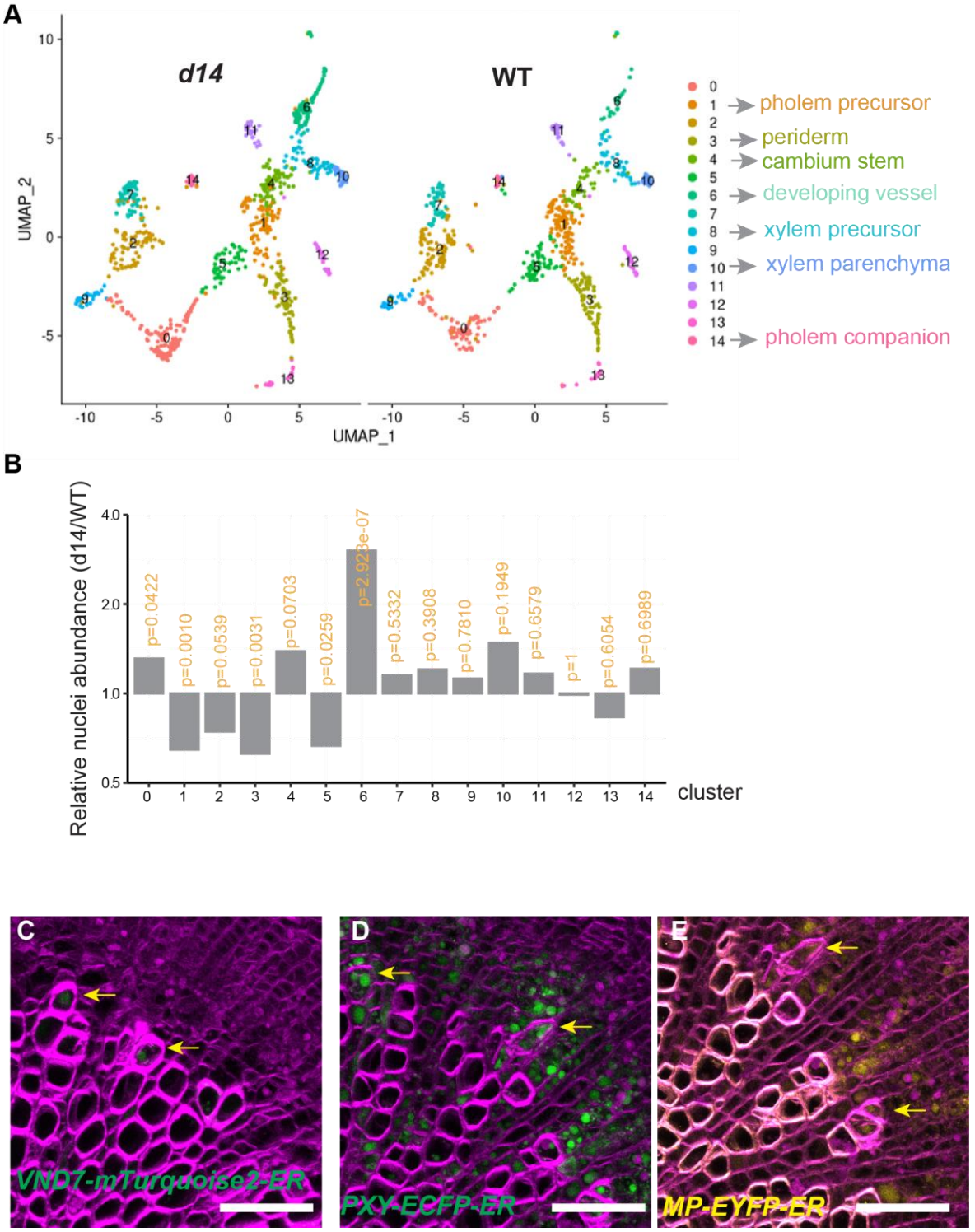

Figure 4.3: More developing vessel cell were detected in *d14* mutant by snRNA-seq analysis

A Cellular identity was assigned to most of the clusters. UMAP dimensional reduction projection of 684 and 822 nuclei from *d14* (left) and wild type (WT) (right). Cells were

grouped into 15 distinct clusters by Seurat. Distinct colours indicated distinct cluster. Clusters assigned to known cell type were labelled with cell identity after grey arrows.

B Fold change of nuclei abundance in *d14* relative to wild type after being normalized to correspondent total nuclei number. Fisher's exact test was used to determine statistical differences in each cluster. Each p-value is shown in the correspondent bar of each cluster.

C-E Hypocotyl cross-sections of plants carrying *VND7:mTurqouise2-ER* in (C), *PXY:ECFP-ER* in (D) and *MP:EYFP-ER* in (E). Yellow arrows point to the developing vessel elements. Scale bars represent 50 µm in (C-E)

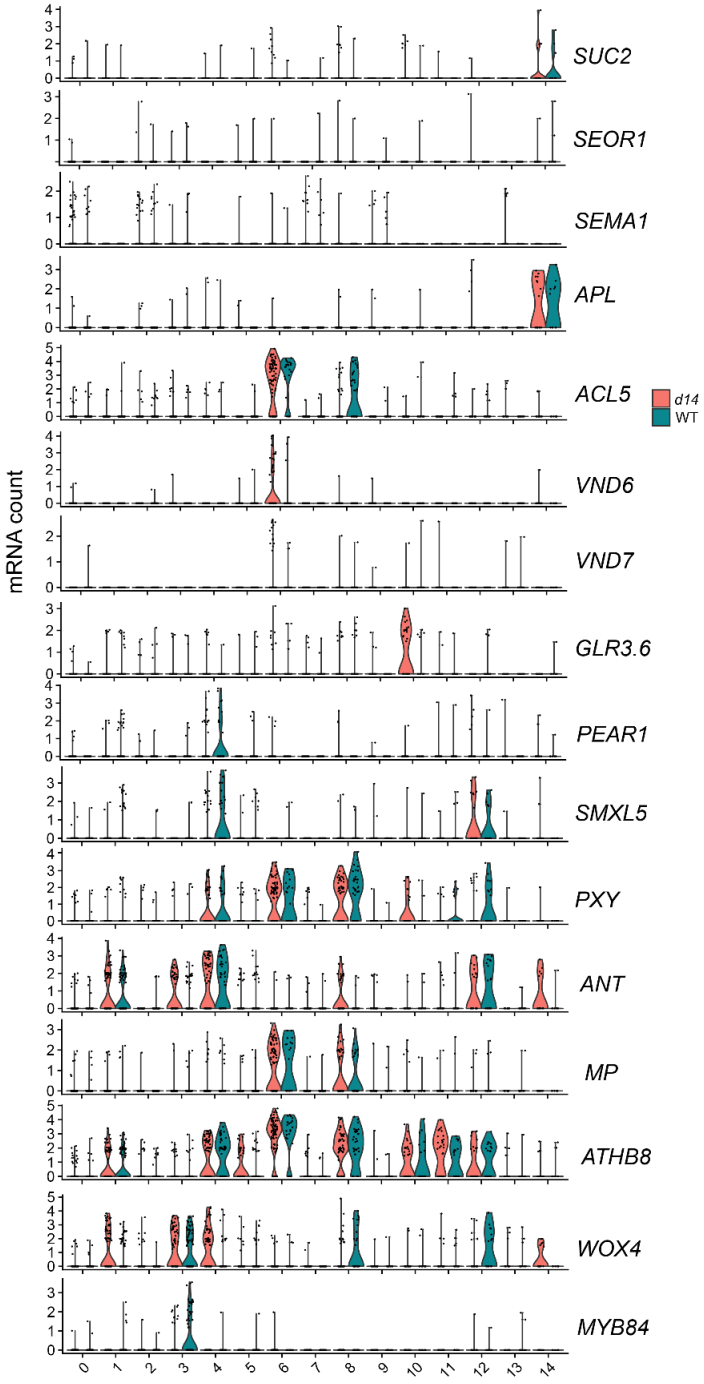

Figure 4.4: mRNA levels of marker genes cross clusters in both wild type and *d14*

Violin plots displaying transcript accumulation of some of the known vascular marker genes across clusters in both wild type and *d14* datasets. Clusters are indicated on the x-axis.

4.1.3 SL signaling suppresses xylem vessel formation in the hypocotyl

To determine whether SL signaling regulates vessel formation in the hypocotyl, I analyzed hypocotyl cross-sections of wild-type and SL signaling mutants. With SCWs deposition, xylem vessels were easily detected in the central region of toluidine blue-stained transverse sections due to the prominent lignified cell wall. In wild-type, the vessel files were spatially separated by large gaps formed by xylem parenchyma cells, while *d14* and *max2* both displayed a xylem pattern without large gaps between the vessel files. In comparison, the xylem pattern of *smxl6;smxl7;smxl8* triple mutants and *d14*;*smxl6;smxl7;smxl8* quadruple mutants was normal (Figure 4.5 A-E). Quantitative analysis of the vessel number demonstrated that *d14* and *max2* produced more vessels, while the vessel number in *smxl6;smxl7;smxl8* was lower than in wild-type (Figure 4.5 F). Importantly, the vessel number in the *d14;smxl6;smxl7;smxl8* background was similar as the number in *smxl6;smxl7;smxl8* triple mutants, suggesting that SL signaling suppressed vessel number via *SMXL6*, *SMXL7* and *SMXL8* (Figure 4.5 F). Furthermore, I determined the mean value of single vessel area, the total vessel area, and the vessel density within these genotypes. Similar as for the number of vessels, enhancements were observed in *d14* and *max2* mutants compared to wild-type (Figure 4.5 G-I). As expected, enhancements observed in *d14* were restored to the level found in *smxl6;7;8* triple mutants when SMXL6, SMXL7 and SMXL8 were deficient (Figure 4.5 G-I), indicating that *SMXL6*, *SMXL7* and *SMXL8* genes function downstream of *D14* in the context of xylem formation. To support the histological phenotype found in *d14* mutants, the expression levels of several vessel-related marker genes was analyzed via qRT-PCR comparing wild type and *d14*. Indeed, the results demonstrated that *d14* mutants showed an increased accumulation of *VND6, VND7* and *IRX3* expression relative to wild type (Figure 4.5 J), confirming the enhancement of xylem formation by histological analysis in *d14* mutants. In addition, as SL and Karrikin

(KAR) signaling both require the F-box protein MAX2, and function convergent in hypocotyl elongation (Wang et al. 2020b), raising a question whether the KAR signaling pathway also involves in vessel formation. KAI2 function as the receptor of KAR signaling. However, the *kai2* mutant displayed reduced vessel number in hypocotyl (Figure 4.6 A-C), supporting a specific role of SL signaling in regulating vessel formation.

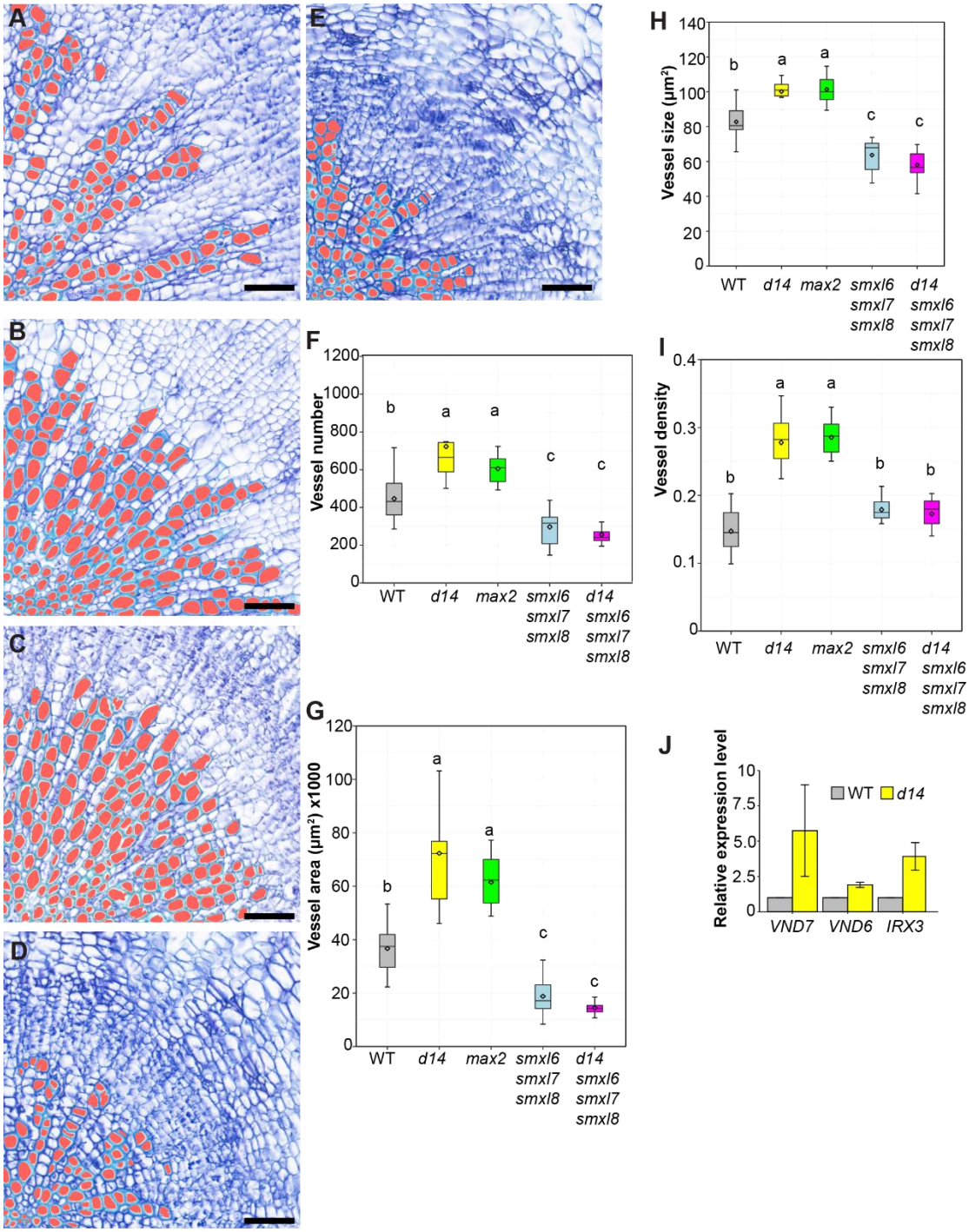

Figure 4.5: SL signaling is required for suppressing xylem vessel formation

A-E Toluidine-blue stained cross-sections of hypocotyl from 5-week-old WT, *d14*, *max2*, *smxl6;smxl7;smxl8* and *d14;smxl6;smxl7;smxl8*. Vessels were automatically searched using ImageJ and marked in red. Scale bars represent 50 µm.

F-I Quantification and comparison of vessels number (F), vessel size (G), vessel area (H) and vessel density (I) between different genotypes (n=10-15). Vessel size represents the mean value of single vessel cell. Vessel density was calculated by the ratio of vessel area to xylem area. Statistical groups were indicated by letters and determined by a one-way ANOVA with post-hoc Tukey-HSD (95 % CI).

J Comparison of relative expression level of xylem related genes *VND7*, *VND6* and *IRX3* between WT and *d14*. Error bars represent ± standard deviation

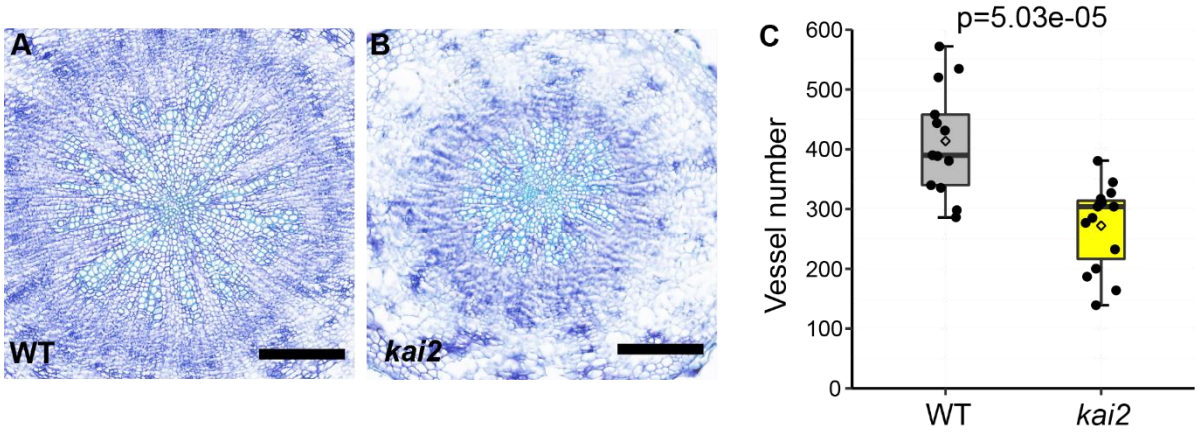

Figure 4.6: The vessel formation in *kai2* shows no enhancement

A-B Toluidine-blue stained cross-sections of hypocotyl from wild type and *kai2*. Vessel cells found in the center of cross-sections were characterized with thick secondary cell wall.

C Quantification and comparison of vessels number between wild type and *kai2* (n=15). The statistical difference is assessed by a one-way ANOVA with post-hoc Tukey-HSD (95 % CI). Scale bars represent 200 µm.

4.1.4 SL signaling acts locally in vessel formation

According to previous report, *d14* mutant also displays developmental defects in above-ground tissues, such as reduced leaf dimensions (Liang et al. 2016). I thus asked whether the enhanced vessel formation in *d14* is a local function of SL

signaling. To testify the local role of *D14* in vessel formation, *D14* was expressed under the control of the WOX4 promoter whose activity is restricted to cambium and xylem cells (Shi et al. 2019). Histological analysis showed the enhanced xylem formation in *d14* was rescued to wild type-like level in vessel number and vessel size, supporting the local role of SL signaling in vessel formation (Figure 4.7 A-C).

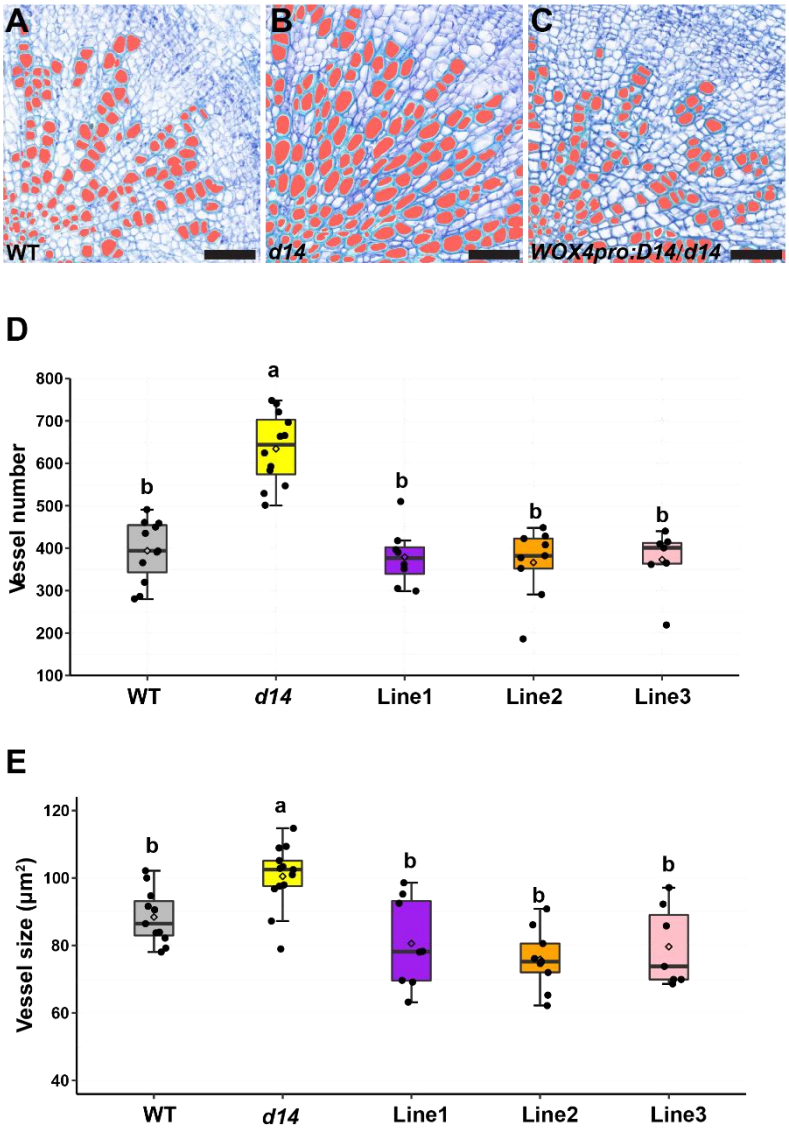

Figure 4.7: Enhanced vessel formation in *d14* was rescued to wild-type level in lines carrying *WOX4pro:D14/d14* construct.

A-C Toluidine-blue stained 5-week-old cross-sections of hypocotyl from WT, *d14* and transgenic lines carrying *WOX4pro:D14/d14* construct**.** Vessels were automatically searched using ImageJ and marked in red. Scale bars represent 50 μm.

D-E Quantification and comparison of vessel number (D) and vessel size (E) between WT, *d14* and three transgenic lines carrying *WOX4pro:D14*/*d14* construct (n=7-12). Vessel size represents the mean value of single vessel cell. Vessel number and vessel size are quantified and compared to each other by one-way ANOVA with post-hoc Tukey_HSD (95 % CI).

4.1.5 The enhanced xylem formation in *d14* is probably not correlated with increased axillary buds

As axillary buds are formed in the junction of stem and petiole, which connects to the vascular tissues in hypocotyl. Therefore, an assumption that the increased axillary buds might act as a driver for the enhanced conduits in hypocotyl is proposed. To testify this assumption, I characterized the xylem vessel number in a mutant with bushy branches. *BRC1,* a key regulator for inhibiting axillary bud outgrowth and suppressing shoot branching (González-Grandío et al. 2013), was reported to be transcriptionally activated by *SMXL6* (Wang et al. 2020a), whose mutation caused increased axillary buds in plants. Therefore, I characterized the vessel number in *brc1*-2 mutant. However, the vessel number in *brc1*-2 exhibited no apparent difference relative to the wild type (Figure 4.8 A-C), arguing that the increased vessel number observed in SL signaling mutants is not caused by increased axillary bus. Meanwhile, the result suggests that axillary bus and vessel formation, acting as two aspects of plants in response to SLs, are mediated by distinct downstream targets.

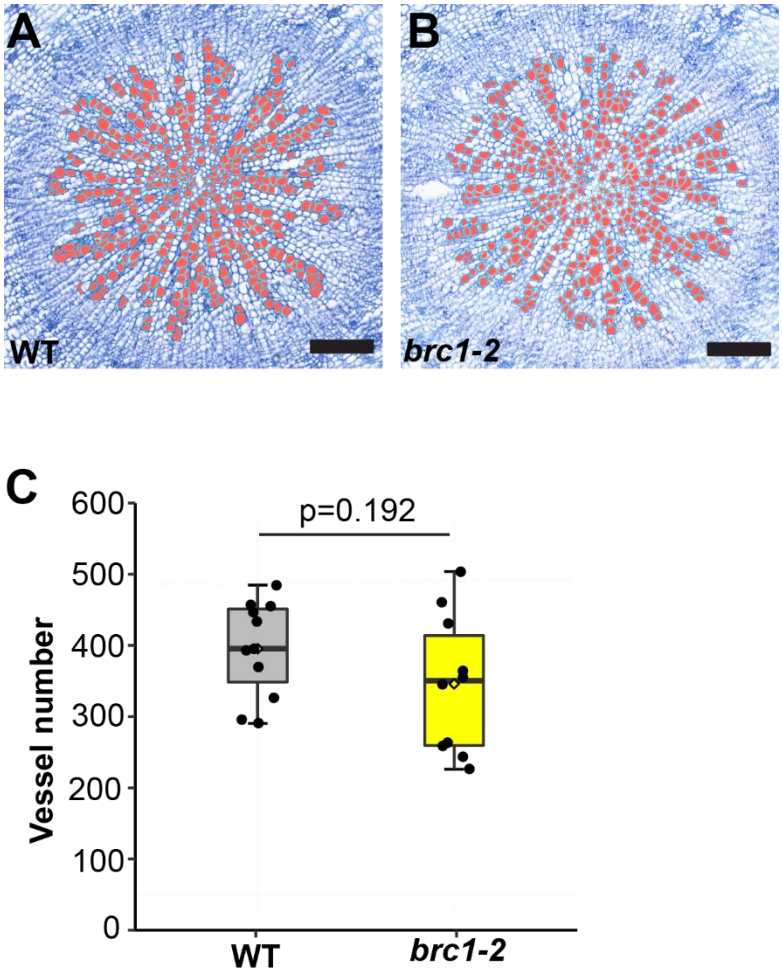

Figure 4.8: *brc1-2* shows normal vessel formation

A-B Toluidine-blue stained 5-week-old cross-sections of hypocotyl from WT and *brc1-2*. Vessels were automatically selected using ImageJ and marked in red. Scale bars represent 100 µm.

C Quantification and comparison of vessels number between WT and *brc1-2* (n=10-11). Vessel number are quantified and assessed by one-way ANOVA with post-hoc Tukey_HSD (95 % CI). No significant difference was detected.

4.1.6 Exogenous GR24^{4DO} application represses vessel number

To assess whether exogenous SLs levels influence vessel formation, I applied the synthetic SL analog GR24^{4DO} to 2-week-old wild type plants. After two weeks of treatment, GR24^{4DO} exposed plants showed a clear decrease in vessel generation

relative to mock-treated plants (Figure 4.9 B-D). In contrast, the above-ground tissues showed no clear difference (Figure 4.9 A), strongly suggesting a specific inhibitory role of exogenous $GR24^{4DO}$ in xylem development.

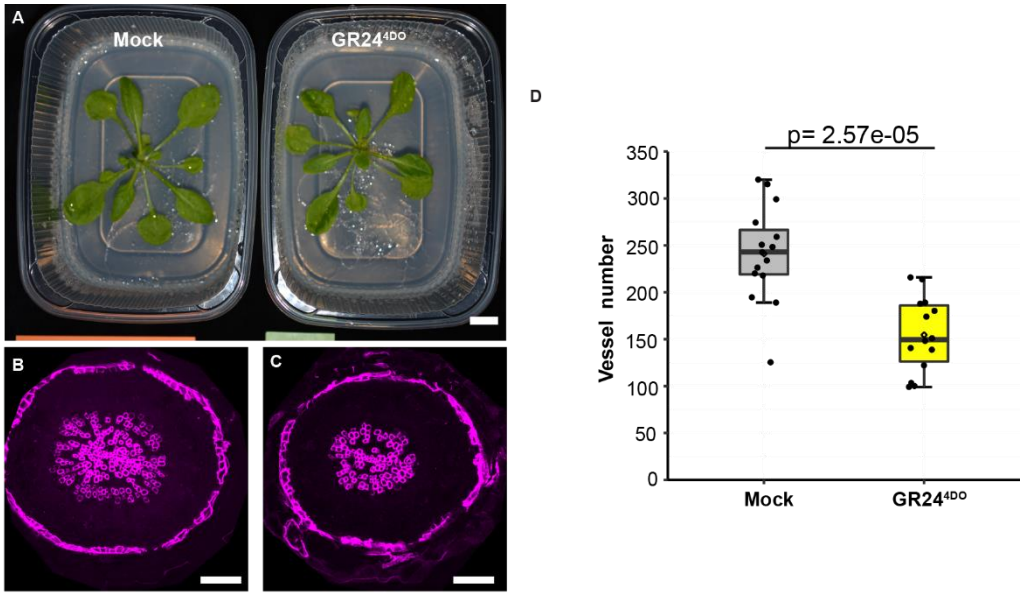

Figure 4.9: Exogenous SL application suppressed xylem vessels generation

A The Picture of representative above-ground 4-week-old tissues after application of 10 µM acetone (left) and $GR24^{4DO}$ (right). Scale bar represents 1 cm in (A)

B-C The hypocotyl cross-sections of 4-week plants after application of 10 µM acetone (B) and $GR24^{4DO}$(C). The cross sections were illuminated under UV laser (405 laser), and the auto-fluorescence from the lignified vessels were captured and shown in magenta. Scale bars represent 100 µm in (B, C).

D Quantification of vessels between plants treated with 10 µM Dex and acetone (n=14-15). Statistical difference was assessed by a one-way ANOVA with post-hoc Tukey-HSD (95 % CI).

4.1.7 SL signaling suppress vessel formation during radial growth

To explore the developmental onset of the xylem vessel number in *d14* mutant, hypocotyl cross-sections were analyzed at several time points. Mild difference was detected in vessel number 2 weeks after germination between wild

type and *d14* (Figure 4.10 A, D and G). Although the vessel number continuously rose in both the wild-type and *d14* over time, still more new vessels were generated in *d14* at the stage of 3 weeks after germination (Figure 4.10 B, E, G). And this tendency continued to be observed in 4-week-old (Figure 4.10 E, F, G) as well as 5-week-old plants (Figure 4.5 A, B and F), implying the increased vessel number in *d14* appeared during radial growth. By contrast, the xylem strand number in primary roots showed no clear difference between *d14* and the wild type. Taken together, SL signaling suppresses the vessel number during radial growth.

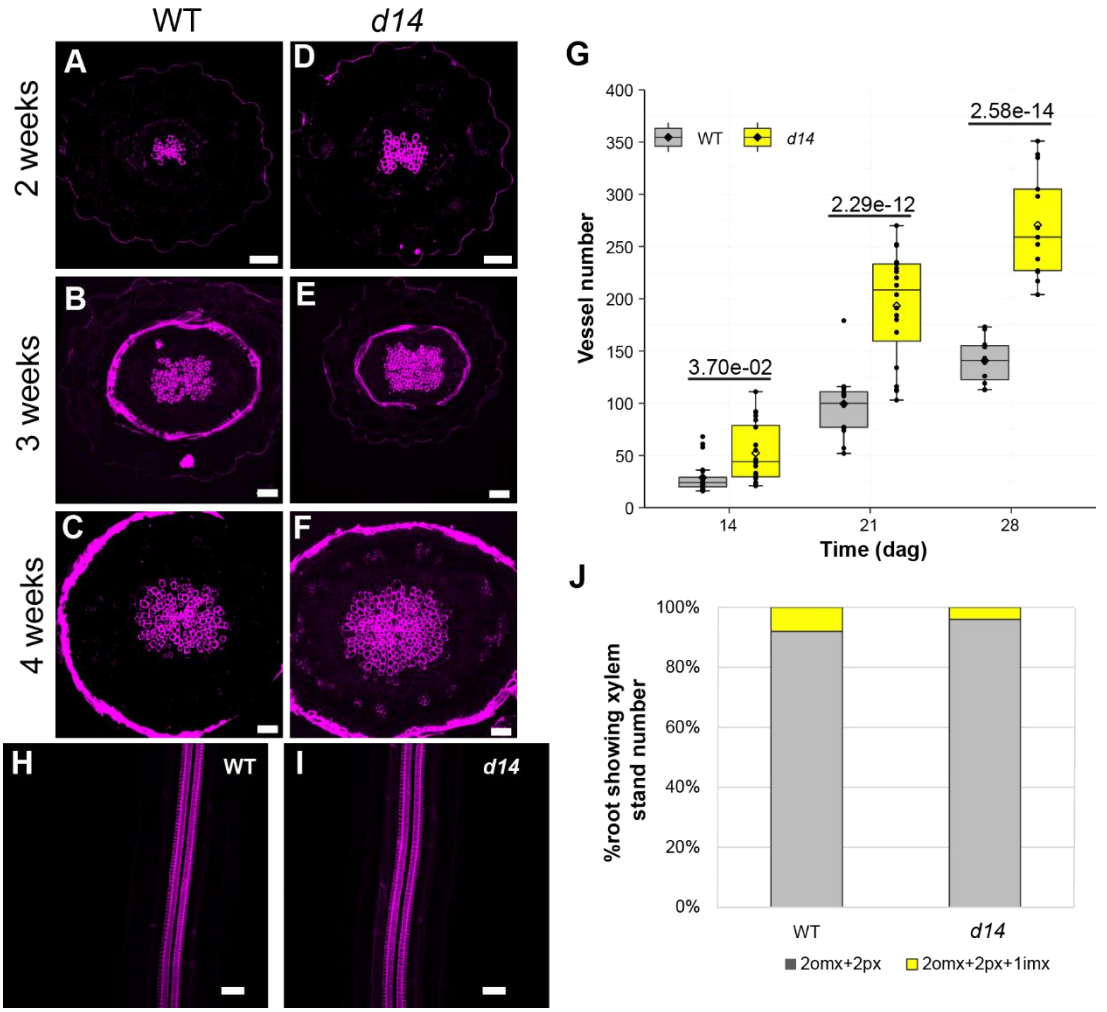

Figure 4.10: SL signaling suppressed xylem vessel formation during radial growth

A-F Hand cross-sections of hypocotyl with indicated genotypes at indicated ages. The cross sections were illuminated under UV laser, and the auto-fluorescence from

the lignified vessels were captured and shown in magenta. Scale bars represent 50 μm in (A-F).

G Grouped time series graph of vessel number compared between WT and *d14* (n=11-20). The way of genotype influences vessel size depends on stage (Two-way ANOVA, F= 19.356, df=2, *p*= 8.66e-08). The statistical differences of genotype for each stage were subsequently determined by a post-hoc Bonferroni test.

H-I Morphology of xylem strand in 5 DAG root observed in WT and *d14*.

J Comparison of xylem strand number between WT and *d14* in a stacked histogram (n=23). 2omx indicates 2 outer metaxylem, 2px indicates two protoxylems, and 1 imx means one inner xylem.

4.1.8 SMXL7 activity is sufficient to promote vessel formation

To probe whether the activity of SMXL7 is sufficient for enhancing vessel formation, I examined the effects of introducing stabilized SMXL7 under the control of its native SMXL7 promoter (*SMXL7pro:SMXL^{d53}-VENUS*) into wild type genetic background. This contrast has been proved to be resistant to *rac*-GR24-induced degradation, resulting in a phenocopy of *d14* in shoot morphology, leaf morphology, as well as shoot branching levels (Liang et al. 2016). I then quantified the phenotypic effect of the stabilized SMXL7 in vessel formation. Likewise, SMXL7 accumulation results in increased vessel number and size relative to wild type, which was close to or resembled those in *d14* (Figure 4.11 A-C). These results suggest that SMXL7 activity is sufficient to promote vessel formation in hypocotyl.

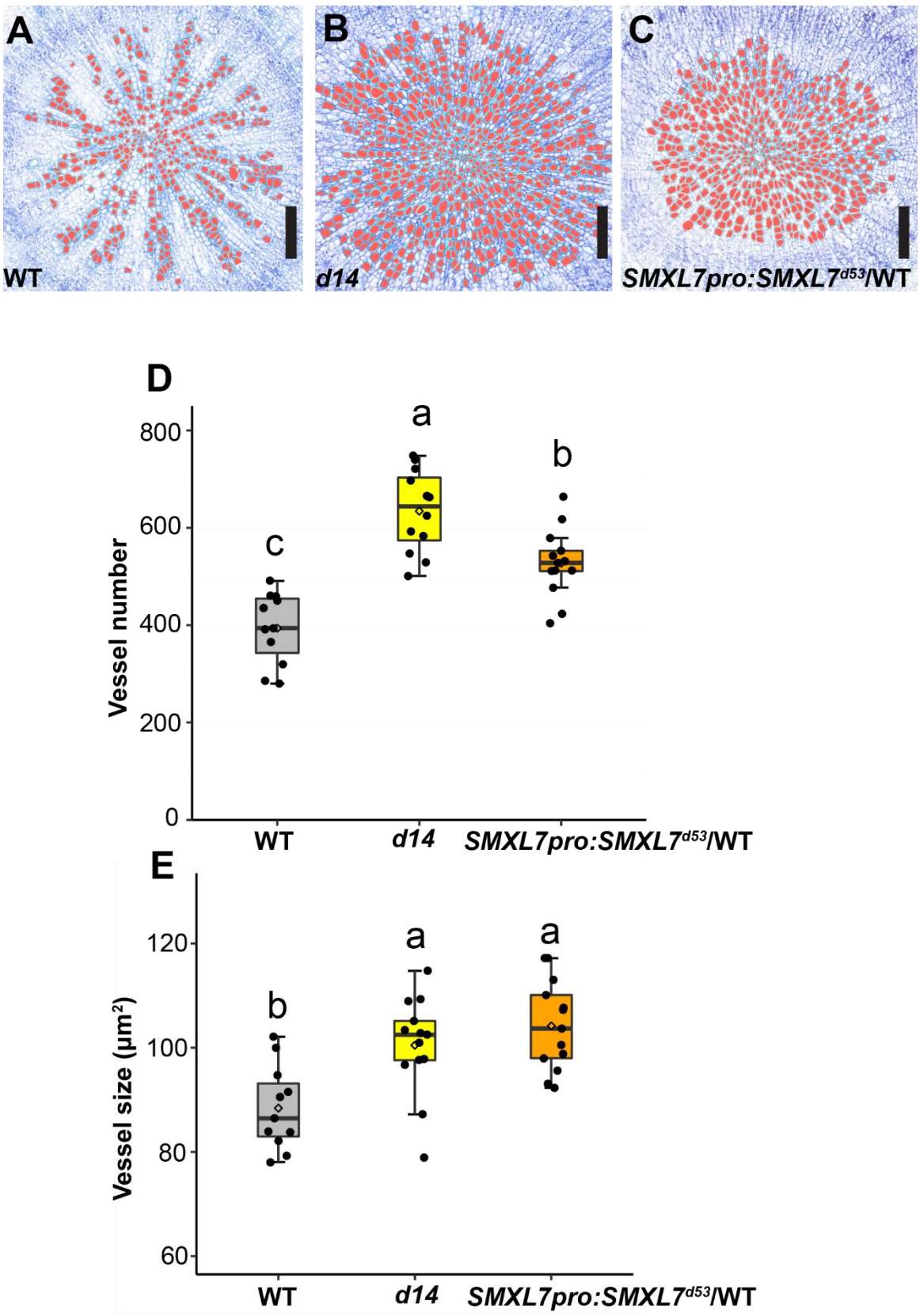

Figure 4.11: Stabilized SMXL7 in wild type promoted vessel formation

A-C Toluidine-blue stained 5-week-old cross-sections of hypocotyl from WT, *d14* and transgenic lines carrying *SMXL7pro:SMXL7*^{d53}*-VENUS*/WT construct**.** Vessels were

automatically searched using ImageJ and marked in red. Scale bars represent 50 µm.

D-E Quantification and comparison of vessel number (D) and vessel size (E) between WT, *d14* and transgenic line carrying *SMXL7pro:SMXL7^{d53}-VENUS* construct (n=11-13). Vessel size represents the mean value of single vessel cell. Vessel number and vessel size are quantified and assessed to each other by one-way ANOVA with post-hoc Tukey_HSD (95 % CI).

4.1.9 Investigating the mechanism of vessel formation regulated by SL signaling

AUXIN RESPONSE FACTOR (ARF) transcription factor-mediated auxin signaling has been shown to promote secondary vessels formation in stems and roots (Smetana et al. 2019; Brackmann et al. 2018). ARF5, also known as *MONOPTEROS* (*MP*), was previously reported to modulate vascular development (Przemeck et al. 1996; Hardtke and Berleth 1998). MPΔIII/IV carries deletions of its domain III and IV and, therefore, is a dominant active variant of MP as it is released from AUX/IAA-mediated repression (Krogan et al. 2012). To investigate whether auxin signaling in vessel-forming cells enhances vessel production, I used the *PXY* promoter, whose activity is high in the proximal cambium, developing vessels as well as in xylem parenchyma (Shi et al. 2019), to express a dexamethasone (Dex)-inducible version of MPΔIII/IV (GR-MPΔIII/IV). After Dex treatment for two weeks, *PXY:GR-MPΔIII/IV* plants displayed a dramatic enhancement of vessel formation relative to mock-treated plants (Figure 4.12 A, B and G), indicating a positive role of auxin signaling in vessel formation in the hypocotyl. Auxin signaling levels (ARF activity) can be repressed by expressing a Dex-inducible variant of the stabilized AUX/IAA protein BODENLOS (GR-bdl) (Hamann et al. 2002). To see whether a reduction in auxin signaling reduces vessel formation, I applied Dex to a transgenic line carrying a *PXY*:*Myc-GR-bdl* construct. After 10-day Dex treatment, *PXY*:*Myc-*

GR-bdl plants showed a reduced xylem formation (Figure 4.12 C, D and H), confirming that auxin signaling promoted vessel formation. As SL signaling functions to suppress vessel formation, I reasoned an interconnected role of SL and auxin signaling in tuning xylem formation. To test this assumption, the *PXY:Myc-GR-bdl* construct was introduced into the *d14* mutant by crossing. Strikingly, the vessel number in *d14* was reduced when auxin signaling was inhibited under 10-day Dex treatment (Figure 4.12 E, F and H). This indicated the enhanced xylem number in *d14* can be alleviated when ARF activity was repressed. In addition, vessel size was reduced to around half in wild type upon Dex treatment, while the effect of size by Dex treatment was weakened in *d14* (Figure 4.12 E, F and I). These results suggested that an interconnected existed between auxin and SL signaling in vessel formation. Furthermore, a *d14;mp-S319* double mutant was generated carrying the weak *mp-S319* allele (Cole et al. 2009)(. Nevertheless, the xylem number in *d14* showed no difference with that in *d14;mp-S319* double mutant (Figure 4.13 A-D). However, a recent study in root showed that ARF7 and ARF19 function redundantly with MP in vessel formation (Smetana et al. 2019), I thus planned to generate *d14;mp-S319;arf7;arf19* quadruple mutant (in progress).

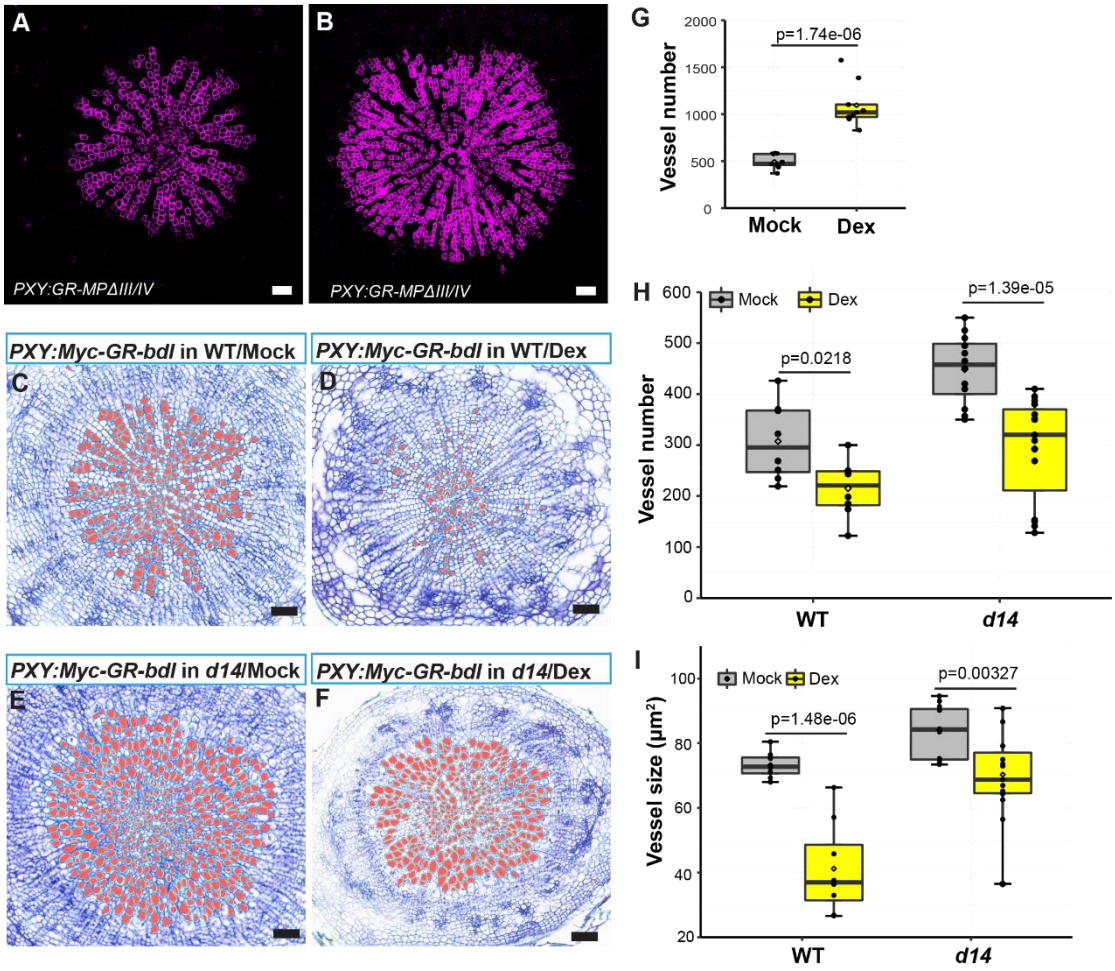

Figure 4.12: The enhanced xylem formation in *d14* was alleviated by repressing auxin signaling

A-B Cross-sections of 5-week-old transgenic plants carrying *PXY:GR-MPΔIII/IV* construct with mock treatment in (A) and Dex treatment in (B) from 3 weeks old onwards for 2 weeks. Xylem autofluorescence was visualized by UV laser and shown in magenta. Scale bars represent 50 μm.

C-F Cross-sections of 31-DAG transgenic plants carrying *PXY:Myc-GR-bdl* in WT (C, D) and *d14* (E, F). Cross-sections in (C, E) was treated with 15 μM Dex and in (D, F) was treated with 15 μM dissolvent from 3 weeks old onwards for 10 Days. Vessels were automatically searched using ImageJ and marked in red. Scale bars represent 50 μm.

G Comparison of vessel number between Dex and Mock-treated plants (n=9). Statistical difference was assessed by a one-way ANOVA with post-hoc Tukey-HSD (95 % CI).

H Comparison of vessel number response to Dex treatment between WT and *d14* mutant (n=8-15). The way of treatment influences vessel number did not depend on genotypes (Two-way ANOVA, F=1.334, df=1, *p*=0.254). The statistical differences of treatment for each genotype were subsequently determined by a post-hoc Bonferroni test.

I Comparison of vessel size response to Dex treatment between WT and *d14* mutant (n=8-15). The way of treatment influences vessel size depends on genotypes (Two-way ANOVA, F=6.578, df=1, *p*=0.014). The statistical differences of treatment for each genotype were subsequently determined by a post-hoc Bonferroni test.

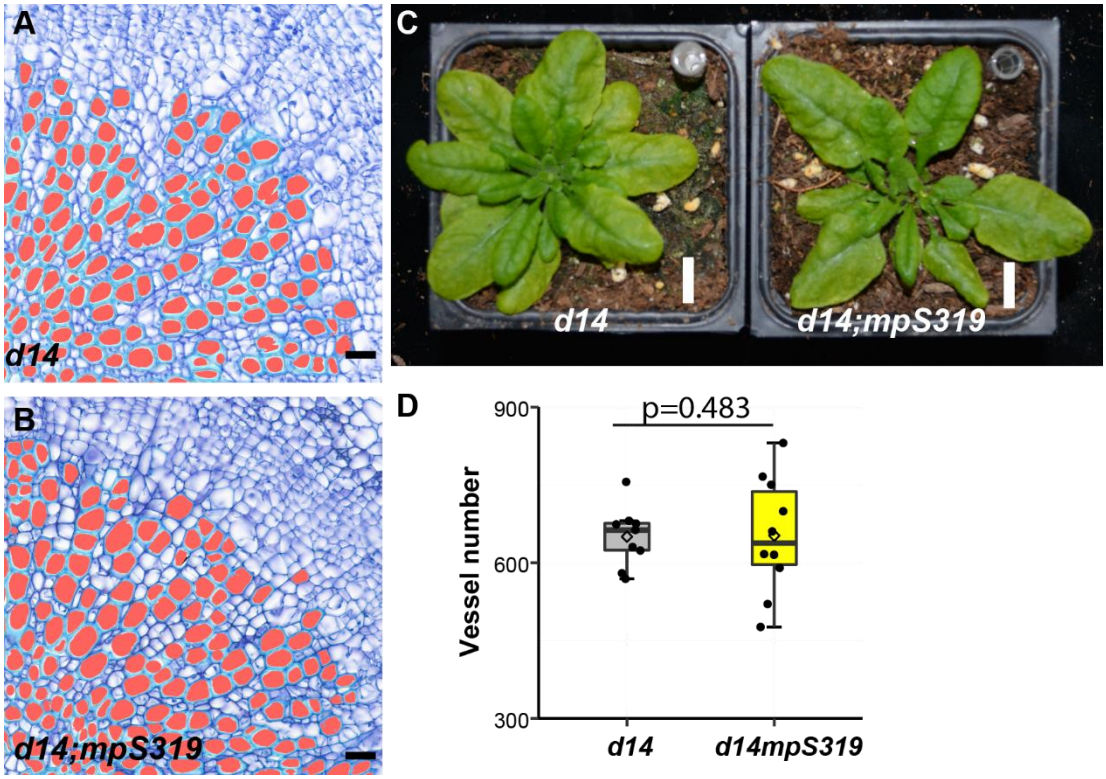

Figure 4.13: Loss of function of MP is not able to suppress vessel formation in *d14*

A-B Toluidine blue stained 5-week-old cross-sections of *d14* single mutant and *d14;mp-S319* double mutant. Vessel cells were marked in red. Scale bars represent 20 µm.

C A Picture of above-ground tissues in *d14* single mutant and *d14;mp-S319* double mutant. Scale bars represent 1 cm.

D Comparison of vessel number between *d14* single mutant and *d14;mp-S319* double mutant (n=10). Statistical difference was determined by a one-way ANOVA with post-hoc Tukey-HSD (95 % CI).

4.1.10 *SMXL7* potentially co-expressed with *ATHB8*

As shown above, SMXL7 promoted vessel formation (Figure 4.10) and was detectable in developing vessels (Figure 4.1 B'). Therefore, I further examined genes co-expressed with SMXL7 from my snRNA-Seq data of wild type and *d14* mutant by evaluating the Pearson correlation coefficient (Yang et al. 2021). The overlapped co-expressed genes found in both wild type and *d14* are listed in table 4.1. Interestingly, *ATHB8* is on the list of the top 22 genes ranked according to the correlation value arranged high to low (Figure 4.14). Consistently, the transcript of *ATHB8* showed highest enrichment in developing vessel cluster from my snRNA-Seq data (Figure 4.4). As the accumulation of ATHB8 facilitate the formation of vessel cell (Baima et al. 2014; Baima et al. 2001), I thus hypothesized that SMXL7 promotes vessel formation potentially through regulation the expression of *ATHB8*.

			Correlation coefficient	
ranking	Gene ID	description	WT	*d14*
1	AT2G29970	SMXL7	1	1
2	AT2G24580	FAD-dependent oxidoreductase family-protein	0.1882862	0.102727
3	AT3G45160	Putative membrane lipoprotein	0.1670842	0.10525745
4	AT1G59740	Major facilitator superfamily protein	0.1377614	0.10104755
5	AT2G31280	Encodes a LONESOME HIGHWAY(LHW)-like protein	0.1370676	0.108072
6	AT3G25710	TARGET OF MONOPTEROS 5	0.1320251	0.10137513
7	AT4G32880	ATHB8	0.1260987	0.10595492
8	AT1G22065	Unknown	0.1248217	0.12926662
9	AT1G12150	Weak chloroplast movement under blue light protein	0.1223944	0.10587884
10	AT2G21050	LIKE AUXIN RESISTANT 2	0.1191098	0.11276062
11	AT1G61660	Encodes a transcriptional activator	0.1175054	0.15326336
12	AT5G53486	unknown transmembrane protein	0.1144103	0.1173048
13	AT3G47510	unknown transmembrane protein	0.1109062	0.12587334
14	AT5G23930	Mitochondrial transcription termination factor family protein	0.1098658	0.10467038
15	AT3G45960	ATEXPL3	0.1089311	0.10502809
16	AT3G56620	Nodulin MtN21-like transporter family protein	0.1028389	0.12025278
17	AT4G32810	Encodes a protein with similarity to carotenoid cleaving deoxygenases	0.1011338	0.16987037
18	AT3G15950	Similar to TSK-associating protein 1 (TSA1)	-0.117212	-0.1074965
19	AT3G16420	PYK10-binding protein 1(PBP1)	-0.121568	-0.1192629
20	AT3G16430	JACALIN-RELATED LECTIN 31	-0.128486	-0.114308
21	AT3G16450	JACALIN-RELATED LECTIN 33	-0.133347	-0.1016256
22	AT3G16460	JACALIN-RELATED LECTIN 34	-0.136101	-0.1187455

Table 4.1 The top 22 overlapped co-expressed genes of SMXL7 according to the wild type and *d14* snRNA-seq data.

4.2 The role of SL signaling during xylem at xylem phase II

The secondary xylem in Arabidopsis hypocotyl develops in two evidently distinguishable phases: at phase I, where parenchyma and vessels are formed, while at phase II, in which vessels and large amounts of fibres occur (Chaffey et al. 2002). As the composition of xylem switches between these two phases, it is worthwhile to explore whether SL signaling plays a role at xylem phase II.

4.2.1 SL signaling is required for maintaining the radial hypocotyl patterning at xylem phase II

In the Arabidopsis hypocotyl, activity of the cylindrical cambium produces three concentric tissue domains: the cambium, the xylem and the phloem (Figure 4.15 A). In wild type hypocotyl, the secondary xylem development occurs in two phases according to the composition of xylem cells (Chaffey et al. 2002). During phase I, xylem consists of lignified vessels and non-lignified parenchyma cells (Figure 4.15 B). Phase II starts with the formation of lignified fibres, and eventually forms a

lignified cell layer that encircles the central area generated at phase I (Figure 4.15 B). As the mutants of certain SL signaling components showed enhanced vessel formation at phase I, I was intrigued to investigate phase II xylem morphology in these mutants. To do so, hypocotyls from 15-20 cm tall wild type, *d14*, *max2*, *smxl6;7;8* and *d14;smxl6;7;8* plants were harvested and histologically analysed. Compared to wild type, the xylem cell layer characterized by massive lignified fibres and vessels was sometimes absent in both *d14*, *max2* mutants. Instead, only type I xylem was observed (Fig 4.15 C, D). Strikingly, some xylem-like cells were discovered in positions normally occupied by phloem cells (Fig 4.15 C, D). To determine the identity of these xylem-like cells, I investigated the activity pattern of the xylem marker *NAC SECONDARY WALL THICKENING PROMOTING FACTOR 3:ECFP-ER* (*NST3:ECFP-ER*, pPS31) in wild type and *d14* mutants. Consistent with a previous report (Mitsuda et al. 2007), the activity of the transcriptional *NST3* marker was strongly detected in developing xylem cells characterized by the deposition of secondary cell walls (Figure 4.16 A, A'), confirming that *NST3* was a xylem marker gene. Also in *d14*, strong activity of *NST3:ECFP* was detected in the usual xylem area. However, prominent *NST3:ECFP* activity was also observed in the xylem-like cells present in the usual phloem area, suggesting a xylem-like identity of these cells (Figure 4.16 B, B'). Therefore, I designated these cells as ectopic xylem. To see whether phloem was in *d14* present only in its usual domain, I analysed the expression of a phloem-specific marker *ALTERED PHLOEM DEVELOPMENT:ECFP-ER* (*APL:ECFP-ER*, pPS10) whose activity was in wild type observed in phloem poles (Figure 4.16 C and C'). In *d14*, the *ER*-localized *APL:ECFP-ER* signal was likewise detected in phloem poles which located between the ectopic xylem, but not appear in the usual xylem area (Figure 4.16 D, and D'), demonstrating that the ectopic xylem was indeed generated in the phloem region, and thus the strict concentric patterning found in wild type was disrupted. Of note, phloem fibres were also generated during phase II stage, which can be distinguished from the ectopic xylem by either the secondary cell wall thickness or the relative locations with respect to the *APL* marker activity (Figure 4.16 C', D'). To explore

whether the core SL signaling pathway is involved in maintaining vascular patterning, I next examined the xylem development organisation of *smxl6;7;8* triple mutants. The analysis suggested that the *smxl6;7;8* mutant displayed a xylem pattern resembling that in wild type in both phase I and phase II (Figure 4.15 E). Importantly, the irregular xylem pattern usually found in *d14* mutants was completely rescued to a wild type-like pattern when SMXL6, SMXL7 and SMXL8 were deficient, demonstrating that SMXL6, SMXL7 and SMXL8 function downstream of *d14* in maintaining radial tissue patterning (Figure 4.15 F). Taken together, my observations demonstrated that the SL signaling is required for the radial tissue patterning during growth phase II in the Arabidopsis hypocotyl.

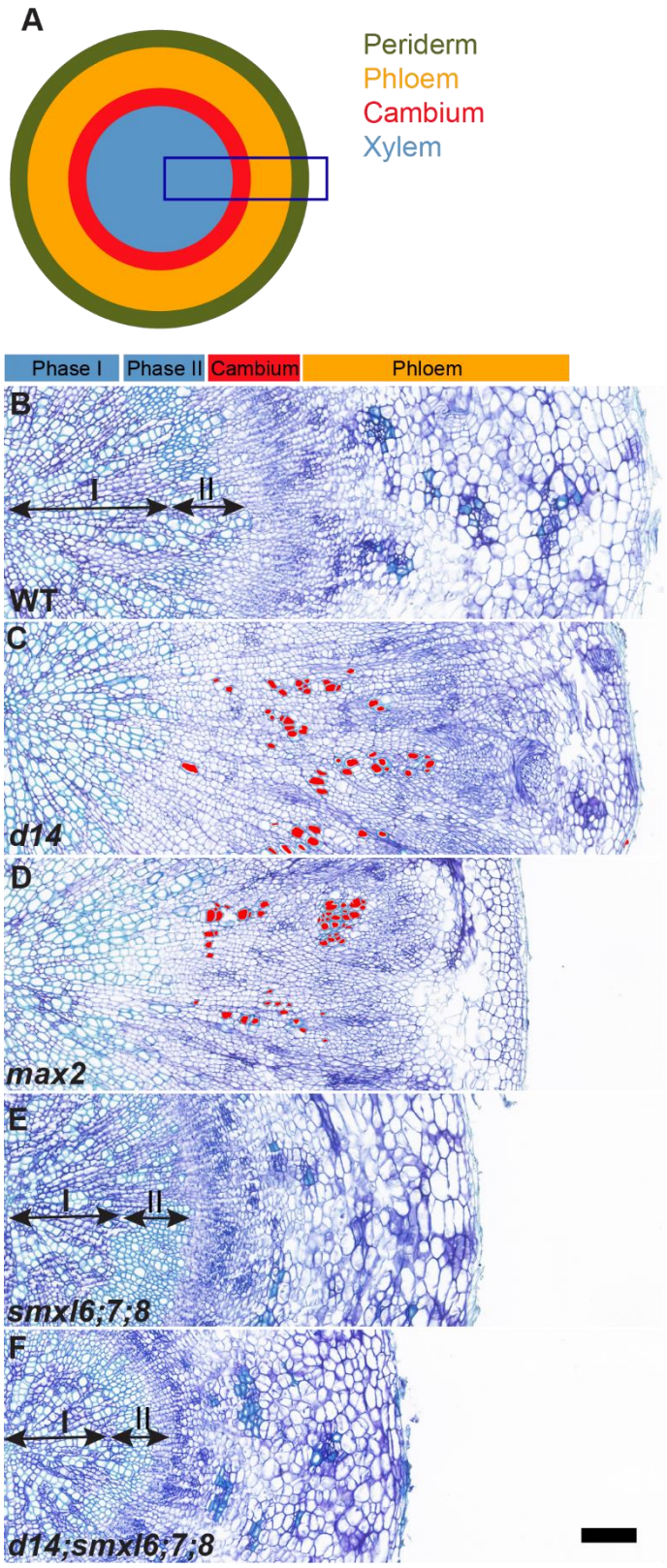

Figure 4.15: The concentric vascular rings were disrupted in *d14* and *max2* mutant

A Schematic cross-section of an Arabidopsis hypocotyl. The blue frame indicates the region analysed in B-F.

B-F Toluidine blue stained hypocotyl cross-sections of WT (B), *d14* (C), *max2* (D), *smxl6;7;8* (E), and *d14;smxl6;7;8* (F). All the hypocotyls were harvested from 15-20 cm tall plants. In WT, three concentric vascular rings are: xylem, cambium and phloem rings from centre to periphery. Xylem produced during phase I and phase II divided by xylem composition. The cells marked in red in *d14* and *max2* cross-sections marked the ectopic xylem-like cells. Bar represent 100 µm in (B-F).

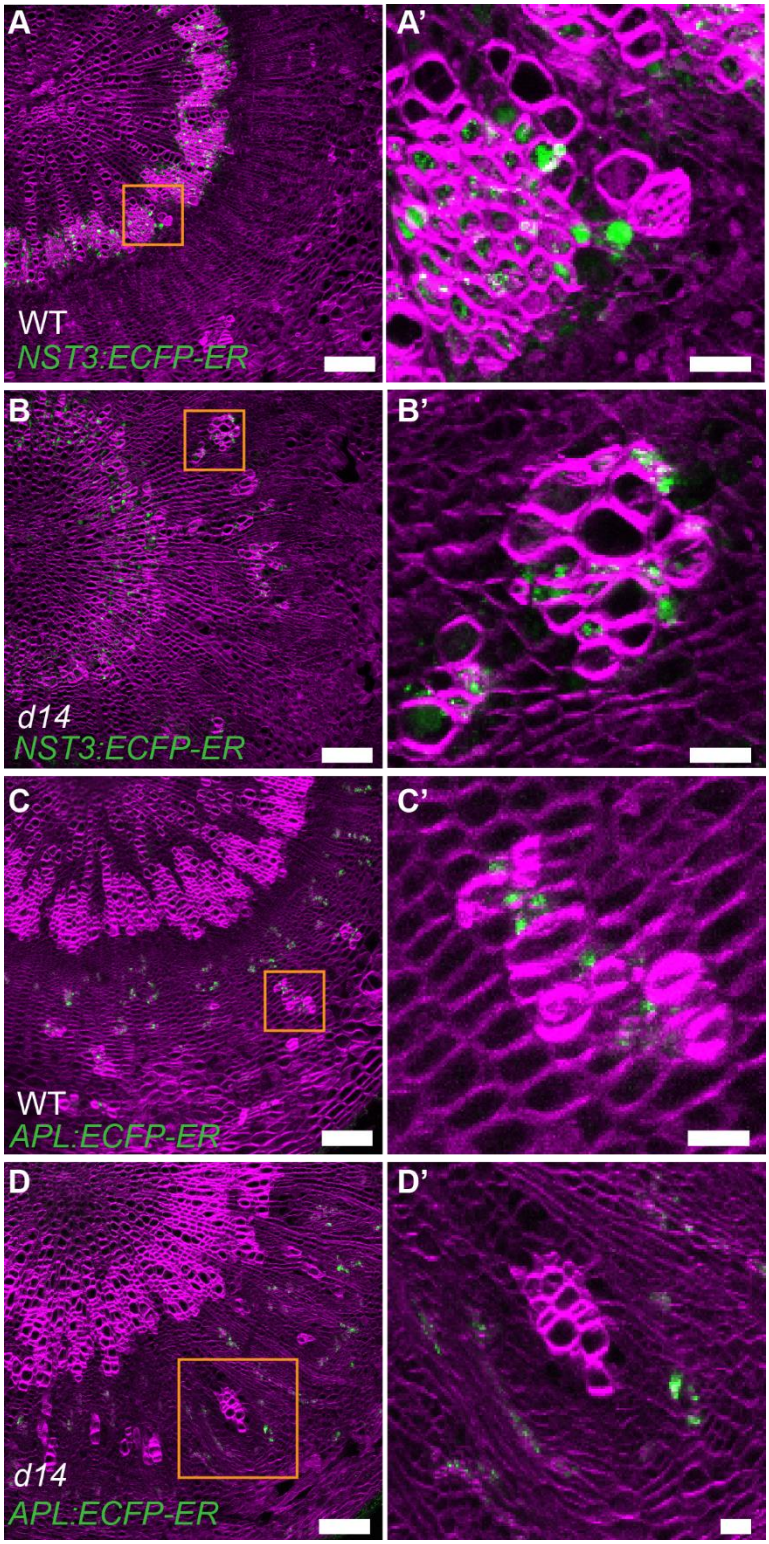

Figure 4.16: The xylem identity confirmation of ectopic xylem-like cells in *d14* mutant

A-D Hand sectioned hypocotyls of 15-20 cm tall *Arabidopsis* plants. ECFP signals (green) were captured by confocal microscope in promoter-reporter lines *NST3:ECFP-ER* (A, B), and *NST3:ECFP-ER* (C, D). Direct Red 23 was used to stain the cell wall shown in magenta.

A'-D' Magnification of the expression regions marked by orange squared frames in A-D. *NST3* activity was specifically found in the xylem area in WT, whose activity was also detected in xylem-like cells in the phloem area in *d14*. As a phloem marker, *APL;ECFP* activity was detected in cells surrounded by phloem fibres in WT, while activity was absent in the xylem-like cells residing on the phloem area. Scale bars represent 100 µm in A-D, and 20 µm in A'-D'.

4.2.2 SL signaling is required for restricting the shift of cambium ring at xylem Phase II

With the disruption of vascular rings, it is impossible to identify the exact cambium region within *d14* hypocotyl by cell wall staining. Thus, I took use of the thymidine analogue 5-ethynyl-2′-deoxyuridine (EdU) (Chehrehasa et al. 2009; Shi et al. 2019) to map the proliferative cambium cells. EdU incorporation was carried out by directly watering 100 μM EdU solution to the soil in which plants with different age were grown. After 3 days of incubation, hypocotyls from *d14* mutants and wild type were harvested and the EdU signals were captured under the microscope. The relative EdU signal intensity was profiled starting from the xylem border to the margin of the cross section. For 4-week-old wild type plants, the maximum of intensity of the EdU signal was detected in cell layers adjacent to the xylem border within the innermost quarter along the radial axis from the xylem border to the section margin (Figure 4.17 A and A'), overlapping with the cambium region. Similarly, the maximum intensity of the EdU signal in *d14* mutants was detected in cell layers adjacent to the xylem border (Figure 4.17 C and C'). The relative location of the EdU signal maximum maintained unchanged in wild type at growth phase II (Figure 4.17 A-B, A'-B'). In comparison, a shift in the position of the EdU signal maximum was detected in *d14* mutants at phase II to the phloem region and located in the second quarter along the radial axis from the xylem border to the section margin (Figure 4.17 D, D'). This indicated that in *d14* mutants the cambium region changed its position during growth phase II. At last, when ectopic xylem islands appeared, EdU signals were prominently observed surrounding the ectopic xylem islands (Figure 4.17 I) indicating enhanced cell division activities at these sites. Together, these results suggested that SL signaling restricted cambium activity to a region close to the initial xylem border during growth phase II.

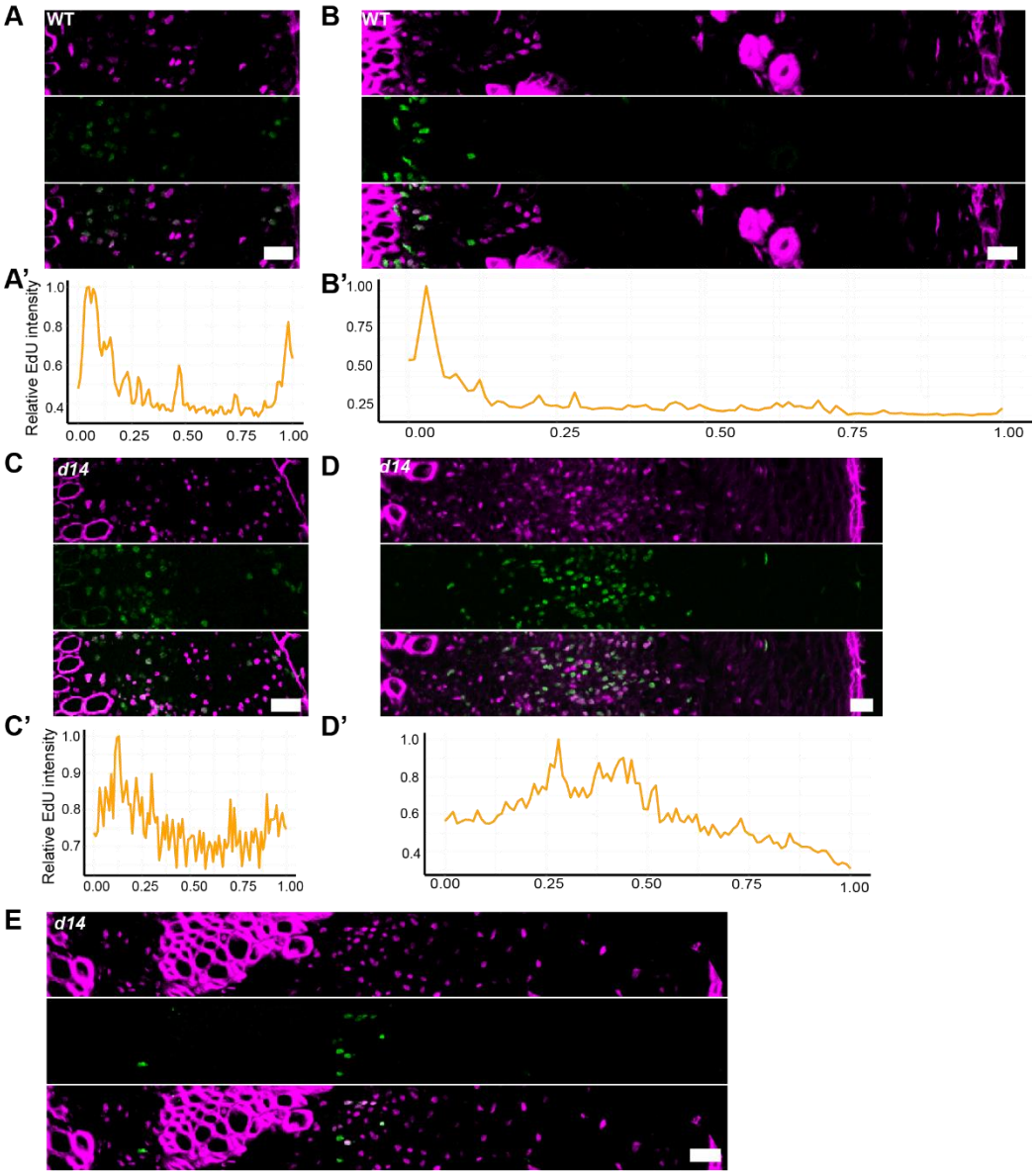

Figure 4.17: The cambium ring shifted in *d14* mutant at phase II.

A-E Hand-sectioned EdU stained hypocotyls from WT and *d14* at growth phase I (4 weeks old) (A, C) and phase II (40-46 DAG) (B, D, E). Plants were treated with 100 µM EdU solution, and incorporated for 3 days. EdU signals were detected using a confocal microscope and are shown in green. Hoechst33342-stained nuclei were visualized under UV light and are shown in magenta. Xylem cells were also visualized under UV light because of their auto-fluorescence due to lignin deposition.

A'-D' The profiles of relative EdU signal intensity at along the radial axis between the xylem border and the section periphery. The mean values of relative EdU signal

intensity were calculated from three replicates in (A, C), five replicates in (B) and six replicates in (D). Scale bars represent 20 μm.

According to a previous report, *PXY* and *SMXL5* gene activities define proximal and distal cambium domains, respectively (Shi et al. 2019). The shifted cambium position in *d14* mutant during phase II was confirmed by characterising promoter activities of *PXY* and *SMXL5* using the XY reporters (Shi et al. 2019) (Figure 4.18). The usual cambium position and organization defined by *PXY* and *SMXL5* promoter activities were observed in both 4-week-old wild type and *d14* plants (phase I) (Figure 4.18 A-F). The cambium position and organization were maintained in 6-week-old wild type plants. (Figure 4.18 G-I, I'). However, cambium organization demonstrated by *PXY* and *SMXL5* promoter activities was disrupted in 6-week-old *d14* plants, which profoundly surrounded the ectopic xylem but not normal xylem border (Figure 4.18 J-L, L'). Taken together, these results demonstrated that cambium activity of *d14* mutant was shifted during growth phase II, giving rise to ectopic xylem islands and disrupted concentric vascular cambium domains. These observations suggested that SL signaling is crucial for maintaining cambium organization.

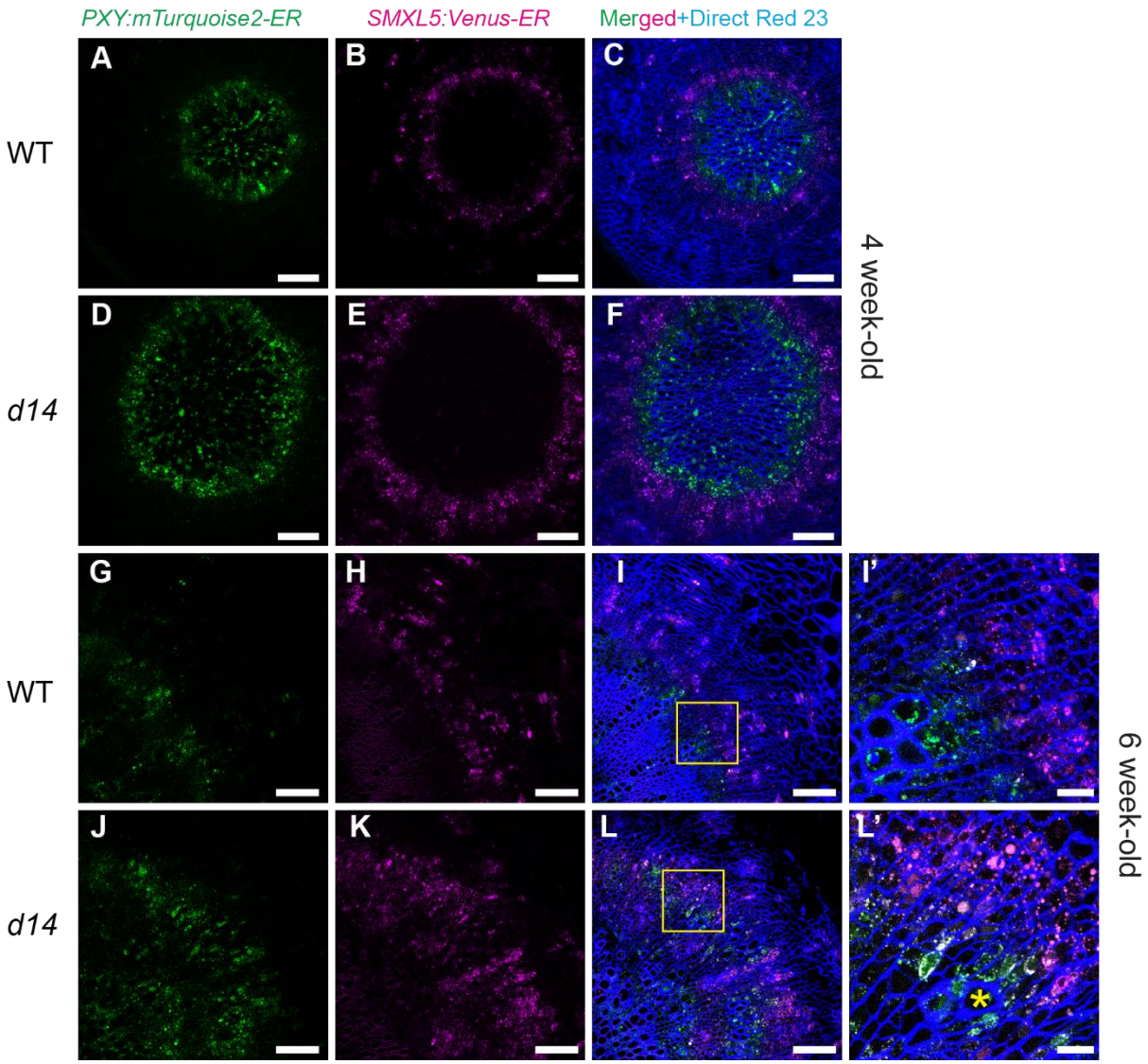

Figure 4.18: The cambium characterised by *SMXL5* and *PXY* promoter activities relocated in *d14* mutants during growth phase II

A-H Hypocotyl cross-sections of 15-20 cm tall plants carrying *PXY:mTurquoise2-ER_SMXL5:VENUS-ER* construct were visualized using a confocal microscope in WT (A, B, C, G, H, I) and *d14* (D, E, F, J, K, L). Cell walls were stained with Direct Red 23 (in blue). mTurquoise2 and Venus signal were shown in green and magenta, respectively. Yellow square frames mark the normal xylem border in (I) and ectopic xylem in (L) shown as close-ups in I' and L'. Yellow asterisk (*) marks the ectopic xylem. Scale bars represent 100 µm in (A-L) and 20 µm in (I', L').

4.2.3 The formation of ectopic xylem in *d14* mutants is independent from inflorescence bolting and enhanced shoot branching

The shift of cambium activity or the formation of ectopic xylem in *d14* mutants was only observed during growth phase II, which is accompanied by the bolting of the inflorescence stem. I thus reasoned that ectopic xylem formation is caused by the bolting event. To test my assumption, wild type and *d14* plants both were grown for six weeks in short day conditions in which bolting is suppressed. In parallel, other plants were kept in normal growth conditions in which they developed an inflorescence stem of around 15 cm (Figure 4.19 A, D). Hypocotyls of these plants were all harvested, sectioned and xylem was visualized based on its lignin-dependent auto-fluorescence under UV light. In wild type, the pattern of vascular tissues was very different comparing bolted and non-bolted plants. In non-bolted plants, only displaying xylem pattern generated at phase I, while the xylem cell layer massively occupied by fibres were missing (Figure 4.19 B, C). It is therefore that the phloem fibres were undetectable in non-bolting plants (Figure 4.19 B, C). By contrast, the unorganized xylem pattern showed no response to bolting and ectopic xylem generated in both cases (Figure 4.19 E, G), suggesting that the ectopic xylem occurred in *d14* mutant is independent of bolting event.

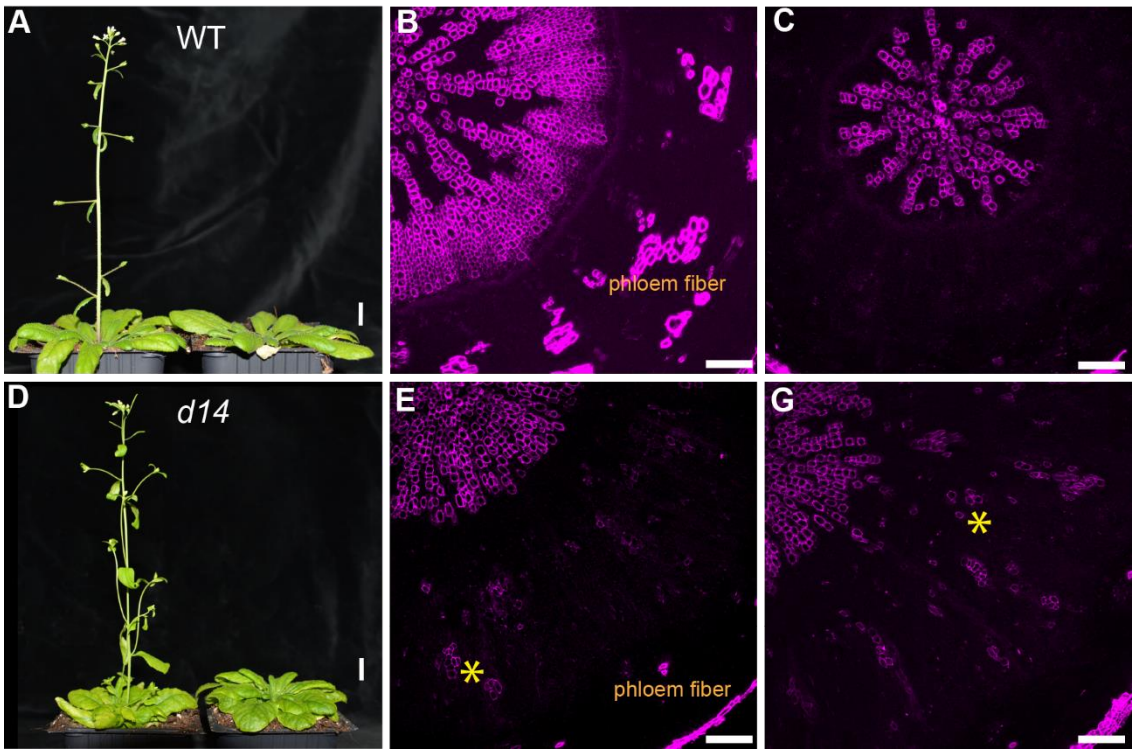

Figure 4.19: The formation of ectopic xylem in *d14* is independent from inflorescence bolting

A, D Representative pictures of above-ground tissues with bolted plants grown in SD conditions for six weeks and non-bolted plants grown in SD condition for three weeks and LD condition for another three weeks.

B, C, E, G Vascular tissue organization visualized in hand-sectioned hypocotyls analysed using a confocal microscope. Xylem and phloem fibres were visualized using the 405 nm laser based on the auto-fluorescence of lignin (in magenta). Hand-sectioned hypocotyl from a bolted wild type plant in (B) and from a non-bolted wild type plant in (C). Hand-sectioned hypocotyl from a bolted *d14* plant in (E) and from a non-bolted *d14* plant in (G). Yellow asterisks mark ectopic xylem. Scale bars represent 1 cm in (A, D) and 100 µm in (B, C, E G)

At growth phase II, the number of outgrown branches differed considerably between wild type and *d14* plants (Figure 4.20 A, B), raising a possibility that the ectopic xylem in *d14* mutant is a secondary effect of enhanced branching. To test this possibility, I analysed *brc1-2* mutants. BRANCHED1 (BRC1) is a key inhibitor of bud outgrowth and *brc1* mutants show an increased branch number relative to wild type

(Aguilar-Martínez et al. 2007). Confirming these observations, *brc1-2* mutants showed increased branching in my hands (Figure 4.20 A, B). However, the xylem pattern in *brc1-2* mutants was comparable to the pattern found in wild type (Figure 4.20 C, D). This result supported the disrupted xylem pattern in d14 is not caused by enhanced branches. (Figure 4.20 A, B, E).

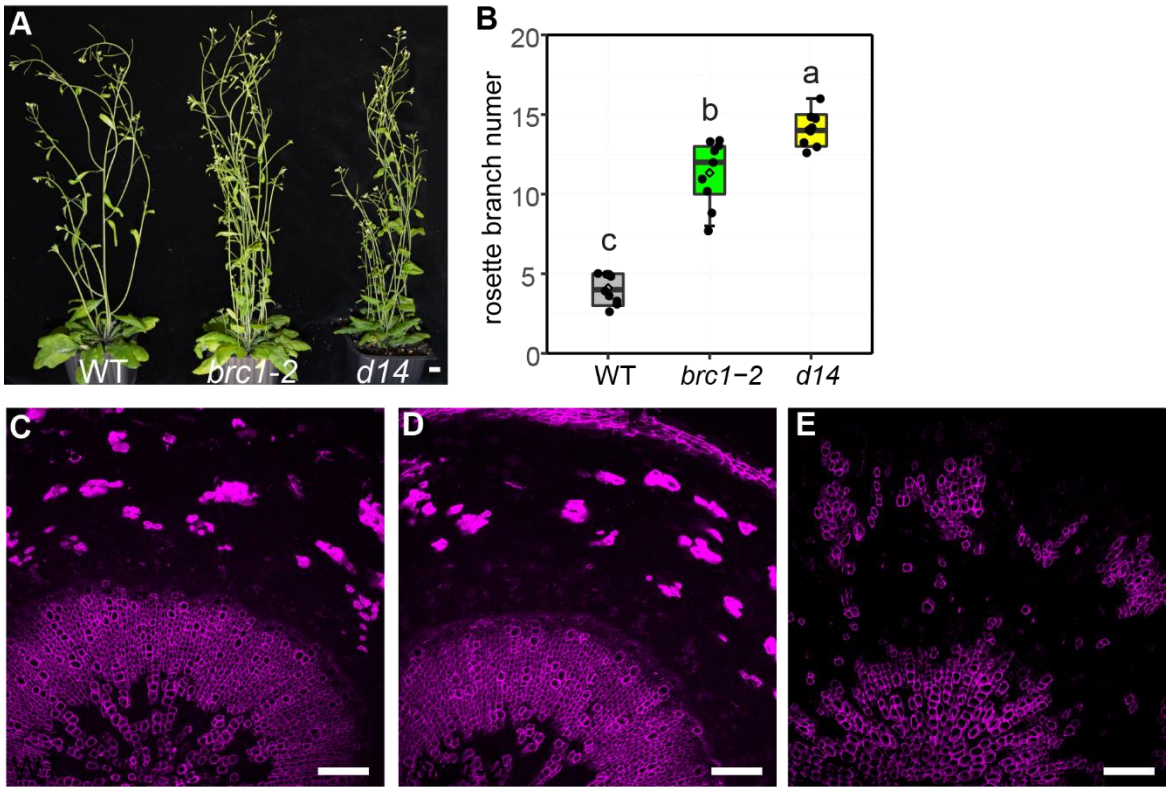

Figure 4.20: The ectopic xylem in *d14* mutant is not a secondary effect of enhanced branching

A The Picture depicts the above-ground tissues of 45-DAG WT, *brc1-2* and *d14*

B The number of outgrown branches was compared between WT, *brc1-2*, and *d14* plants (n=9). Statistical groups were indicated by letters and determined by a one-way ANOVA with post-hoc Tukey-HSD (95 % CI). Scale bars represent 1 cm in (A), and 100 µm in (C-E).

C-E Hypocotyl cross-sections from 45-DAG WT (C), *brc1-2* (D), and *d14* (E) plants were analysed using a confocal microscope. The lignified cell walls were visualized under UV light, by which the autofluorescence of lignin can be captured (in magenta).

4.2.4 High auxin signaling levels in the phloem region causes the formation of ectopic xylem in *d14*

According to a previous report, high levels of auxin signaling is sufficient to trigger the formation of ectopic xylem in phloem region (Smetana et al. 2019). As ectopic xylem occurred in the phloem region in *d14*, I speculated that the ectopic xylem is caused by enhanced auxin signaling levels. Therefore, the activity of the auxin response reporter *DR5revV2:EYFP-ER* (Brackmann et al. 2018) was determined in wild type and *d14* mutant plants. In wild type, high auxin response was observed in the xylem region, whereas very weak auxin response was detected in the phloem area (Figure 4.21 A, B). In comparison, in *d14* plants high auxin response was not only detected in the xylem region, but also found in the cells next to the ectopic xylem (Figure 4.21 C, D), proposing that a high auxin response accompanied the formation of ectopic xylem.

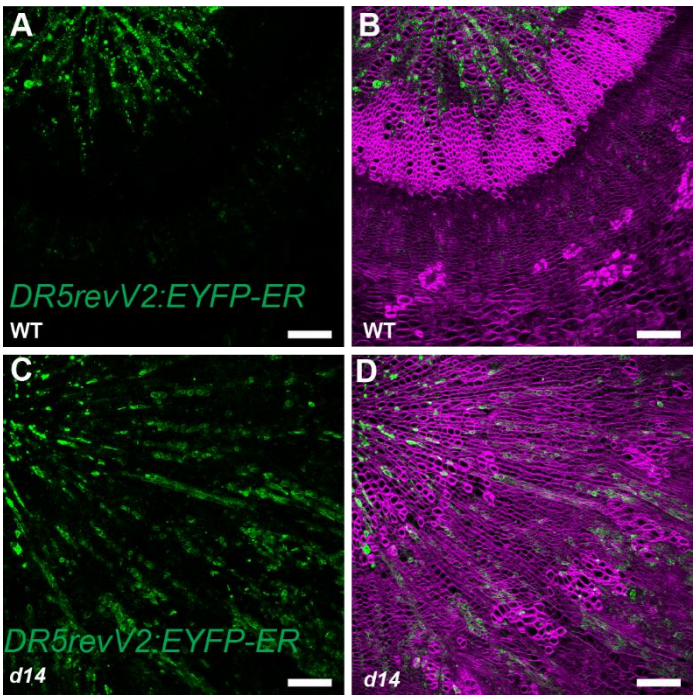

Figure 4.21: High auxin response accompanies ectopic xylem formation in *d14*

A-D Hypocotyl cross-sections from 15-20 cm tall WT (A, B) and *d14* (C, D) plants carrying the *DR5revV2:EYFP-ER* reporter were analysed using a confocal microscope. EYFP signals are shown in green. Cell walls were stained by Direct Red 23 (in magenta). Scale bars represent 100 μm.

To test if the high auxin response is the precondition for ectopic xylem formation, I repressed auxin signaling in phloem-related cells using a *SMXL5:Myc-GR-bdl* transgene specifically active in the phloem area. After two weeks of treatment, the above-ground organs and the xylem pattern in hypocotyls showed no difference comparing Dex- and mock-treated wild type plants (Figure 4.22 A-E). Similarly, the above-ground organs of *d14* mutants displayed no difference comparing Dex- and mock-treated plants (Figure 4.22 A). In contrast, the ectopic xylem in Dex-treated *d14* mutants was absent and the cell arrangement in the phloem region were completely restored back to the situation in wild type (Figure 4.22 F-I, G' and I'). This result strongly suggested that the formation of the ectopic xylem in *d14* mutants was caused by enhanced auxin signaling levels in the phloem region.

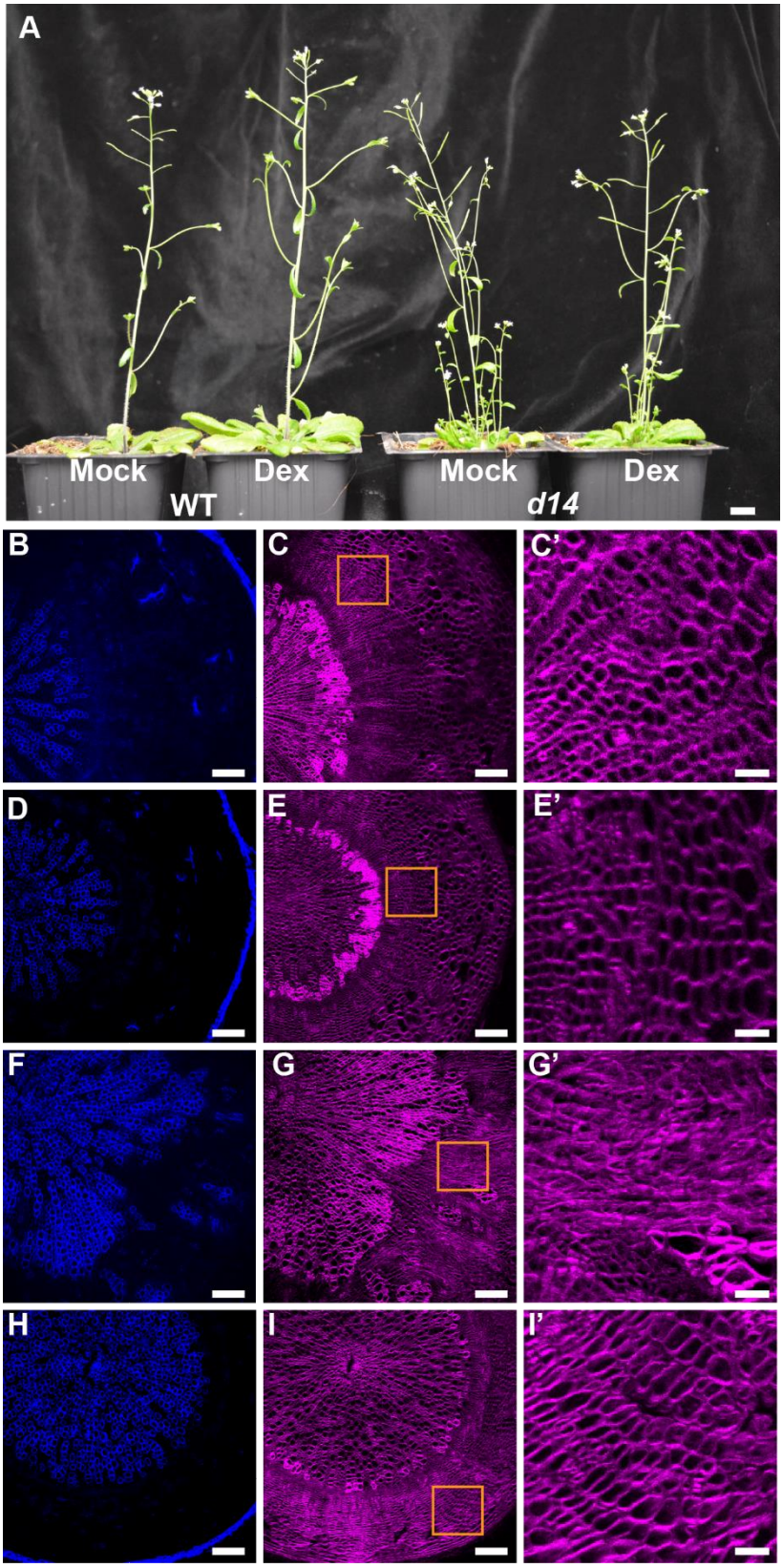

Figure 4.22: High auxin signaling causes the formation of ectopic xylem in *d14* mutants

A The above-ground habitus of plants carrying a *SMXL5:Myc-GR-bdl* transgene under Dex or mock treatment.

B-I Hypocotyl cross-sections of mock-treated WT (B, C), Dex-treated WT (D, E), mock-treated *d14* (F, G) and Dex-treated *d14* (H, I) plants carrying a *SMXL5:Myc-GR-bdl* transgene. The lignified cell walls were visualized under UV light, by which the autofluorescence of lignin can be captured (in blue). Cell walls were stained by Direct Red 23 and are shown in magenta.

C', E', G', I' Magnification of orange squared areas in phloem regions in (C, E, G, I).

4.2.5 SL signaling modulates radial vascular patterning via *MONOPTEROS*

The ectopic xylem occurred in *d14* mutants caused by high auxin response in phloem region. Meanwhile, ARFs as the effector of auxin response which regulate the transcription of auxin-responsive genes (Salehin et al. 2015). Therefore, the relationship between ARFs and the *d14* mutant phenotype was genetically analysed. MP has been proposed to be involved in xylem formation (Brackmann et al. 2018; Smetana et al. 2019). To test whether MP functions downstream of SL signaling in maintaining a concentric vascular patterning, I generated *d14;mp-S319* double mutants. Carrying a weak *MP* mutant allele, *mp-S319* plants display partially compromised flower initiation (Chung et al. 2019). Similar to the *mp-S319* single mutant, flower initiation in *d14;mp-S319* double mutants was also affected (Figure 4.23 A). Interestingly, the disruption of the concentric vascular organization which occurred in hypocotyls of *d14* single mutants was completely rescued in *d14* mutants carrying also the *mp-S319* allele (Figure 4.23 B, C, D, E). This observation demonstrated that the vascular defects in *d14* mutants was *MP*-dependent. In parallel, the *DR5revV2:YFP* reporter was introduced into the *d14;mp-S319* double mutant. With *MP* deficiency, the high auxin response in the phloem region usually

observed in *d14* single mutants was rescued (Figure 4.23 F, G, H, I), suggesting that the high auxin response was induced by enhanced *MP* activity. Taken together, I concluded that SL signaling is required for stabilizing concentric organization of vascular tissues and that this function depends on *MP*.

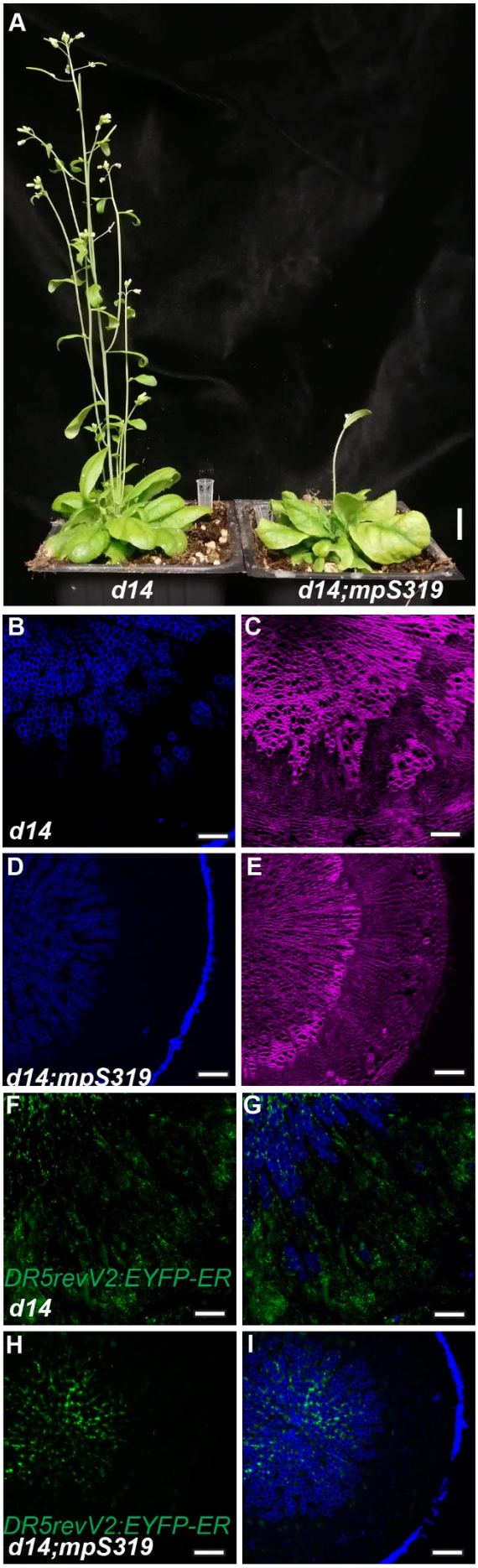

Figure 4.23: SL signaling determines concentric organization of vascular tissues via *MONOPTEROS*.

A The above-ground appearance of *d14* single and *d14;mp-S319* double mutants.

B-E Histological analysis of the xylem pattern in (B, D) and vascular pattern in (C, E) comparing 15-20 cm tall *d14* single and *d14;mp-S319* double mutants. Xylem pattern was visualized by the auto fluorescence of the lignin deposited in cell walls of xylem cells and is shown in blue. Direct Red 23 was used to stain cell walls and is shown in magenta.

F-I Hypocotyl cross-sections of *d14* single and *d14;mp-S319* double mutants carrying the *DR5revV2:EYFP-ER* transgene . EYFP signals are shown in green (F, H). Xylem pattern was analysed by using 405 nm laser to excite the autofluorescence of xylem-deposited lignin (in blue).

5 Discussion

Secondary xylem is an essential conduit for transporting water and minerals from roots throughout the plant; meanwhile, it constitutes a large part of the plant biomass on earth as a result of the deposition of cell-wall material. It is therefore important to investigate and understand the spatio-temporal regulation networks that control secondary xylem formation. In this study, I demonstrated novel roles of SL signaling in vascular development in *Arabidopsis thaliana*: SL signaling suppresses secondary vessel formation at xylem phase I and maintains the radial hypocotyl patterning at xylem phase II. During xylem phase I, SL signaling is highly associated with most of the differentiated tissues. In comparison, a relatively low SL signaling level is detected in developing vessels. With the deficiency of SL signaling, secondary vessel formation is evidently enhanced in *d14*, while an increase in secondary vessel number is found when enhancing auxin signaling in the *PXY* expression domain. Strikingly, the vessel number enhancement in *d14* mutants is alleviated by repressing auxin signaling in the *PXY* domain. At phase II, the disrupted radial hypocotyl patterning present in *d14* mutants is accompanied by an altered auxin response along the radial sequence of hypocotyl tissues. Importantly, the disrupted radial hypocotyl patterning is completely rescued when auxin signaling is repressed in the *SMXL5* expression domain or under *MP* deficiency conditions. This demonstrates that SL signaling is required for maintaining the radial hypocotyl patterning via regulating the radial auxin response pattern mainly mediated by MP.

5.1 A novel role of the core SL signaling pathway in secondary vessel formation

The core SL signaling pathway has been well defined in Arabidopsis. The pathway is mediated by SCF^{MAX2} and D14 proteins and depends on the degradation of SMXL proteins (Bennett et al. 2016; Soundappan et al. 2015; Wang et al. 2015). In this study, I showed that *d14* and *max2* mutants both display increments in vessel

number, vessel size, vessel area as well as vessel density, and that the enhanced vessel formation shown in *d14* is completely rescued to the level of *smxl6;7;8* triple mutants when *SMXL6*, *SMXL7* and *SMXL8* genes are deficient. This shows that the core SL signaling pathway suppresses vessel formation in the Arabidopsis hypocotyl. A notable feature of my genetic data is that the suppression of the *d14* phenotype by *SMXL6*, *SMXL7* and *SMXL8* deficiency often rescues the phenotype to the level of *smxl6;smxl7;smxl8*, meaning beyond wild type-like levels. Thus, rendering the phenotypes in *d14*;*smxl6;smxl7;smxl8* that are quantitively opposite to *d14*. For instance, vessel number and vessel area are ~50% less than wild type in *d14*;*smxl6;smxl7;smxl8*, while vessel size is ~25% less than wild type. Intriguingly, the above-mentioned phenotypes are also occurred in *D14* background, such that *smxl6;smxl7;smxl8* shows similar level with *d14*;*smxl6;smxl7;smxl8* in view of vessel number, area and size. Of note, similar suppression is also described in other actions of SL signaling. For instance, *max2* mutants have increased lateral root density than wild type, while lateral root density in *max2*;*smxl6;smxl7;smxl8* mutants display a ~50% decrease in lateral root density compared to wild type (Soundappan et al. 2015). As such, these results suggest that *SMXL6*, *SMXL7* and *SMXL8* are genetically epistatic to *D14*-mediated SL signaling, meaning that their mutation makes it irrelevant whether SL signaling is present or absent.

An inhibitory role of the core SL signaling pathway exists also in the context of other developmental process, such as axillary bud outgrowth, adventitious rooting, lateral root emergence, vascularization of leaves, and vasculature regeneration after wounding (Bennett et al. 2016; Soundappan et al. 2015; Wang et al. 2015; Rasmussen et al. 2012; Koltai 2015; Zhang et al. 2020). However, an inhibitory role of SL signaling during vessel formation has not yet been reported previously. Of note, *BRC1* functions downstream of the core SL signaling module and its absence results in a bushy phenotype comparable to that of *d14* mutants (Aguilar-Martínez et al. 2007; Wang et al. 2020a). However, I observed normal vessel formation in *brc1-2* mutants. It is thus likely that the enhanced vessel formation is not a secondary effect of the bushy growth habitus found in *d14* mutants. Moreover, these results indicate

that axillary bud outgrowth and vessel formation are regulated through distinct SMXL targets. SL signaling exerts a negative role in vessel formation, and the involvement of SLs in suppressing cell wall defects has been described previously (Ramírez et al. 2018; Ramírez and Pauly 2019). *trichome birefringence-like 29 (tbl29*) mutants show drastic xylem collapse in stems caused by the reduction of xylan *O*-acetylation levels (Xiong et al. 2013). Interestingly, the collapsed xylem pattern observed in *tbl29* is rescued to normal xylem morphology by *MAX3* and *MAX4* deficiency (Ramírez et al. 2018). *MAX3* and *MAX4* encode CCD7 and CCD8, respectively, which are key enzymes in SL biosynthesis (Sorefan et al. 2003; Booker et al. 2004), implying that the *tbl29*-triggered deficiency in xylem morphology is SL dependent. Moreover, *tbl29;max4* double mutants exhibit collapsed xylem after application of GR24, confirming the involvement of SLs in the collapsed xylem observed in *tbl29* mutants (Ramírez et al. 2018). Notably, SL-mutants also displayed enhanced vessel formation similar to that in *d14* mutants (data not shown). It is therefore possible that the enhanced vessel number in SL-mutants causes a reduction in hydraulic pressure, such that prevents xylem collapse shown in *tbl29* mutants.

5.1.1 SL signaling in the context of xylem regulation by other factors

The fact that SL signaling suppresses vessel formation is an important and promising discovery, which substantially contributes to the existing regulatory network of xylem regulation. To integrate this new finding into the existing regulatory network, it is pivotal to discuss the potential relationship between SL signaling and exiting factors in xylem regulation.

In my study, I showed that SL signaling is spatially associated with differentiated vascular tissues, but that the activities of the SL signaling-related genes *D14*, *SMXL6*, *SMXL7*, and *SMXL8* (except for *MAX2*) could hardly be detected in cambial cells in the hypocotyl. These results indicate that the suppression of vessel formation by SL signaling happens not via repressing the proliferation of cambium

cells. This conclusion can be supported by the similar stem cell number between *d14* and wild type found from snRNA-seq analysis. Instead, SL signaling rather seems to inhibit the differentiation of cambium-derived daughter cells into xylem-related cells, such that coordinates the allocation of cambium derivatives between phloem and xylem. It is supported by the increased xylem precursor cells and developing vessel cells in *d14* mutants; and decreased number in phloem precursor cells in *d14* mutants relative to wild type from the snRNA-seq analysis. An increased vessel formation via trans-differentiation of various cell types into xylem vessels is observed when *VND6* and/or *VND7* genes are ectopically expressed (Kubo et al. 2005). However, in *d14*, enhanced vessel formation is observed already at the very beginning of vessel development as revealed by the expression of known organizer genes of stem cell (*PXY*, *ATHB8*, *MP*) based on snRNA-seq and promoter activity analyses in developing vessels. *VND6* and *VND7* expressions are likely to simply induce the terminal differentiation of xylem vessels, as trans-differentiation only involves the deposition of SCW, while the cell shape of other cell types transforming into vessel cells maintains unchanged (Kubo et al. 2005; Smetana et al. 2019). These observations suggest that distinct mechanisms of vessel formation promotion exist between *d14* and *VND* genes. In addition, I found increased expression of *VND6* and *VND7* in *d14* mutants compared to wild type, implying that promotion of vessel formation in *d14* mutants probably requires the involvement of *VND6* and/or *VND7*

5.1.2 SL signaling in the context of xylem regulation by auxin

MP, as an auxin response transcription factor, whose mutation results in defective division in the provascular initial cells during embryogenesis, is tightly associated with vascular tissue formation (Hardtke and Berleth 1998). Auxin synthesis, transport, and signaling regulate the expression level of HD-ZIP III transcription factors thereby mediating the specification of xylem cells during primary

growth (Donner et al. 2009; Ursache et al. 2014). Interestingly, high and low activities of *HD-ZIP III* genes confer metaxylem and protoxylem specification, respectively (Carlsbecker et al. 2010). In particular, the expression of *ATHB8* in the protoxylem is reduced when interfering with PIN-mediated polar auxin transport through NPA treatment, leading to defective protoxylem specification (Bishopp et al. 2011). Moreover, MP directly binds a regulatory element in the promoter region of *ATHB8*, thus identifying *ATHB8* as a primary auxin response gene (Donner et al. 2009). Metaxylem formation in primary roots requires high *HD-ZIP III* expression, which is mediated by auxin synthesis (Ursache et al. 2014). Based on these observations, auxin transport, signaling and synthesis play important roles in the specification of the central xylem axis during primary root growth. This is not the case for SL signaling. As shown within this project, five-day-old *d14* mutants show normal primary xylem patterning and cell file numbers relative to wild type, which indicates that SL signaling plays a very limited role in xylem formation during primary root growth.

Unlike during primary growth, the role of SL signaling in vessel formation becomes evident during secondary growth. During secondary growth, I observed a vessel number increment in *d14* mutants relative to wild type at several time points, demonstrating an inhibitory role of SL signaling during wood formation in the hypocotyl. In this regard, it is important to mention that auxin signaling mediated by *MP*, *ARF7*, and *ARF19* transcription factors is likewise required for secondary vessel formation (Smetana et al. 2019). *MP*, *ARF7*, and *ARF19* function redundantly, which is revealed by the observation that *arf7;arf19* double mutants show a reduced vessel number relative to wild type, and additional vessel formation defects are detected when *MP* is knocked down in an *arf7;arf19* mutant background by the induction of an inducible artificial miRNA (Smetana et al. 2019). Interestingly, a similar secondary vessel reduction is found in quintuple *HD-ZIP III* mutants. Moreover, upon the reduction of *MP* transcript levels in *arf7;arf19* backgrounds, a downregulation of *HD-ZIP III* gene expression is observed. Therefore, auxin signaling mediated by the MP, ARF7 and ARF19 auxin response factors promotes secondary vessel formation in

roots, as it seems, mainly by regulating *HD-ZIP III* genes (Smetana et al. 2019). Along the same lines, I detected enhanced vessel formation in hypocotyls when I increased auxin signaling by expressing a gain-of-function version of *MP* in the *PXY* expression domain. In turn, a reduction of auxin signaling by a Dex-dependent *PXY*:*Myc-GR-bdl* transgene reduced vessel formation in my hands. In particular, the files of vessel elements which are successively produced by cambium stem cells usually found in wild type plants were broken in this case. Consistently, I observed a xylem patterning with random absence of vessel files in Dex-treated *PXY*:*Myc-GR-bdl* plants. Moreover, the vessel cells generated after Dex-induction were very small and similar in size to cambium stem cells. This effect is probably caused by premature differentiation of developing vessel elements. Under similar growth conditions, I found that the enhanced vessel number in *d14*;*PXY*:*Myc-GR-bdl* plants is alleviated after Dex-treatments. In addition, the smaller vessels that are normally detected in Dex-treated *PXY*:*Myc-GR-bdl* plants are hardly observed in Dex-treated *d14*;*PXY*:*Myc-GR-bd* plants. These results suggest that auxin signaling is crucial for the formation of secondary vessel elements in hypocotyls, and that the effects caused by repressing auxin signaling are weaker when SL signaling is deficient. It thus can be speculated that there are interconnected roles between SL and auxin signaling in maintaining proper secondary vessel formation.

Recently, it was demonstrated that SLs inhibit the formation of vasculature regeneration mediated by auxin transport and canalization (Zhang et al. 2020). Of note, auxin transport and canalization has also been proposed to be targeted by SL signaling in the context of shoot branching (Shinohara et al. 2013; Bennett et al. 2016). Combined with the observations that auxin transport and PIN1 levels in the plasma membrane of xylem parenchyma cells are increased in the inflorescence stem of SL signaling mutants (Bennett et al. 2016; Bennett et al. 2006). it can be hypothesized that the enhanced secondary vessel formation found in *d14* mutants is likely caused by an altered PIN1 accumulation in xylem parenchyma cells. According to previous reports, auxin transport capacity is severely dampened along the inflorescence stem in *pin1-613* mutants, and the enhanced auxin transport observed

in *d14* can be suppressed by *PIN1* deficiency (Bennett et al. 2016; Agusti et al. 2011). As such, one could answer the question whether PIN1 accumulation is the reason for increased vessel formation in *d14* mutants by simply analysing vessel morphology in *pin1-613, d14;pin1-613,* and *d14* mutants. However, *PIN1* expression is regulated by MP during secondary vein formation (Scarpella et al. 2006; Wenzel et al. 2007), which opens up the possibility that increased PIN1 accumulation in *d14* mutants is caused by increased MP activity. Therefore, I generated and analysed a *d14;mp-S319* double mutant. As a weak *mp* allele, *mpS-319* only displays defects in flower initiation (Cole et al. 2009). However, *d14;mp-S319* double mutants showed no clear difference in secondary vessel formation compared to *d14* mutants. Considering the redundancy of *MP* with *ARF7* and *ARF19* in secondary vessel formation (Smetana et al. 2019), I expect that higher order *arf* and *d14* mutants and, ultimately, *d14;mp-S319;arf7;arf19* quadruple mutants are required to tackle this aspect.

5.2 The ATHB8/ACL5–BUD2 transcription module

It has been demonstrated that thermospermine produced by ACL5 and BUD2 is one of the factors contributing to the regulation of xylem differentiation in Arabidopsis (Muñiz et al. 2008; Ge et al. 2006; Knott et al. 2007). Loss-of-function mutations of *ACL5* and *BUD2* both result in more vessels in vascular tissues (Muñiz et al. 2008; Ge et al. 2006). Interestingly, expression of *ACL5* and *BUD2* both can be promoted by auxin (Milhinhos et al. 2013; Tong et al. 2014; Vera-Sirera et al. 2015; Ge et al. 2006), while exogenous application of thermospermine in turn suppresses auxin-dependent xylem differentiation (Yoshimoto et al. 2012). Moreover, ATHB8 directly promotes the expression of *ACL5* and *BUD2* via a cis-regulatory element (Baima et al. 2014). Reciprocally, ACL5 represses the expression of *HD–ZIP III* and auxin signaling genes by an unknown thermospermine-dependent mechanism (Baima et al. 2014). In this way, a negative feedback regulation of auxin signaling

mediated by the ATHB8/ACL5–BUD2 transcriptional module is proposed to fine-tune vessel production (Baima et al. 2014). Interestingly, several differences are found in vessel morphology and development between *d14* and *acl5* mutants in spite of both show increased vessel number. Firstly, enhanced and distorted vessel formation is already apparent in 7-day-old *acl5* roots (Muñiz et al. 2008), while *d14* produces normal root xylem patterning at this stage. Moreover, the additional vessel elements in *d14* mutants are larger than those in wild type but smaller in *acl5* mutants (Muñiz et al. 2008). Importantly, vessel elements can be enlarged by increasing the duration of vessel differentiation in *Zinnia* xylogenic cultures (Muñiz et al. 2008). As such, it is possible that a longer duration of vessel differentiation exists in *d14* mutants relative to wild type. Baima et al. (2014) further demonstrated that the formation of additional veins in *acl5* leaves is mainly caused by the accumulation of HD-ZIPIII proteins. In agreement with this conclusion, *ATHB8* has been shown to promote xylem differentiation based on the fact that the overproduction of ATHB8 leads to an excess of secondary vessel formation (Baima et al. 2001). However, the following fact argues that vessel defects in *acl5* are not simply caused by an ATHB8 overproduction: Hypocotyls of 35-day-old *acl5* mutants are substantially thinner than wild type and show a complete absence of xylem fibres (Muñiz et al. 2008). By contrast, *ATHB8* overexpressing lines show a much larger diameter than wild type at the hypocotyl-root junction at similar stage (Baima et al. 2001). Unlike *acl5*, *d14* shows continuous secondary growth, and vessel formation enhancement in 35-day-old hypocotyl is still apparent compared with wild type. As such, enhanced vessel formation in *d14* mutants can also be likely caused by the overproduction of ATHB8.

5.3 SL signaling pattern along the radial sequence of vascular tissues

It has been proposed that a local auxin response maximum is present in the xylem domain, and tapers off towards the cambium where a moderate level of signaling is pivotal for cambium activity (Brackmann et al. 2018; Smetana et al. 2019). Compared to auxin signaling, however, the spatial distribution of SL signaling

was unknown. In this study, I established the spatial distribution of SL signaling along the radial sequence of vascular tissues in the hypocotyl. According to this, the level of SL signaling peaks in the xylem parenchyma, and a signaling gradient exists across xylem parenchyma, developing vessel and cambium cells from high to low levels. Meanwhile, SL signaling shows an overall higher level within the phloem region.

5.3.1 High SL signaling levels in most differentiated vascular tissues

I found high promoter activities of *D14*, *SMXL6*, *SMXL7* and *SMXL8* genes in differentiated vascular tissues, whereas their promoter activities can hardly be detected in the cambium region. However, MAX2 is an important component of both SL and KAR signaling (Nelson et al. 2011; Waters et al. 2012) and I detected promoter activity of *MAX2* in all vascular tissues. Collectively, SL signaling is high in most of the differentiated vascular tissues. The high activity of SL signaling in differentiated vascular tissues is confirmed by quantitative analysis of the Strigo-D2 sensor. Using this ratiometric sensor (Song et al. 2022), I observed high SL signaling levels in most differentiated tissues, whereas in the cambium zone SL signaling level were relatively low.

So far, the molecular control of the spatial distribution of SL signaling in the radial sequence of the hypocotyl is poorly understood. However, it could be substantiated by reported crosstalk between SLs and auxin. The auxin-biosynthesis genes *YUC3* and *YUC5* can be repressed by exogenous application of SLs, indicating that SLs or SL signaling represses auxin biosynthesis (Wang et al. 2020a). Nevertheless, it has been demonstrated that the activities of almost all *YUCCA* genes and the major bioactive auxin (IAA) peak in the middle of the cambium zone, where actively dividing cambium cells are located (Immanen et al. 2016; Uggla et al. 1996; Tuominen et al. 1997; Uggla et al. 1998). It thus indicates that SL signaling in

the cambium should be low indicated by high activities of auxin-biosynthesis genes. The fact that SLs inhibit auxin transport and canalization, and a 30% increase in PIN1 levels occurs in xylem parenchyma cells when SL signaling is not functional (Bennett et al. 2016; Zhang et al. 2020) supports an active SL signaling in xylem parenchyma cells.

5.3.2 Moderate SL signaling levels in developing vessel elements

The expression patterns of *SMXL6*, *SMXL7*, and *SMXL8* are generally comparable in vascular tissues, however, only *SMXL7* shows a clear expression in developing vessel cells. Importantly, transgenic lines expressing a stabilized SMXL7^{d53} protein containing the same mutation as being present in the gain-of-function *d53* allele in rice (Liang et al. 2016), display similar vessel enhancements as found in *d14* mutants. These results therefore indicate that the SMXL7 protein promotes vessel formation in a cell-autonomous manner. However, only moderate SL signaling levels are detected in developing vessels according to the Strigo-D2 sensor. As such, there is an SL signaling gradient from xylem parenchyma, over developing vessels, to the cambium where signaling levels are very low. In addition, according to my snRNA-Seq data, some known vascular marker genes show massive expression in developing vessel cells, such as *MP, ATHB8*, *PXY*, *ACL5, VND6*, and *VND7*. As such, auxin signaling mediated by MP should be high in developing vessels, thus promoting xylem identity (Smetana et al. 2019; Donner et al. 2009). SL signaling suppresses the formation of secondary vessels, it is therefore possible that the moderate SL signaling in developing vessels is required to prevent premature xylem differentiation.

5.4 Spatially restriction of cambium zone by SL signaling during phase II

A disrupted radial hypocotyl pattern is observed in *d14* mutants during xylem phase II, while the radial pattern is well organized in several successive cylindrical rings at phase I. In addition to be present in the normal xylem region, cells with xylem-like identity occur in the phloem region during phase II in *d14*, whereas cells with phloem identity are restricted to the normal phloem zone as in wild type. Interestingly, similar ectopic xylem islands are found in tap roots in sugar beet (*Beta vulgaris* L.) (Jammer et al. 2020), demonstrating the existence of ectopic xylem islands in plants in a natural context. Strikingly, I detected massively proliferating cells by EdU staining in areas surrounding the ectopic xylem. By contrast, only certain cells located in the cambium domain were stained by EdU in wild type. This result suggests that cambium activity is shifted to the phloem region in *d14* mutants. The ectopic xylem always appears together with EdU positive cells, but the opposite is not the case. This indicates the ectopic xylem differentiates from EdU positive, i.e. dividing, cells. However, the origin of the EdU positive cells in the phloem region is still unclear. One assumption is that EdU positive cells originate from phloem cells by dedifferentiation. Alternatively, normal cambium stem cells may divide but cease differentiation until being located in the phloem region. Of note, a spatially interspersed xylem and phloem vascular pattern is also observed in PXY-CLE41 module-related mutants (Fisher and Turner 2007; Yang et al. 2020), which phloem tissues extend almost to hypocotyl centres. In addition, the strict spatial separation of phloem and xylem can be disturbed when *CLE41* is ectopically expressed in the xylem domain (Etchells and Turner 2010). I therefore analysed the expression pattern of *CLE41* in wild type and *d14* hypocotyls. Similar to wild type, I found expression of *CLE41* only in the phloem region (data not shown), suggesting that the disturbed spatial separation of xylem and phloem in *d14* is not caused by altered *CLE41* expression.

5.4.1 MP mediated auxin signaling in the phloem region

My work demonstrates that SL signaling modulates radial vascular patterning via MP-mediated auxin signaling. This is supported by three observations: (1) the ectopic xylem occurring in *d14* is accompanied by a high auxin response in the phloem region; (2) ectopic xylem formation found in *d14* can be suppressed when auxin signaling is repressed by the stabilized *bdl* protein expressed in the phloem area; (3) the ectopic xylem found in *d14* is fully repressed when MP activity is abolished. In line with this conclusion, when the *MPΔIII/IV* gain-of-function protein is conditionally expressed in the phloem region, an ectopic vascular organizer and, subsequently, ectopic xylem is formed in roots, showing that MP is sufficient for the formation of an ectopic organizer and of ectopic xylem (Smetana et al. 2019). Of note, MP-mediated auxin signaling is required, but not sufficient, for the initiation of vascular identity in the embryo (Smit et al. 2020). Interestingly, the high auxin response in the phloem is also recovered to wild-type level with the abolishment of MP, whereas the high auxin response in the xylem region is not evidently affected. This observation suggests that MP and no other ARFs contribute to the high auxin response in the *d14* phloem region. This therefore brings up the question whether the expression of *MP* is promoted when SL signaling is deficient. Indeed, I detected strong *MP* activity in areas surrounding the ectopic xylem islands in *d14* mutants (preliminary data). By contrast, *MP* activity is hardly detected in the wild type phloem region. It is thus reasonable to think that SL signaling is required for repressing *MP* expression in the wild type phloem. Given the fact that complex crosstalk exists between SL and auxin signaling, and that there is a positive feedback loop consisting of auxin-MP-ATHB8-PIN1 in vascular stem cells establishment (Scarpella et al. 2006; Donner et al. 2009; Scarpella et al. 2010), more research is needed to characterize the interaction between SL signaling and *MP* activity.

5.4.2 Why does ectopic xylem only appear during xylem phase II?

A phase switch occurs during secondary xylem development in Arabidopsis, and xylem composition and production rate display remarkable differences between phase I and II (Chaffey et al. 2002; Ragni and Hardtke 2014). It is thus likely that different regulatory networks are required for xylem generation during phase I and II and it is possible that SL signaling is important only during xylem phase II for repressing *MP* expression in the phloem. The differences of expression patterns of SL signaling-related components are very minor between phase I and phase II (data not shown). Thus, the possibility that altered SL signaling domains cause ectopic xylem emergence during phase II is rather unlikely.

5.5 Speculating about a SMXL7-ATHB8 transcriptional module

In Arabidopsis, SMXL6, SMXL7 and SMXL8 function as mediators of SL signaling in different contexts, such as shoot branching, lateral root density, leaf morphology (Soundappan et al. 2015; Gomez-Roldan et al. 2008; Umehara et al. 2008; Rasmussen et al. 2012; Kapulnik et al. 2011; Yamada et al. 2014; Ueda and Kusaba 2015). Since the activity of *SMXL6*, *SMXL7* and *SMXL8* genes are all strongly detected in vascular tissues, it is possible that *SMXL6*, *SMXL7* and *SMXL8* function redundantly during secondary vessel formation. However, only the activity of *SMXL7* but not *SMXL6* and *SMXL8* are clearly detected in developing vessel cells, indicating that *SMXL7* plays a dominant role in vessel formation. A dominant role of *SMXL7* is also demonstrated in the context of branching by the observation that *smxl6;8;max2* mutants only show a slight decrease in branching compared to *max2* mutants (Soundappan et al. 2015). Indeed, when a stabilized SMXL7 protein is expressed under the control of its native promoter, a prominent vessel enhancement, reminiscent to that shown in *d14* mutants is observed. Interestingly, the expression of *ATHB8* is clearly observed in developing vessel elements in Arabidopsis hypocotyls as revealed by a *ATHB8::GUS* reporter (Ilegems et al. 2010). In line with this result, the expression of *ATHB8* is strong in the developing vessel cluster in my snRNA-Seq

sequencing. Therefore, both *SMXL7* and *ATHB8* are expressed in developing vessel cells in the hypocotyl. Based on this observation, I identified genes co-expressed with SMXL7 via evaluating the Pearson correlation coefficient for my snRNA-Seq data (refer to (Yang et al. 2021)). Strikingly, *ATHB8* is on the list of the top overlapped 22 genes in wild type and *d14* ranked according to the correlation value from high to low. Therefore, I hypothesize that proper secondary vessel formation demands the concerted action of SL and auxin signaling: SMXL7 as a positive regulator of *ATHB8* or other HD-ZIP III genes, and the degradation of SMXL7 upon SL signaling consequently would suppress vessel formation via repressing HD-ZIP III genes; meanwhile MP, ARF7 and ARF19-mediated auxin signaling promotes expression of HD-ZIP III genes to enhance xylem formation. According to this model, HD-ZIP III genes function as common targets of auxin and SL signaling. However, it is generally considered that SMXL6, SMXL7 and SMXL8 act as transcriptional repressors, and the following facts challenge the positive regulation of *ATHB8* by SMXL7. Firstly, SMXL7 has been recently demonstrated to act as transcription factor, which binds directly to the promoters of *SMXL6*, *SMXL7* and *SMXL8* to inhibit their expression (Wang et al. 2020a). Secondly, it has been proposed that SMXL6, SMXL7 and SMXL8 function as transcriptional repressors by interacting with other transcription factors, as well as with the transcriptional corepressors TOPLESS (TPL) and TPL RELATED (TPR) (Waters et al. 2017; Jiang et al. 2013; Zhou et al. 2013; Soundappan et al. 2015; Wang et al. 2015; Song et al. 2017). Nevertheless, SMXL7 may still promote the expression of *ATHB8* by interacting with other transcriptional regulators as revealed by the co-expression analysis that a gene encodes a transcriptional activator co-expressed with SMXL7.

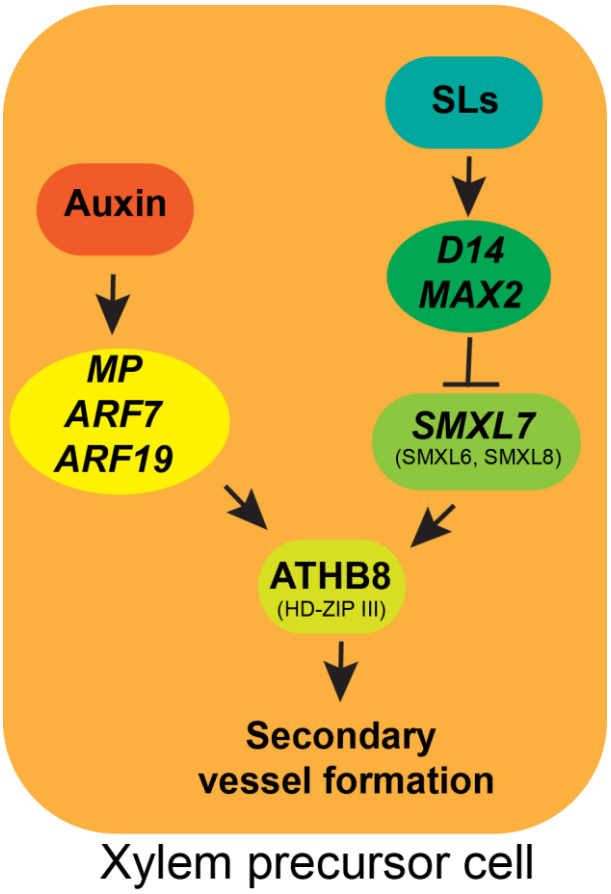

Figure 5.1 A possible regulation network for secondary vessel formation in hypocotyl
Shown are schematic representations of a possible regulation network for secondary xylem formation. Auxin promotes secondary vessel formation by positively regulating *ATHB8* via MP (ARF7 and ARF19). Meanwhile SL signaling suppresses vessel formation by repressing expression of *ATHB8* via SMXL7 (SMXL6, SMXL8).

6 List of publications

Co-first authorships:

Strigo-D2—a bio-sensor for monitoring spatio-temporal strigolactone signaling patterns in intact plants **(2021)** Changzheng Song*, Jiao Zhao*, Marjorie Guichard, Dongbo Shi, Guido Grossmann, Christian Schmitt, Virginie Jouannet, Thomas Greb Plant Physiology

In preparation:

- SL signaling suppresses secondary vessel formation (working title)
- SL signaling maintains radial hypocotyl patterning via MP mediated auxin signaling (working title)

7 References

Abe S, Sado A, Tanaka K, Kisugi T, Asami K, Ota S, Kim HI, Yoneyama K, Xie X, Ohnishi T (2014) Carlactone is converted to carlactonoic acid by MAX1 in Arabidopsis and its methyl ester can directly interact with AtD14 in vitro. Proceedings of the National Academy of Sciences 111 (50):18084-18089

Absmanner B, Stadler R, Hammes UZ (2013) Phloem development in nematode-induced feeding sites: the implications of auxin and cytokinin. Frontiers in plant science 4:241

Aguilar-Martínez JA, Poza-Carrión C, Cubas P (2007) Arabidopsis BRANCHED1 acts as an integrator of branching signals within axillary buds. The Plant Cell 19 (2):458-472

Agusti J, Herold S, Schwarz M, Sanchez P, Ljung K, Dun EA, Brewer PB, Beveridge CA, Sieberer T, Sehr EM (2011) Strigolactone signaling is required for auxin-dependent stimulation of secondary growth in plants. Proceedings of the National Academy of Sciences 108 (50):20242-20247

Akiyama K, Matsuzaki K-i, Hayashi H (2005) Plant sesquiterpenes induce hyphal branching in arbuscular mycorrhizal fungi. Nature 435 (7043):824-827

Al-Babili S, Bouwmeester HJ (2015) Strigolactones, a novel carotenoid-derived plant hormone. Annual review of plant biology 66:161-186

Alder A, Jamil M, Marzorati M, Bruno M, Vermathen M, Bigler P, Ghisla S, Bouwmeester H, Beyer P, Al-Babili S (2012) The path from β-carotene to carlactone, a strigolactone-like plant hormone. Science 335 (6074):1348-1351

Arite T, Iwata H, Ohshima K, Maekawa M, Nakajima M, Kojima M, Sakakibara H, Kyozuka J (2007) DWARF10, an RMS1/MAX4/DAD1 ortholog, controls lateral bud outgrowth in rice. The Plant Journal 51 (6):1019-1029

Arite T, Umehara M, Ishikawa S, Hanada A, Maekawa M, Yamaguchi S, Kyozuka J (2009) d14, a strigolactone-insensitive mutant of rice, shows an accelerated outgrowth of tillers. Plant and Cell Physiology 50 (8):1416-1424

Baima S, Forte V, Possenti M, Peñalosa A, Leoni G, Salvi S, Felici B, Ruberti I, Morelli G (2014) Negative feedback regulation of auxin signaling by ATHB8/ACL5–BUD2 transcription module. Molecular plant 7 (6):1006-1025

Baima S, Possenti M, Matteucci A, Wisman E, Altamura MM, Ruberti I, Morelli G (2001) The Arabidopsis ATHB-8 HD-zip protein acts as a differentiation-promoting transcription factor of the vascular meristems. Plant physiology 126 (2):643-655

Ben-Targem M, Ripper D, Bayer M, Ragni L (2021) Auxin and gibberellin signaling cross-talk promotes hypocotyl xylem expansion and cambium homeostasis. Journal of Experimental Botany 72 (10):3647-3660

Bennett T, Leyser O (2014) Strigolactone signalling: standing on the shoulders of DWARFs. Current opinion in plant biology 22:7-13

Bennett T, Liang Y, Seale M, Ward S, Müller D, Leyser O (2016) Strigolactone regulates shoot development through a core signalling pathway. Biology Open 5 (12):1806-1820

Bennett T, Sieberer T, Willett B, Booker J, Luschnig C, Leyser O (2006) The Arabidopsis MAX pathway controls shoot branching by regulating auxin transport. Current Biology 16 (6):553-563

Bishopp A, Help H, El-Showk S, Weijers D, Scheres B, Friml J, Benková E, Mähönen AP, Helariutta Y (2011) A mutually inhibitory interaction between auxin and cytokinin specifies vascular pattern in roots. Current Biology 21 (11):917-926

Björklund S, Antti H, Uddestrand I, Moritz T, Sundberg B (2007) Cross-talk between gibberellin and auxin in development of Populus wood: gibberellin stimulates polar auxin transport and has a common transcriptome with auxin. The Plant Journal 52 (3):499-511

Booker J, Auldridge M, Wills S, McCarty D, Klee H, Leyser O (2004) MAX3/CCD7 is a carotenoid cleavage dioxygenase required for the synthesis of a novel plant signaling molecule. Current biology 14 (14):1232-1238

Boyer F-D, de Saint Germain A, Pillot J-P, Pouvreau J-B, Chen VX, Ramos S, Stévenin A, Simier P, Delavault P, Beau J-M (2012) Structure-activity relationship studies of strigolactone-related molecules for branching inhibition in garden pea: molecule design for shoot branching. Plant physiology 159 (4):1524-1544

Brackmann K, Qi J, Gebert M, Jouannet V, Schlamp T, Grünwald K, Wallner E-S, Novikova DD, Levitsky VG, Agustí J (2018) Spatial specificity of auxin responses coordinates wood formation. Nature communications 9 (1):1-15

Braun N, de Saint Germain A, Pillot J-P, Boutet-Mercey S, Dalmais M, Antoniadi I, Li X, Maia-Grondard A, Le Signor C, Bouteiller N (2012) The pea TCP transcription factor PsBRC1 acts downstream of strigolactones to control shoot branching. Plant physiology 158 (1):225-238

Brewer PB, Dun EA, Ferguson BJ, Rameau C, Beveridge CA (2009) Strigolactone acts downstream of auxin to regulate bud outgrowth in pea and Arabidopsis. Plant physiology 150 (1):482-493

Brewer PB, Dun EA, Gui R, Mason MG, Beveridge CA (2015) Strigolactone inhibition of branching independent of polar auxin transport. Plant physiology 168 (4):1820-1829

Brewer PB, Yoneyama K, Filardo F, Meyers E, Scaffidi A, Frickey T, Akiyama K, Seto Y, Dun EA, Cremer JE (2016) LATERAL BRANCHING OXIDOREDUCTASE acts in the final stages of strigolactone biosynthesis in Arabidopsis. Proceedings of the National Academy of Sciences 113 (22):6301-6306

Bu Q, Lv T, Shen H, Luong P, Wang J, Wang Z, Huang Z, Xiao L, Engineer C, Kim TH (2014) Regulation of drought tolerance by the F-box protein MAX2 in Arabidopsis. Plant Physiology 164 (1):424-439

Caño-Delgado A, Yin Y, Yu C, Vafeados D, Mora-García S, Cheng J-C, Nam KH, Li J, Chory J (2004) BRL1 and BRL3 are novel brassinosteroid receptors that function in vascular differentiation in Arabidopsis.

Carlsbecker A, Lee J-Y, Roberts CJ, Dettmer J, Lehesranta S, Zhou J, Lindgren O, Moreno-Risueno MA, Vatén A, Thitamadee S (2010) Cell signalling by

microRNA165/6 directs gene dose-dependent root cell fate. Nature 465 (7296):316-321

Cayla T, Batailler B, Le Hir R, Revers F, Anstead JA, Thompson GA, Grandjean O, Dinant S (2015) Live imaging of companion cells and sieve elements in Arabidopsis leaves. PloS one 10 (2):e0118122

Chaffey N, Cholewa E, Regan S, Sundberg B (2002) Secondary xylem development in Arabidopsis: a model for wood formation. Physiologia plantarum 114 (4):594-600

Chehrehasa F, Meedeniya AC, Dwyer P, Abrahamsen G, Mackay-Sim A (2009) EdU, a new thymidine analogue for labelling proliferating cells in the nervous system. Journal of neuroscience methods 177 (1):122-130

Chevalier F, Nieminen K, Sánchez-Ferrero JC, Rodríguez ML, Chagoyen M, Hardtke CS, Cubas P (2014) Strigolactone promotes degradation of DWARF14, an α/β hydrolase essential for strigolactone signaling in Arabidopsis. The Plant Cell 26 (3):1134-1150

Chung Y, Zhu Y, Wu M-F, Simonini S, Kuhn A, Armenta-Medina A, Jin R, Østergaard L, Gillmor CS, Wagner D (2019) Auxin response factors promote organogenesis by chromatin-mediated repression of the pluripotency gene SHOOTMERISTEMLESS. Nature communications 10 (1):1-11

Cole M, Chandler J, Weijers D, Jacobs B, Comelli P, Werr W (2009) DORNROSCHEN is a direct target of the auxin response factor MONOPTEROS in the Arabidopsis embryo.

Cook C, Whichard LP, Turner B, Wall ME, Egley GH (1966) Germination of witchweed (Striga lutea Lour.): isolation and properties of a potent stimulant. Science 154 (3753):1189-1190

Crawford S, Shinohara N, Sieberer T, Williamson L, George G, Hepworth J, Müller D, Domagalska MA, Leyser O (2010) Strigolactones enhance competition between shoot branches by dampening auxin transport. Development 137 (17):2905-2913

Cui X, Ge C, Wang R, Wang H, Chen W, Fu Z, Jiang X, Li J, Wang Y (2010) The BUD2 mutation affects plant architecture through altering cytokinin and auxin responses in Arabidopsis. Cell research 20 (5):576-586

Czarnecki O, Yang J, Weston DJ, Tuskan GA, Chen J-G (2013) A dual role of strigolactones in phosphate acquisition and utilization in plants. International journal of molecular sciences 14 (4):7681-7701

De Rybel B, Adibi M, Breda AS, Wendrich J, Smit ME, Novák O, Yamaguchi N, Yoshida S, Van Isterdael G, Palovaara J, Nijsse B, Boekschoten MV, Hooiveld G, Beeckman T, Wagner D, Ljung K, Fleck C, Weijers D (2014) Integration of growth and patterning during vascular tissue formation in Arabidopsis. Science 345 (6197):1255215

De Rybel B, Mähönen AP, Helariutta Y, Weijers D (2016) Plant vascular development: from early specification to differentiation. Nature reviews Molecular cell biology 17 (1):30-40

de Saint Germain A, Clavé G, Badet-Denisot M-A, Pillot J-P, Cornu D, Le Caer J-P,

Burger M, Pelissier F, Retailleau P, Turnbull C (2016) An histidine covalent receptor and butenolide complex mediates strigolactone perception. Nature Chemical Biology 12 (10):787-794

Domagalska MA, Leyser O (2011) Signal integration in the control of shoot branching. Nature Reviews Molecular Cell Biology 12 (4):211-221

Donner TJ, Sherr I, Scarpella E (2009) Regulation of preprocambial cell state acquisition by auxin signaling in Arabidopsis leaves. Development 136 (19):3235-3246

Drummond RS, Martínez-Sánchez NM, Janssen BJ, Templeton KR, Simons JL, Quinn BD, Karunairetnam S, Snowden KC (2009) Petunia hybrida CAROTENOID CLEAVAGE DIOXYGENASE7 is involved in the production of negative and positive branching signals in petunia. Plant physiology 151 (4):1867-1877

Dun EA, de Saint Germain A, Rameau C, Beveridge CA (2012) Antagonistic action of strigolactone and cytokinin in bud outgrowth control. Plant physiology 158 (1):487-498

Dupuy L, Mackenzie J, Haseloff J (2010) Coordination of plant cell division and expansion in a simple morphogenetic system. Proceedings of the National Academy of Sciences 107 (6):2711-2716

Etchells JP, Provost CM, Mishra L, Turner SR (2013) WOX4 and WOX14 act downstream of the PXY receptor kinase to regulate plant vascular proliferation independently of any role in vascular organisation. Development 140 (10):2224-2234

Etchells JP, Smit ME, Gaudinier A, Williams CJ, Brady SM (2016) A brief history of the TDIF-PXY signalling module: balancing meristem identity and differentiation during vascular development. New Phytologist 209 (2):474-484

Etchells JP, Turner SR (2010) The PXY-CLE41 receptor ligand pair defines a multifunctional pathway that controls the rate and orientation of vascular cell division. Development 137 (5):767-774

Fisher K, Turner S (2007) PXY, a receptor-like kinase essential for maintaining polarity during plant vascular-tissue development. Current Biology 17 (12):1061-1066

Flematti GR, Ghisalberti EL, Dixon KW, Trengove RD (2004) A compound from smoke that promotes seed germination. Science 305 (5686):977-977

Flematti GR, Scaffidi A, Waters MT, Smith SM (2016) Stereospecificity in strigolactone biosynthesis and perception. Planta 243 (6):1361-1373

Fukuda H, Komamine A (1980) Establishment of an experimental system for the study of tracheary element differentiation from single cells isolated from the mesophyll of Zinnia elegans. Plant physiology 65 (1):57-60

Ge C, Cui X, Wang Y, Hu Y, Fu Z, Zhang D, Cheng Z, Li J (2006) BUD2, encoding an S-adenosylmethionine decarboxylase, is required for Arabidopsis growth and development. Cell research 16 (5):446-456

Gomez-Roldan V, Fermas S, Brewer PB, Puech-Pagès V, Dun EA, Pillot J-P, Letisse

F, Matusova R, Danoun S, Portais J-C (2008) Strigolactone inhibition of shoot branching. Nature 455 (7210):189-194

González-Grandío E, Poza-Carrión C, Sorzano COS, Cubas P (2013) BRANCHED1 promotes axillary bud dormancy in response to shade in Arabidopsis. The Plant Cell 25 (3):834-850

Graeff M, Hardtke CS (2021) Metaphloem development in the Arabidopsis root tip. Development 148 (18):dev199766

Green KA, Prigge MJ, Katzman RB, Clark SE (2005) CORONA, a member of the class III homeodomain leucine zipper gene family in Arabidopsis, regulates stem cell specification and organogenesis. The Plant Cell 17 (3):691-704

Haas AS, Shi D, Greb T Cell Fate Decisions Within the Vascular Cambium–Initiating Wood and Bast formation. Frontiers in Plant Science:911

Hamann T, Benkova E, Bäurle I, Kientz M, Jürgens G (2002) The Arabidopsis BODENLOS gene encodes an auxin response protein inhibiting MONOPTEROS-mediated embryo patterning. Genes & development 16 (13):1610-1615

Hamiaux C, Drummond RS, Janssen BJ, Ledger SE, Cooney JM, Newcomb RD, Snowden KC (2012) DAD2 is an α/β hydrolase likely to be involved in the perception of the plant branching hormone, strigolactone. Current biology 22 (21):2032-2036

Hanzawa Y, Takahashi T, Komeda Y (1997) ACL5: an Arabidopsis gene required for internodal elongation after flowering. The Plant Journal 12 (4):863-874

Hardtke CS, Berleth T (1998) The Arabidopsis gene MONOPTEROS encodes a transcription factor mediating embryo axis formation and vascular development. The EMBO journal 17 (5):1405-1411

Hirakawa Y, Kondo Y, Fukuda H (2010) TDIF peptide signaling regulates vascular stem cell proliferation via the WOX4 homeobox gene in Arabidopsis. The Plant Cell 22 (8):2618-2629

Hirakawa Y, Shinohara H, Kondo Y, Inoue A, Nakanomyo I, Ogawa M, Sawa S, Ohashi-Ito K, Matsubayashi Y, Fukuda H (2008) Non-cell-autonomous control of vascular stem cell fate by a CLE peptide/receptor system. Proceedings of the National Academy of Sciences 105 (39):15208-15213

Hu J, Hu X, Yang Y, He C, Hu J, Wang X (2022) Strigolactone signaling regulates cambial activity through repression of WOX4 by transcription factor BES1. Plant Physiology 188 (1):255-267

Ikematsu S, Tasaka M, Torii KU, Uchida N (2017) ERECTA-family receptor kinase genes redundantly prevent premature progression of secondary growth in the Arabidopsis hypocotyl. New Phytologist 213 (4):1697-1709

Ilegems M, Douet V, Meylan-Bettex M, Uyttewaal M, Brand L, Bowman JL, Stieger PA (2010) Interplay of auxin, KANADI and Class III HD-ZIP transcription factors in vascular tissue formation. Development 137 (6):975-984

Imai A, Hanzawa Y, Komura M, Yamamoto KT, Komeda Y, Takahashi T (2006) The dwarf phenotype of the Arabidopsis acl5 mutant is suppressed by a mutation

in an upstream ORF of a bHLH gene.
Immanen J, Nieminen K, Smolander O-P, Kojima M, Serra JA, Koskinen P, Zhang J, Elo A, Mähönen AP, Street N (2016) Cytokinin and auxin display distinct but interconnected distribution and signaling profiles to stimulate cambial activity. Current Biology 26 (15):1990-1997
Israelsson M, Sundberg B, Moritz T (2005) Tissue-specific localization of gibberellins and expression of gibberellin-biosynthetic and signaling genes in wood-forming tissues in aspen. The Plant Journal 44 (3):494-504
Ito Y, Nakanomyo I, Motose H, Iwamoto K, Sawa S, Dohmae N, Fukuda H (2006) Dodeca-CLE peptides as suppressors of plant stem cell differentiation. Science 313 (5788):842-845
Jammer A, Albacete A, Schulz B, Koch W, Weltmeier F, van der Graaff E, Pfeifhofer HW, Roitsch TG (2020) Early-stage sugar beet taproot development is characterized by three distinct physiological phases. Plant direct 4 (7):e00221
Jiang L, Liu X, Xiong G, Liu H, Chen F, Wang L, Meng X, Liu G, Yu H, Yuan Y (2013) DWARF 53 acts as a repressor of strigolactone signalling in rice. Nature 504 (7480):401-405
Kakehi J-i, Kuwashiro Y, Niitsu M, Takahashi T (2008) Thermospermine is required for stem elongation in Arabidopsis thaliana. Plant and Cell Physiology 49 (9):1342-1349
Kapulnik Y, Resnick N, Mayzlish-Gati E, Kaplan Y, Wininger S, Hershenhorn J, Koltai H (2011) Strigolactones interact with ethylene and auxin in regulating root-hair elongation in Arabidopsis. Journal of experimental botany 62 (8):2915-2924
Knott JM, Römer P, Sumper M (2007) Putative spermine synthases from Thalassiosira pseudonana and Arabidopsis thaliana synthesize thermospermine rather than spermine. FEBS letters 581 (16):3081-3086
Kohlen W, Charnikhova T, Liu Q, Bours R, Domagalska MA, Beguerie S, Verstappen F, Leyser O, Bouwmeester H, Ruyter-Spira C (2011) Strigolactones are transported through the xylem and play a key role in shoot architectural response to phosphate deficiency in nonarbuscular mycorrhizal host Arabidopsis. Plant physiology 155 (2):974-987
Koltai H (2015) Cellular events of strigolactone signalling and their crosstalk with auxin in roots. Journal of experimental botany 66 (16):4855-4861
Kondo Y, Fujita T, Sugiyama M, Fukuda H (2015) A novel system for xylem cell differentiation in Arabidopsis thaliana. Molecular plant 8 (4):612-621
Kondo Y, Ito T, Nakagami H, Hirakawa Y, Saito M, Tamaki T, Shirasu K, Fukuda H (2014) Plant GSK3 proteins regulate xylem cell differentiation downstream of TDIF–TDR signalling. Nature communications 5 (1):1-11
Krogan NT, Ckurshumova W, Marcos D, Caragea AE, Berleth T (2012) Deletion of MP/ARF5 domains III and IV reveals a requirement for Aux/IAA regulation in Arabidopsis leaf vascular patterning. New Phytologist 194 (2):391-401

Kubo M, Udagawa M, Nishikubo N, Horiguchi G, Yamaguchi M, Ito J, Mimura T, Fukuda H, Demura T (2005) Transcription switches for protoxylem and metaxylem vessel formation. Genes & development 19 (16):1855-1860

Lampropoulos A, Sutikovic Z, Wenzl C, Maegele I, Lohmann JU, Forner J (2013) GreenGate-a novel, versatile, and efficient cloning system for plant transgenesis. PloS one 8 (12):e83043

Liang Y, Ward S, Li P, Bennett T, Leyser O (2016) SMAX1-LIKE7 signals from the nucleus to regulate shoot development in Arabidopsis via partially EAR motif-independent mechanisms. The Plant Cell 28 (7):1581-1601

Lin H, Wang R, Qian Q, Yan M, Meng X, Fu Z, Yan C, Jiang B, Su Z, Li J (2009) DWARF27, an iron-containing protein required for the biosynthesis of strigolactones, regulates rice tiller bud outgrowth. The Plant Cell 21 (5):1512-1525

Mähönen AP, Bishopp A, Higuchi M, Nieminen KM, Kinoshita K, Törmäkangas K, Ikeda Y, Oka A, Kakimoto T, Helariutta Y (2006) Cytokinin signaling and its inhibitor AHP6 regulate cell fate during vascular development. Science 311 (5757):94-98

Mähönen AP, Bonke M, Kauppinen L, Riikonen M, Benfey PN, Helariutta Y (2000) A novel two-component hybrid molecule regulates vascular morphogenesis of the Arabidopsis root. Genes & development 14 (23):2938-2943

Mallory A, Vaucheret H (2010) Form, function, and regulation of ARGONAUTE proteins. Plant Cell 22 (12):3879-3889. doi:10.1105/tpc.110.080671

Mashiguchi K, Sasaki E, Shimada Y, Nagae M, Ueno K, Nakano T, Yoneyama K, Suzuki Y, Asami T (2009) Feedback-regulation of strigolactone biosynthetic genes and strigolactone-regulated genes in Arabidopsis. Bioscience, Biotechnology, and Biochemistry 73 (11):2460-2465

Mauriat M, Moritz T (2009) Analyses of GA20ox-and GID1-over-expressing aspen suggest that gibberellins play two distinct roles in wood formation. The Plant Journal 58 (6):989-1003

McCarthy RL, Zhong R, Ye Z-H (2009) MYB83 is a direct target of SND1 and acts redundantly with MYB46 in the regulation of secondary cell wall biosynthesis in Arabidopsis. Plant and Cell Physiology 50 (11):1950-1964

McConnell JR, Emery J, Eshed Y, Bao N, Bowman J, Barton MK (2001) Role of PHABULOSA and PHAVOLUTA in determining radial patterning in shoots. Nature 411 (6838):709-713

Milhinhos A, Prestele J, Bollhöner B, Matos A, Vera-Sirera F, Rambla JL, Ljung K, Carbonell J, Blazquez MA, Tuominen H (2013) Thermospermine levels are controlled by an auxin-dependent feedback loop mechanism in Populus xylem. The Plant Journal 75 (4):685-698

Mitsuda N, Iwase A, Yamamoto H, Yoshida M, Seki M, Shinozaki K, Ohme-Takagi M (2007) NAC transcription factors, NST1 and NST3, are key regulators of the

formation of secondary walls in woody tissues of Arabidopsis. The Plant Cell 19 (1):270-280

Miyashima S, Roszak P, Sevilem I, Toyokura K, Blob B, Heo J-o, Mellor N, Help-Rinta-Rahko H, Otero S, Smet W (2019) Mobile PEAR transcription factors integrate positional cues to prime cambial growth. Nature 565 (7740):490-494

Miyashima S, Sebastian J, Lee JY, Helariutta Y (2013) Stem cell function during plant vascular development. The EMBO journal 32 (2):178-193

Muñiz L, Minguet EG, Singh SK, Pesquet E, Vera-Sirera F, Moreau-Courtois CL, Carbonell J, Blázquez MA, Tuominen H (2008) ACAULIS5 controls Arabidopsis xylem specification through the prevention of premature cell death.

Nelson DC, Flematti GR, Riseborough J-A, Ghisalberti EL, Dixon KW, Smith SM (2010) Karrikins enhance light responses during germination and seedling development in Arabidopsis thaliana. Proceedings of the National Academy of Sciences 107 (15):7095-7100

Nelson DC, Scaffidi A, Dun EA, Waters MT, Flematti GR, Dixon KW, Beveridge CA, Ghisalberti EL, Smith SM (2011) F-box protein MAX2 has dual roles in karrikin and strigolactone signaling in Arabidopsis thaliana. Proceedings of the National Academy of Sciences 108 (21):8897-8902

Niwa M, Daimon Y, Kurotani K-i, Higo A, Pruneda-Paz JL, Breton G, Mitsuda N, Kay SA, Ohme-Takagi M, Endo M (2013) BRANCHED1 interacts with FLOWERING LOCUS T to repress the floral transition of the axillary meristems in Arabidopsis. The Plant Cell 25 (4):1228-1242

Ohashi-Ito K, Fukuda H (2003) HD-Zip III homeobox genes that include a novel member, ZeHB-13 (Zinnia)/ATHB-15 (Arabidopsis), are involved in procambium and xylem cell differentiation. Plant and Cell Physiology 44 (12):1350-1358

Ohta M, Matsui K, Hiratsu K, Shinshi H, Ohme-Takagi M (2001) Repression domains of class II ERF transcriptional repressors share an essential motif for active repression. The plant cell 13 (8):1959-1968

Pauwels L, Barbero GF, Geerinck J, Tilleman S, Grunewald W, Pérez AC, Chico JM, Bossche RV, Sewell J, Gil E (2010) NINJA connects the co-repressor TOPLESS to jasmonate signalling. Nature 464 (7289):788-791

Prigge MJ, Otsuga D, Alonso JM, Ecker JR, Drews GN, Clark SE (2005) Class III homeodomain-leucine zipper gene family members have overlapping, antagonistic, and distinct roles in Arabidopsis development. The Plant Cell 17 (1):61-76

Prusinkiewicz P, Crawford S, Smith RS, Ljung K, Bennett T, Ongaro V, Leyser O (2009) Control of bud activation by an auxin transport switch. Proceedings of the National Academy of Sciences 106 (41):17431-17436

Przemeck GK, Mattsson J, Hardtke CS, Sung ZR, Berleth T (1996) Studies on the role of the Arabidopsis gene MONOPTEROS in vascular development and plant cell axialization. Planta 200 (2):229-237

Ragni L, Greb T Secondary growth as a determinant of plant shape and form. In:

Seminars in Cell & Developmental Biology, 2018. Elsevier, pp 58-67
Ragni L, Hardtke CS (2014) Small but thick enough–the Arabidopsis hypocotyl as a model to study secondary growth. Physiologia plantarum 151 (2):164-171
Ragni L, Nieminen K, Pacheco-Villalobos D, Sibout R, Schwechheimer C, Hardtke CS (2011) Mobile gibberellin directly stimulates Arabidopsis hypocotyl xylem expansion. The Plant Cell 23 (4):1322-1336
Ramírez V, Pauly M (2019) Genetic dissection of cell wall defects and the strigolactone pathway in Arabidopsis. Plant direct 3 (6):e00149
Ramírez V, Xiong G, Mashiguchi K, Yamaguchi S, Pauly M (2018) Growth-and stress-related defects associated with wall hypoacetylation are strigolactone-dependent. Plant direct 2 (6):e00062
Rasmussen A, Mason MG, De Cuyper C, Brewer PB, Herold S, Agusti J, Geelen D, Greb T, Goormachtig S, Beeckman T (2012) Strigolactones suppress adventitious rooting in Arabidopsis and pea. Plant physiology 158 (4):1976-1987
Růžička K, Ursache R, Hejátko J, Helariutta Y (2015) Xylem development–from the cradle to the grave. New Phytologist 207 (3):519-535
Salehin M, Bagchi R, Estelle M (2015) SCFTIR1/AFB-based auxin perception: mechanism and role in plant growth and development. The Plant Cell 27 (1):9-19
Sang D, Chen D, Liu G, Liang Y, Huang L, Meng X, Chu J, Sun X, Dong G, Yuan Y (2014) Strigolactones regulate rice tiller angle by attenuating shoot gravitropism through inhibiting auxin biosynthesis. Proceedings of the National Academy of Sciences 111 (30):11199-11204
Scaffidi A, Waters MT, Sun YK, Skelton BW, Dixon KW, Ghisalberti EL, Flematti GR, Smith SM (2014) Strigolactone hormones and their stereoisomers signal through two related receptor proteins to induce different physiological responses in Arabidopsis. Plant Physiology 165 (3):1221-1232
Scarpella E, Barkoulas M, Tsiantis M (2010) Control of leaf and vein development by auxin. Cold Spring Harbor perspectives in biology 2 (1):a001511
Scarpella E, Marcos D, Friml J, Berleth T (2006) Control of leaf vascular patterning by polar auxin transport. Genes & development 20 (8):1015-1027
Seto Y, Yasui R, Kameoka H, Tamiru M, Cao M, Terauchi R, Sakurada A, Hirano R, Kisugi T, Hanada A (2019) Strigolactone perception and deactivation by a hydrolase receptor DWARF14. Nature Communications 10 (1):1-10
Shabek N, Ticchiarelli F, Mao H, Hinds TR, Leyser O, Zheng N (2018) Structural plasticity of D3–D14 ubiquitin ligase in strigolactone signalling. Nature 563 (7733):652-656
Shi D, Lebovka I, López-Salmerón V, Sanchez P, Greb T (2019) Bifacial cambium stem cells generate xylem and phloem during radial plant growth. Development 146 (1):dev171355
Shinohara N, Taylor C, Leyser O (2013) Strigolactone can promote or inhibit shoot

branching by triggering rapid depletion of the auxin efflux protein PIN1 from the plasma membrane. PLoS biology 11 (1):e1001474

Smetana O, Mäkilä R, Lyu M, Amiryousefi A, Sánchez Rodríguez F, Wu M-F, Sole-Gil A, Leal Gavarrón M, Siligato R, Miyashima S (2019) High levels of auxin signalling define the stem-cell organizer of the vascular cambium. Nature 565 (7740):485-489

Smit ME, Llavata-Peris CI, Roosjen M, van Beijnum H, Novikova D, Levitsky V, Sevilem I, Roszak P, Slane D, Jürgens G (2020) Specification and regulation of vascular tissue identity in the Arabidopsis embryo. Development 147 (8):dev186130

Snowden KC, Simkin AJ, Janssen BJ, Templeton KR, Loucas HM, Simons JL, Karunairetnam S, Gleave AP, Clark DG, Klee HJ (2005) The Decreased apical dominance1/Petunia hybrida CAROTENOID CLEAVAGE DIOXYGENASE8 gene affects branch production and plays a role in leaf senescence, root growth, and flower development. The Plant Cell 17 (3):746-759

Song C, Zhao J, Guichard M, Shi D, Grossmann G, Schmitt C, Jouannet V, Greb T (2022) Strigo-D2—a bio-sensor for monitoring spatio-temporal strigolactone signaling patterns in intact plants. Plant Physiology 188 (1):97-110

Song X, Lu Z, Yu H, Shao G, Xiong J, Meng X, Jing Y, Liu G, Xiong G, Duan J (2017) IPA1 functions as a downstream transcription factor repressed by D53 in strigolactone signaling in rice. Cell research 27 (9):1128-1141

Sorefan K, Booker J, Haurogné K, Goussot M, Bainbridge K, Foo E, Chatfield S, Ward S, Beveridge C, Rameau C (2003) MAX4 and RMS1 are orthologous dioxygenase-like genes that regulate shoot branching in Arabidopsis and pea. Genes & development 17 (12):1469-1474

Soundappan I, Bennett T, Morffy N, Liang Y, Stanga JP, Abbas A, Leyser O, Nelson DC (2015) SMAX1-LIKE/D53 family members enable distinct MAX2-dependent responses to strigolactones and karrikins in Arabidopsis. The Plant Cell 27 (11):3143-3159

Stanga JP, Morffy N, Nelson DC (2016) Functional redundancy in the control of seedling growth by the karrikin signaling pathway. Planta 243 (6):1397-1406

Stanga JP, Smith SM, Briggs WR, Nelson DC (2013) SUPPRESSOR OF MORE AXILLARY GROWTH2 1 controls seed germination and seedling development in Arabidopsis. Plant physiology 163 (1):318-330

Stirnberg P, van De Sande K, Leyser HO (2002) MAX1 and MAX2 control shoot lateral branching in Arabidopsis.

Sun Y, Fan X-Y, Cao D-M, Tang W, He K, Zhu J-Y, He J-X, Bai M-Y, Zhu S, Oh E (2010) Integration of brassinosteroid signal transduction with the transcription network for plant growth regulation in Arabidopsis. Developmental cell 19 (5):765-777

Szemenyei H, Hannon M, Long JA (2008) TOPLESS mediates auxin-dependent transcriptional repression during Arabidopsis embryogenesis. Science 319 (5868):1384-1386

Talbert PB, Adler HT, Parks DW, Comai L (1995) The REVOLUTA gene is necessary for apical meristem development and for limiting cell divisions in the leaves and stems of Arabidopsis thaliana. Development 121 (9):2723-2735

Tong W, Yoshimoto K, Kakehi J-I, Motose H, Niitsu M, Takahashi T (2014) Thermospermine modulates expression of auxin-related genes in Arabidopsis. Frontiers in plant science 5:94

Tuominen H, Puech L, Fink S, Sundberg B (1997) A radial concentration gradient of indole-3-acetic acid is related to secondary xylem development in hybrid aspen. Plant Physiology 115 (2):577-585

Turco GM, Rodriguez-Medina J, Siebert S, Han D, Valderrama-Gómez MÁ, Vahldick H, Shulse CN, Cole BJ, Juliano CE, Dickel DE (2019) Molecular mechanisms driving switch behavior in xylem cell differentiation. Cell reports 28 (2):342-351. e344

Ueda H, Kusaba M (2015) Strigolactone regulates leaf senescence in concert with ethylene in Arabidopsis. Plant Physiology 169 (1):138-147

Uggla C, Mellerowicz EJ, Sundberg Br (1998) Indole-3-acetic acid controls cambial growth in Scots pine by positional signaling. Plant Physiology 117 (1):113-121

Uggla C, Moritz T, Sandberg G, Sundberg B (1996) Auxin as a positional signal in pattern formation in plants. Proceedings of the national academy of sciences 93 (17):9282-9286

Umehara M, Cao M, Akiyama K, Akatsu T, Seto Y, Hanada A, Li W, Takeda-Kamiya N, Morimoto Y, Yamaguchi S (2015) Structural requirements of strigolactones for shoot branching inhibition in rice and Arabidopsis. Plant and Cell Physiology 56 (6):1059-1072

Umehara M, Hanada A, Yoshida S, Akiyama K, Arite T, Takeda-Kamiya N, Magome H, Kamiya Y, Shirasu K, Yoneyama K (2008) Inhibition of shoot branching by new terpenoid plant hormones. Nature 455 (7210):195-200

Ursache R, Miyashima S, Chen Q, Vatén A, Nakajima K, Carlsbecker A, Zhao Y, Helariutta Y, Dettmer J (2014) Tryptophan-dependent auxin biosynthesis is required for HD-ZIP III-mediated xylem patterning. Development 141 (6):1250-1259

Van Ha C, Leyva-González MA, Osakabe Y, Tran UT, Nishiyama R, Watanabe Y, Tanaka M, Seki M, Yamaguchi S, Van Dong N (2014) Positive regulatory role of strigolactone in plant responses to drought and salt stress. Proceedings of the National Academy of Sciences 111 (2):851-856

Vera-Sirera F, De Rybel B, Urbez C, Kouklas E, Pesquera M, Alvarez-Mahecha JC, Minguet EG, Tuominen H, Carbonell J, Borst JW (2015) A bHLH-based feedback loop restricts vascular cell proliferation in plants. Developmental cell 35 (4):432-443

Villaécija-Aguilar JA, Hamon-Josse M, Carbonnel S, Kretschmar A, Schmidt C, Dawid C, Bennett T, Gutjahr C (2019) SMAX1/SMXL2 regulate root and root hair development downstream of KAI2-mediated signalling in Arabidopsis. PLoS genetics 15 (8):e1008327

Wallner E-S, López-Salmerón V, Belevich I, Poschet G, Jung I, Grünwald K, Sevilem

I, Jokitalo E, Hell R, Helariutta Y (2017) Strigolactone-and karrikin-independent SMXL proteins are central regulators of phloem formation. Current Biology 27 (8):1241-1247

Wang L, Wang B, Jiang L, Liu X, Li X, Lu Z, Meng X, Wang Y, Smith SM, Li J (2015) Strigolactone signaling in Arabidopsis regulates shoot development by targeting D53-like SMXL repressor proteins for ubiquitination and degradation. The Plant Cell 27 (11):3128-3142

Wang L, Wang B, Yu H, Guo H, Lin T, Kou L, Wang A, Shao N, Ma H, Xiong G (2020a) Transcriptional regulation of strigolactone signalling in Arabidopsis. Nature 583 (7815):277-281

Wang L, Xu Q, Yu H, Ma H, Li X, Yang J, Chu J, Xie Q, Wang Y, Smith SM (2020b) Strigolactone and karrikin signaling pathways elicit ubiquitination and proteolysis of SMXL2 to regulate hypocotyl elongation in Arabidopsis. The Plant Cell 32 (7):2251-2270

Waters MT, Gutjahr C, Bennett T, Nelson DC (2017) Strigolactone signaling and evolution. Annual review of plant biology 68:291-322

Waters MT, Nelson DC, Scaffidi A, Flematti GR, Sun YK, Dixon KW, Smith SM (2012) Specialisation within the DWARF14 protein family confers distinct responses to karrikins and strigolactones in Arabidopsis. Development 139 (7):1285-1295

Wendrich JR, Weijers D (2013) The Arabidopsis embryo as a miniature morphogenesis model. New Phytol 199 (1):14-25. doi:10.1111/nph.12267

Wenzel CL, Schuetz M, Yu Q, Mattsson J (2007) Dynamics of MONOPTEROS and PIN-FORMED1 expression during leaf vein pattern formation in Arabidopsis thaliana. The Plant Journal 49 (3):387-398

Whitford R, Fernandez A, De Groodt R, Ortega E, Hilson P (2008) Plant CLE peptides from two distinct functional classes synergistically induce division of vascular cells. Proceedings of the National Academy of Sciences 105 (47):18625-18630

Wunderling A, Ripper D, Barra-Jimenez A, Mahn S, Sajak K, Targem MB, Ragni L (2018) A molecular framework to study periderm formation in Arabidopsis. New Phytologist 219 (1):216-229

Xie X (2016) Structural diversity of strigolactones and their distribution in the plant kingdom. Journal of Pesticide Science:J16-02

Xie X, Yoneyama K, Kisugi T, Uchida K, Ito S, Akiyama K, Hayashi H, Yokota T, Nomura T, Yoneyama K (2013) Confirming stereochemical structures of strigolactones produced by rice and tobacco. Molecular plant 6 (1):153-163

Xie X, Yoneyama K, Yoneyama K (2010) The strigolactone story. Annual review of phytopathology 48:93-117

Xiong G, Cheng K, Pauly M (2013) Xylan O-acetylation impacts xylem development and enzymatic recalcitrance as indicated by the Arabidopsis mutant tbl29. Molecular Plant 6 (4):1373-1375

Yamada Y, Furusawa S, Nagasaka S, Shimomura K, Yamaguchi S, Umehara M (2014) Strigolactone signaling regulates rice leaf senescence in response to a phosphate deficiency. Planta 240 (2):399-408

Yamaguchi M, Mitsuda N, Ohtani M, Ohme-Takagi M, Kato K, Demura T (2011) VASCULAR-RELATED NAC-DOMAIN 7 directly regulates the expression of a broad range of genes for xylem vessel formation. The Plant Journal 66 (4):579-590

Yamaguchi M, Nadia G, Igarashi H, Ohtani M, Nakano Y, Mortimer JC, Nishikubo N, Kubo M, Katayama Y, Kakegawa K (2010) VASCULAR-RELATED NAC-DOMAIN6 (VND6) and VND7 effectively induce transdifferentiation into xylem vessel elements under control of an induction system. Plant Physiology:pp. 110.154013

Yamamoto R, Fujioka S, Demura T, Takatsuto S, Yoshida S, Fukuda H (2001) Brassinosteroid levels increase drastically prior to morphogenesis of tracheary elements. Plant Physiology 125 (2):556-563

Yamamoto R, Fujioka S, Iwamoto K, Demura T, Takatsuto S, Yoshida S, Fukuda H (2007) Co-regulation of brassinosteroid biosynthesis-related genes during xylem cell differentiation. Plant and cell physiology 48 (1):74-83

Yang B, Minne M, Brunoni F, Plačková L, Petřík I, Sun Y, Nolf J, Smet W, Verstaen K, Wendrich JR (2021) Non-cell autonomous and spatiotemporal signalling from a tissue organizer orchestrates root vascular development. Nature Plants 7 (11):1485-1494

Yang JH, Lee KH, Du Q, Yang S, Yuan B, Qi L, Wang H (2020) A membrane-associated NAC domain transcription factor XVP interacts with TDIF co-receptor and regulates vascular meristem activity. New Phytologist 226 (1):59-74

Yao R, Ming Z, Yan L, Li S, Wang F, Ma S, Yu C, Yang M, Chen L, Chen L (2016) DWARF14 is a non-canonical hormone receptor for strigolactone. Nature 536 (7617):469-473

Yao R, Wang F, Ming Z, Du X, Chen L, Wang Y, Zhang W, Deng H, Xie D (2017) ShHTL7 is a non-canonical receptor for strigolactones in root parasitic weeds. Cell Research 27 (6):838-841

Yin Y, Vafeados D, Tao Y, Yoshida S, Asami T, Chory J (2005) A new class of transcription factors mediates brassinosteroid-regulated gene expression in Arabidopsis. Cell 120 (2):249-259

Yin Y, Wang Z-Y, Mora-Garcia S, Li J, Yoshida S, Asami T, Chory J (2002) BES1 accumulates in the nucleus in response to brassinosteroids to regulate gene expression and promote stem elongation. Cell 109 (2):181-191

Yoneyama K, Awad AA, Xie X, Yoneyama K, Takeuchi Y (2010) Strigolactones as germination stimulants for root parasitic plants. Plant and Cell Physiology 51

(7):1095-1103
Yoneyama K, Xie X, Yoneyama K, Kisugi T, Nomura T, Nakatani Y, Akiyama K, McErlean CS (2018) Which are the major players, canonical or non-canonical strigolactones? Journal of experimental botany 69 (9):2231-2239
Yoneyama K, Xie X, Yoneyama K, Takeuchi Y (2009) Strigolactones: structures and biological activities. Pest Management Science: formerly Pesticide Science 65 (5):467-470
Yoshimoto K, Noutoshi Y, Hayashi K-i, Shirasu K, Takahashi T, Motose H (2012) A chemical biology approach reveals an opposite action between thermospermine and auxin in xylem development in Arabidopsis thaliana. Plant and Cell Physiology 53 (4):635-645
Yu X, Li L, Li L, Guo M, Chory J, Yin Y (2008) Modulation of brassinosteroid-regulated gene expression by Jumonji domain-containing proteins ELF6 and REF6 in Arabidopsis. Proceedings of the National Academy of Sciences 105 (21):7618-7623
Zandalinas SI, Fichman Y, Mittler R (2020) Vascular bundles mediate systemic reactive oxygen signaling during light stress. Plant Cell 32 (11):3425-3435
Zhang H, Lin X, Han Z, Qu L-J, Chai J (2016a) Crystal structure of PXY-TDIF complex reveals a conserved recognition mechanism among CLE peptide-receptor pairs. Cell research 26 (5):543-555
Zhang H, Lin X, Han Z, Wang J, Qu L-J, Chai J (2016b) SERK family receptor-like kinases function as co-receptors with PXY for plant vascular development. Molecular plant 9 (10):1406-1414
Zhang J, Elo A, Helariutta Y (2011) Arabidopsis as a model for wood formation. Current Opinion in Biotechnology 22 (2):293-299
Zhang J, Mazur E, Balla J, Gallei M, Kalousek P, Medveďová Z, Li Y, Wang Y, Prát T, Vasileva M (2020) Strigolactones inhibit auxin feedback on PIN-dependent auxin transport canalization. Nature communications 11 (1):1-10
Zhang J, Nieminen K, Serra JAA, Helariutta Y (2014a) The formation of wood and its control. Current opinion in plant biology 17:56-63
Zhang Y, Van Dijk AD, Scaffidi A, Flematti GR, Hofmann M, Charnikhova T, Verstappen F, Hepworth J, Van Der Krol S, Leyser O (2014b) Rice cytochrome P450 MAX1 homologs catalyze distinct steps in strigolactone biosynthesis. Nature chemical biology 10 (12):1028-1033
Zhao J, Peng P, Schmitz RJ, Decker AD, Tax FE, Li J (2002) Two putative BIN2 substrates are nuclear components of brassinosteroid signaling. Plant physiology 130 (3):1221-1229
Zhao L-H, Zhou XE, Wu Z-S, Yi W, Xu Y, Li S, Xu T-H, Liu Y, Chen R-Z, Kovach A (2013) Crystal structures of two phytohormone signal-transducing α/β hydrolases: karrikin-signaling KAI2 and strigolactone-signaling DWARF14. Cell research 23 (3):436-439
Zhao Q-P, Wang X-N, Li N-N, Zhu Z-Y, Mu S-C, Zhao X, Zhang X (2018) Functional analysis of MAX2 in phototropins-mediated cotyledon flattening in Arabidopsis. Frontiers in plant science:1507

Zhou F, Lin Q, Zhu L, Ren Y, Zhou K, Shabek N, Wu F, Mao H, Dong W, Gan L (2013) D14–SCFD3-dependent degradation of D53 regulates strigolactone signalling. Nature 504 (7480):406-410

Zwanenburg B, Mwakaboko AS, Reizelman A, Anilkumar G, Sethumadhavan D (2009) Structure and function of natural and synthetic signalling molecules in parasitic weed germination. Pest Management Science: formerly Pesticide Science 65 (5):478-491